THE EFFECTS OF OXIDIZERS ON THE DIAMETERS OF THE CARBON NANOTUBES GROWN BY CHEMICAL VAPOR DEPOSITION METHOD

A Thesis Submitted to
the Graduate School of Engineering and Sciences of
İzmir Institute of Technology
in Partial Fulfillment of the Requirements for the Degree of

MASTER OF SCIENCE

in Physics

by

Gülay BÜLBÜL

October 2012
İZMİR

We approve the thesis of **Gülay BÜLBÜL**

Examining Committee Members:

Assoc. Prof. Dr. Yusuf SELAMET
Department of Physics, İzmir Institute of Technology

Assoc. Prof. Dr. Özgür ÇAKIR
Department of Physics, İzmir Institute of Technology

Assoc. Prof. Dr. Mustafa Muammer DEMİR
Department of Chemistry, İzmir Institute of Technology

2 October 2012

Assoc. Prof. Dr. Yusuf SELAMET
Supervisor, Department of Physics
İzmir Institute of Technology

Prof. Dr. Nejat BULUT
Head of the Department of Physics

Prof. Dr. R. Tuğrul SENGER
Dean of the Graduate School of
Engineering and Sciences

ACKNOWLEDGEMENTS

During my master thesis, lots of people helped and supported me, therefore I would like to thank all of them.

Firstly, I would like to thank my advisor Assoc. Prof. Dr. Yusuf Selamet for his help, patience, guidance and encouragement. He always made me feel in confidence while I was preparing my thesis.

A special thank goes to Assist. Prof. Dr. Enver Tarhan for help with Raman Spectroscopy.

I thankfully acknowledge TUBITAK for financial support during this project (TUBITAK 211T151).

In addition, I am very thankful to my lab mates at Carbon Nanostructure Laboratory Deniz Söylev and Atike İnce.

For SEM and AFM analysis, I send my thanks to IYTE Material Research Center staff. Moreover, I want to thank Hasan Aydın and Nesli Yağmurcukardeş for spending his time for AFM measurements in the laboratory, IYTE. Other thanks go to Dr. Sinem Bezircilioğlu for controlling academic writing of my thesis with a warm and friendship attitude.

Thanks to each of my friends in Prep Class at Izmir Institute of Technology for sharing unforgettable memories. Especially, I feel very lucky to have Gülden Yorgancıoğlu by my side since my first day at IYTE. I could not have finished this thesis without her encouragement and warm friendship. Although she has not been at IYTE for one year, she always has been in contact both in my good days and bad days. I feel more than lucky to have such a friend!

My special thanks go to Serkan Serdar for breathing with me on my hardest days and his supports from the beginning, till the end.

To my family, my mother Leman Bülbül, my father Coşkun Bülbül I wish to say a big thank you. Without your motivation, love, positive attitudes and financial supports I never would have been able to keep going. Brother Koray Bülbül, I always felt you as the safety net I could lean on if things go wrong, thanks for being there, always. I am also grateful to express my satisfactions with my other family members. I always need my family in my life!!!

ABSTRACT

THE EFFECTS OF OXIDIZERS ON THE DIAMETERS OF THE CARBON NANOTUBES GROWN BY CHEMICAL VAPOR DEPOSITION METHOD

This thesis was focused on growing high quality and small-diameter carbon (C) nanotube (NT) on $Fe/Al_2O_3/SiO_2/Si$ thin film catalyst by ethylene decomposition thermal chemical vapor deposition (CVD) method in the presence of a weak oxidizer (CO_2). Moreover, the importance and functional properties of the oxidizer in pretreatment and CNT growth were determined.

At first, it was worked in different growth conditions to examine the effects of CO_2 in CNT growth. The main parameters were pretreatment time, CO_2 gas flow rates during pretreatment and growth, growth temperature. Pretreatment and growth times were kept at 15 min. each and CO_2 introduced 5 and 10 min. during pretreatment stage prior to the CNT growth with the flow rates 8:2, 10:2, 10:8 and 10:10 sccm, respectively. Additionally, three different growth temperatures; 750 ^oC, 760 ^oC and 770 ^oC were studied.

Secondly, pretreatment time was kept at 15 min. The effects of CO_2, which was sent in the system at 8:2, 10:2, 10:8 and 10:10 sccm ratios, on density and height of the catalyst particles were investigated.

At last, all catalyst particles and CNTs obtained from the experiments were analyzed by several characterization techniques such as AFM, EDX, SEM, STEM and Raman Spectroscopy, respectively. The optimal values of amount and introduction time of CO_2, the ratio of CO_2 in growth to that in pretreatment were identified. Moreover, the relation between currently obtained catalyst particles and previously being grown CNTs on them were determined. It was observed that using the appropriate amount of CO_2 in pretreatment and growth process positively affected the catalyst sizes and CNT diameter distributions.

ÖZET

KİMYASAL BUHAR BİRİKTİRME YÖNTEMİ İLE BÜYÜTÜLEN KARBON NANOTÜPLERİN ÇAPLARINA OKSİTLEYİCİLERİN ETKİLERİ

Bu tez, $Fe/Al_2O_3/SiO/Si$ ince film kataliz üzerine, zayıf oksitleyici (CO_2) varlığında etilen dekompozisyonu termal kimyasal buhar biriktirme (CVD) tekniği ile kaliteli ve düşük çaplı karbon (C) nanotüp (NT) sentezlenmesine odaklandı. Ayrıca, oksitleyicinin önişlem ve CNT büyütmesi üzerindeki önemi ve işlevsel özellikleri belirlendi.

İlk olarak, CNT büyümesinde CO_2 gazının etkisinin araştırılması için farklı büyütme koşullarında çalışıldı. Önişlem süresi, önişlem ve büyütme süresi boyunca gönderilen CO_2 gaz akış oranları ve büyütme sıcaklığı çalışılan ana parametrelerdir. Deneyler boyunca önişlem ve büyütme süresi 15 dakika olarak seçilmekle birlikte, CO_2 gazı bu süre içinde gaz akış oranları sırasıyla 8:2, 10:2, 10:8 ve 10:10 sccm olarak önişlem süresi boyunca 5 ve 10 dakikalık sürelerle sisteme gönderildi. Diğer bir parametre olan sıcaklık ise 750 ^oC, 760 ^oC ve 770 ^oC değerlerinde çalışıldı.

İkinci olarak, 15 dakika seçilen önişlem süresince 8: 2, 10: 2, 10: 8 ve 10: 10 sccm oranlarında gönderilen CO_2 gazının kataliz parçacıklarının yoğunlukları ve yükseklikleri üzerindeki etkileri araştırıldı.

Son olarak, bahsedilen parametreler kullanılarak yapılan deneyler sonucunda elde edilen kataliz ve CNT'ler sırasıyla AFM, EDX, SEM, STEM ve Raman Spektroskopi gibi çeşitli karakterizasyon teknikleriyle analiz edildi. CO_2 gazının optimal miktarı ve gönderme süresi ile önişlem ve büyütme evrelerindeki oranı belirlendi. Elde edilen kataliz parçacıkları ve daha önce bunlar üzerlerine büyütülen CNT'ler arasındaki ilişki değerlendirildi. Önişlem ve büyütme işlemlerinde uygun miktarda kullanılan CO_2 gazının kataliz büyüklüğü ve CNT çap dağılımlarını olumlu etkilediği gözlendi.

Dedicated to;

My lovely family

For being always with me!

TABLE OF CONTENTS

LIST OF FIGURES

LIST OF TABLES

Table **Page**

CHAPTER 1

INTRODUCTION

The synthesis of carbon nanotubes (CNTs) has been extensively investigated by a large number of research groups, since the current explosion of interest in CNTs began with the discovery by Iijima in 1991 (Iijima 1991). A great number of works performed on CNTs have shown that they offer tremendous opportunities for novel applications, and the development of new nanoscale devices.

CNTs are extraordinary nano materials in terms of their excellent structural, mechanical and electronic properties: Their tensile strength is at least 10 times stronger than conventional graphite fibers. They have thermal conductivity better than all but the purest diamond and their electrical conductivity is much higher than copper (Schwartz 2006). Additionally, CNTs have high Young modulus and low weight (Saito, et al. 1992). Therefore, they can serve multifunctional roles in molecular electronics (Bachtold, et al. 2001, Frackowiak, et al. 2000, Martel, et al. 1998), field emission devices (Zhu, et al. 1999), flat panel display (Collins and Zettl 1997), scanning probes (Dai, et al. 1998), chemical force sensors (Kong, et al. 2000, Wong, et al. 1998), hydrogen storage (Darkrim, et al. 2002, Liu, et al. 1999) and composite materials (Paradise and Goswami 2007).

CNTs can be considered as the result of rolling graphite layers onto themselves, which is also an allotrope of carbon, forming carbon cylinders and may be composed of a single shell which is called single-walled carbon nanotube (SWNT) or of several shells which is called multi-walled carbon nanotube (MWNT) (Dresselhaus, et al. 2001). A SWNT can be classified into three types; chiral, zigzag or armchair. The most exciting CNT property is related to its electronic band structure which depends on the folding angle and the chiral vector $\overrightarrow{C_h} = n\overrightarrow{a_1} + m\overrightarrow{a_2}$ of the tube, so that a CNT can be semiconducting or metallic (Dresselhaus and Dai, 2004). Though zigzag CNTs are to be either semiconducting or metallic, all armchair CNTs are metallic nanotubes (Saito, et al. 1992, Schwartz 2006).

Arc discharge, laser vaporization and chemical vapor deposition (CVD) methods (Baddour and Briens 2005) are the three main methods used for CNT synthesis. The

first two methods, arc discharge and laser vaporization, have some limitations, so they are not suitable for mass production. On the other hand, CVD is regarded as one of the most promising growth technique because of its advantages. As the process of CVD technique is considered, it depends on passing carbon-containing gas through a furnace where metal catalysts are present at the growth temperature to decompose the gas (Ando, et al. 2004, Merkoçi 2006, Nessim 2010).

When growing CNTs are considered, catalyst materials are of vital importance. Among transition metals, Fe, Co, Ni are the most common catalysts used in CVD process (Baddour and Briens 2005) due to the fact that these metals have finite solubility of carbon at high temperatures (Ando, et al. 2004, Dai 2002).

The aim of this study was to investigate the growth mechanism and the effects of the oxidizers on the diameter of CNTs grown by CVD method. Pretreatment time, growth temperature, time and flow rate of oxidizer (CO_2) were the studied parameters in this work. This thesis includes six chapters. The first chapter is a general description of carbon nanotubes and content of this thesis. In Chapter 2, carbon nanotubes, their discovery, types, structure, synthesis methods and growth mechanism are focused on in detail. Chapter 3 is devoted to a brief literature survey on oxidizer use in CNT growth. In the experimental section, Chapter 4, the catalyst film deposition process by DC magnetron sputtering, the Thermal Chemical Vapor Deposition (TCVD) process with a detailed explanation and the characterization techniques of CNTs are given. Chapter 5 presents the experimental results and discussions part. The final part Chapter 6 includes conclusions of this study.

CHAPTER 2

CARBON NANOTUBES

2.1. Carbon Structures

Carbon is a fascinating element in the universe because of its two unique features: a carbon atom is able to make bonding with another carbon atom in many configurations resulting in allotropic forms of carbon from 0-dimensions to 3-dimensions; fullerene is 0-dimensional, carbon nanotube is 1-dimensional, graphene is 2-dimensional, and diamond is 3-dimensional. The other feature of a carbon atom is that it can also bond with many elements such as hydrogen, oxygen, and nitrogen (Bonard 2006).

Fullerene, the first nano structured crystalline form of carbon, can consist of 60, 70 or 82 carbon atoms which are arranged in hexagon and pentagon configurations (Dai 2002). According to the arrangements of the carbon atoms, a fullerene can form a hollow sphere, cylinder, or similar figure. In the fullerene structure, each carbon atom takes part in one double bond and in two single bonds. The bonding is an admixture of sp^2 and sp^3. The structure of a C_{60} molecule is called Buckminsterfullerene and has the form of a soccer ball as shown in Figure 2.1.

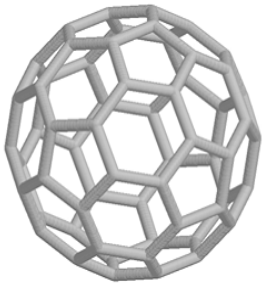

Figure 2.1. C_{60} Buckminsterfullerene
(Source: Stahl, et al. 2000)

Graphite is the most stable allotrope of carbon at room temperature, and atmospheric pressure (Baddour and Briens 2005, Petrucci, et al. 1993), and is a zero band gap semiconductor. In graphite, carbon atoms are in fact only bonded to three other carbon atoms, not four. The remaining electron detaches from the carbon atom, and is free to move between sheets of the carbon rings**.** Each carbon atom possesses a sp^2 orbital hybridization to form three in plane σ bonds with an out of plane π bond. Figure 2.2 shows the structure of graphite.

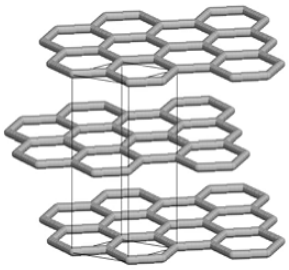

Figure 2.2. The structure of graphite
(Source: Stahl, et al. 2000)

Diamond is one of the best known allotropes of carbon. In diamond, all four electrons in the outer shell of the carbon atom are used in bonds with other carbon atoms in the four tetrahedral directions, therefore, diamond does not have a free electron. Hence, it is electrically insulating with a large band gap. This three dimensional sp^3 (diamond) structure makes diamond the hardest material in nature. The unusual property of diamond is its high thermal conductivity (Meyyappan 2005). Diamond structure is shown in Figure 2.3.

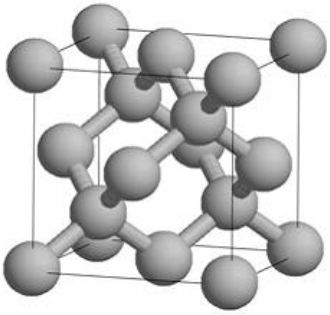

Figure 2.3. Diamond in the cubic structure
(Source: Stahl, et al. 2000)

Carbon nanotube (CNT) is the last carbon structure to be dealt with in the following section in this thesis.

2.2. Carbon Nanotubes

2.2.1. Historical Background

When electron microscopes became popular in the research fields, Radushkevich et al. discovered the first tubular form of carbon by using an electron microscope in 1952 (Radushkevich, et al. 1952). However, not much interest was shown to the early reports of carbon nanotubes by the scientists. In 1991, while the Japanese scientist Sumio Ijima was doing some experiments to observe fullerene, he observed another form of carbon (graphitic tubules). After the discovery, that structure of carbon has been given a name, 'carbon nanotube'(CNT) (Dupuis 2005).

The first observed and described CNT was multi-walled carbon nanotube (MWNT) which was grown by using arc-discharge method. A few years later, the second type of CNT called single-walled carbon nanotube (SWNT) was discovered by using two different growth methods (chemical vapor deposition (CVD) and laser ablation method) (Dupuis 2005, Iijima and Ichihashi 1993).

2.2.2. Types of Carbon Nanotubes

Depending on the number of a CNT's graphene cylinders, there are two types of CNT. When a CNT contains one graphene cylinder, it is called single-walled carbon nanotube. On the other hand, the second type of CNT, multi-walled carbon nanotube, has more than one concentric cylinder.

2.2.2.1. Single-Walled Carbon Nanotube

A single-walled carbon nanotube (SWNT) can be considered to be formed by the rolling of a single graphene cylinder with the diameter ranging from 0.4 to 5 nm, and also it can be classified as either metallic or semiconducting. SWNTs are mostly

preferred nanotube type because of their perfect electrical, mechanical and structural properties as well as their having less defects with compared to MWNT (Dai 2002). The shape of a SWNT is depicted in Figure 2.4.

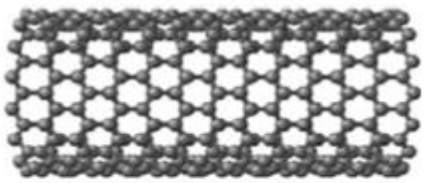

Figure 2.4. An illustration of a SWNT
(Source: Dresselhaus, et al. 2003)

2.2.2.2. Multi-Walled Carbon Nanotube

A multi-walled carbon nanotube (MWNT) consists of two or more concentric cylindrical shells with an interlayer spacing of 0.34 nm (Popov 2004) of graphene sheets coaxially arranged around a central hollow core. Each individual tube can have different chirality (Thostenson, et al. 2001). The diameter of this type of CNT ranges from 2 to 100 nm (Merkoçi 2006), depending on the method of synthesis, and their lengths up to μm or even cm (Dai 2002). The shape of a MWNT is shown in Figure 2.5.

Although the atoms of SWNT are held with covalent bonding, the concentric tubes are held together by Van der Waals bonding in MWNT (Thostenson, et al. 2001). MWNT acts primarily like metallic conductors (some can be semiconducting with very small band gaps). MWNT is stronger than SWNT, but they have more defects than SWNT (Dai 2002). MWNT contains imperfections that can limit their properties because of having multiple walls with concentric cylinders around the inner tube (Schwartz 2006).

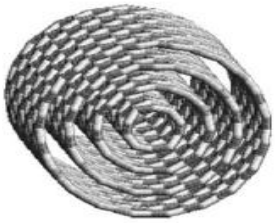

Figure 2.5. An illustration of a MWNT
(Source: Dresselhaus, et al. 2003)

2.2.3. Classification of Carbon Nanotubes

When a graphene sheet is rolled into tubular form, the structure can be in three different configurations such as; armchair, zigzag, and finally chiral carbon nanotube. The formations of three different CNTs are shown in Figure 2.6.

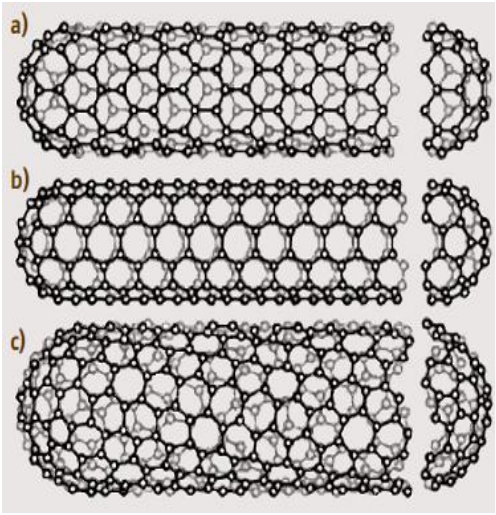

Figure 2.6. Classification of CNTs a) Zigzag (n, 0) b) Armchair (n=m) c) Chiral (n≠m) CNTs (Source: Dresselhaus, et al. 1998)

As shown in Figure 2.7, the orientation of chiral vector is $\overrightarrow{C_h} = n\overrightarrow{a_1} + m\overrightarrow{a_2}$ where $\overrightarrow{a_1}$ and $\overrightarrow{a_2}$ are the unit base cell vectors of graphene honeycomb lattice and n and m are integers. The diameter of CNT is determined by the (n,m) or (m,n) indices called 'chirality' (Dai 2002). 'Chiral angle (θ)' is known as the angle between the chiral vector ($\overrightarrow{C_h}$) and the unit vector ($\overrightarrow{a_1}$), which determines the direction of the chiral vector and gives information about orientations of CNTs.

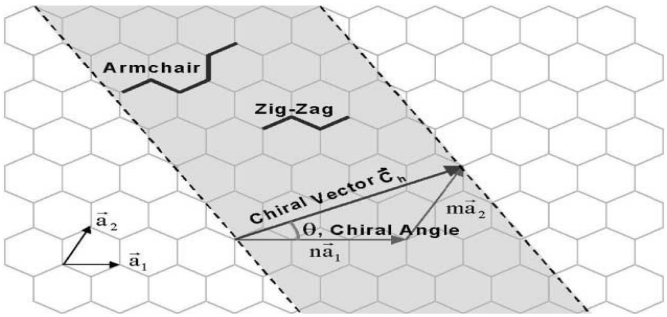

Figure 2.7. An illustration of unrolled grapheme
(Source: Thostenson, et al. 2001)

The chiral angle for armchair tubes (n=m) is $\theta=0^o$, for zigzag tubes (m=0) $\theta=30^o$, and for all chiral tubes (n≠m) $0< \theta<30^o$ (Belin and Epron 2005). Depending on the tube chirality, CNTs have different electrical properties, that's why they can be metallic or semiconducting. If n-m=3q, where q is an integer, CNTs are metallic; while n-m≠3q, CNTs are semiconducting (Ivchenko and Spivak 2002). However, armchair CNTs (no band gap because of symmetrical structures) always show metallic character, zig-zag CNT (large band gap) and chiral CNTs (small band gap) indicate either metallic or semiconducting behavior (Hornyak, et al. 2008, Kaufmann and Star 2008). In Figure 2.8, metallic and semiconducting CNTs are shown. The metallic CNTs are represented by encircled dots, the semiconducting CNTs are represented by dots.

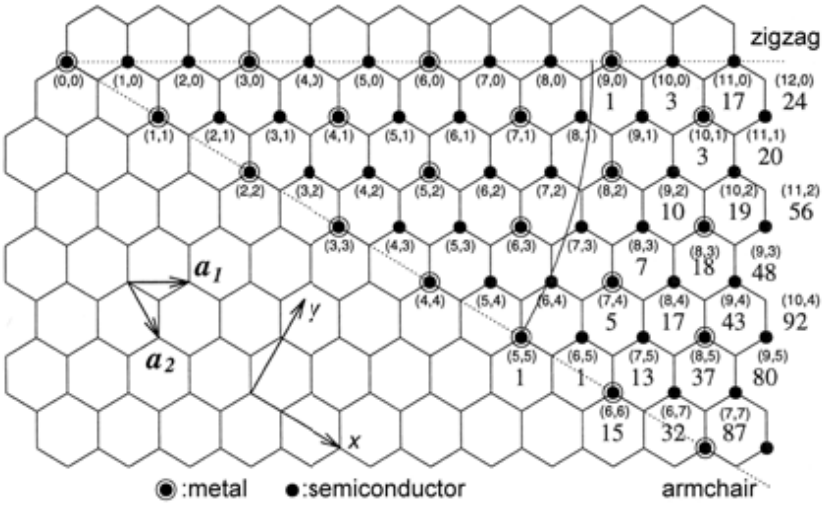

Figure 2.8. Possible vector space specified by the pairs of integers (n, m) for general CNTs (Source: Dresselhaus, et al. 1998)

2.3. Carbon Nanotube Synthesis Methods

Since the discovery of CNTs, several different production methods, the most common of which are arc-discharge (Journet and Bernier 1998), the laser-ablation (Thess, et al. 1996) and chemical vapor deposition (CVD) (Niu and Fang 2006), have been used to synthesize them. These methods can be divided as physical and chemical processes according to the method applied to release carbon atoms from carbon-containing precursor molecules (Moisala, et al. 2003). Arc-discharge and laser-ablation methods are the physical methods, CVD is the chemical method (Moisala, et al. 2003).

Each method has unique properties in terms of the results obtained, since they have advantages or disadvantages as shown in Table 2.1, which are focused in this section.

Table 2.1. Advantages and disadvantages of three main techniques used for CNT growth.

Method	**Arc-discharge**	**Laser-ablation**	**CVD**
Pioneer	Iijima (1991)	Guo et al. (1995)	Yacaman et al. (1993)
Kind of CNT	MWNT	SWNT	Both
Yields	High	Low	High
Advantages	-the high growth rate	-the conditions easily optimized - narrow diameter range	-simple mechanism -low cost -low temperature production -growth control -aligned growth
Disadvantages	-simple and inexpensive -expensive equipment -the large amount of energy consumed	-expensive equipment -high temperature production -the large amount of energy consumed	-impurity -high structural defects

2.3.1. Arc-Discharge Method

Arc-discharge method by which the CNTs have been produced by Iijima (Iijima 1991) is the most common and perhaps the easiest way (Journet and Bernier 1998) to produce CNTs, fullerenes and amorphous carbon (Bonard 2006). A typical illustration of an arc-discharge apparatus is shown in Figure 2.9.

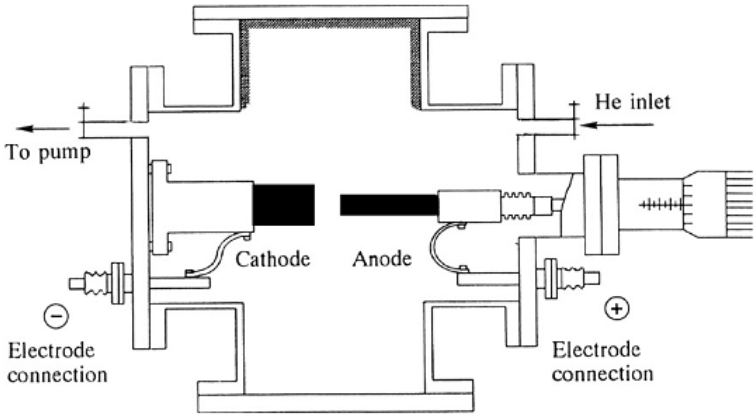

Figure 2.9. Schematic illustration of an arc-discharge apparatus
(Source: Harris 2007)

The principle of this method depends on an electric discharge produced by applying direct current (DC) of ~200 A at a low voltage (20-40 V) (Iijima 1991) between anode and cathode under an inert atmosphere of helium or argon (Journet and Bernier 1998, Popov 2004) and also in methane (Ando, et al. 2004).

Arc-discharge method can be utilized with or without catalyst (such as Fe, Co, Ni); catalyst is necessary for the production of SWNT while for the production of MWNT is not, (Journet and Bernier 1998). The temperature of the anode surface (~4000 ^{o}C) is higher than the cathode surface (~3500 ^{o}C) during the process, so that carbon atoms evaporate from the anode and accumulate on the cathode, and the length of the anode decreases with the nano particles forming.

The voltage and current are the parameters of the arc-discharge method (Zhu, et al. 2002). Furthermore, the conditions and choice of catalyst are important (Baddour and Briens 2005) and the pressure of inert gas has a strong influence on the CNTs grown.

Even though this technique is simple, inexpensive and the most widely used synthesis method, CNT yields can be limited. Moreover, the purification of CNTs is a problem due to their location among vaporized debris (Hornyak, et al. 2008, Merkoçi 2006), so it needs to be separated from the crude product containing various side products and catalytic metals (Baddour and Briens 2005). The other drawback of this method is that CNTs may be damaged during the process.

2.3.2. The Laser-Ablation Method

The first CNT synthesis by laser-ablation method was reported by Guo (Guo, et al. 1995). This method, which is useful, more simple and powerful for producing CNT, has a similar principle with the arc-discharge method. It can be considered as a thermal and a high-energy method (Hornyak, et al. 2008). A typical illustration of a laser-ablation apparatus is depicted in Figure 2.10.

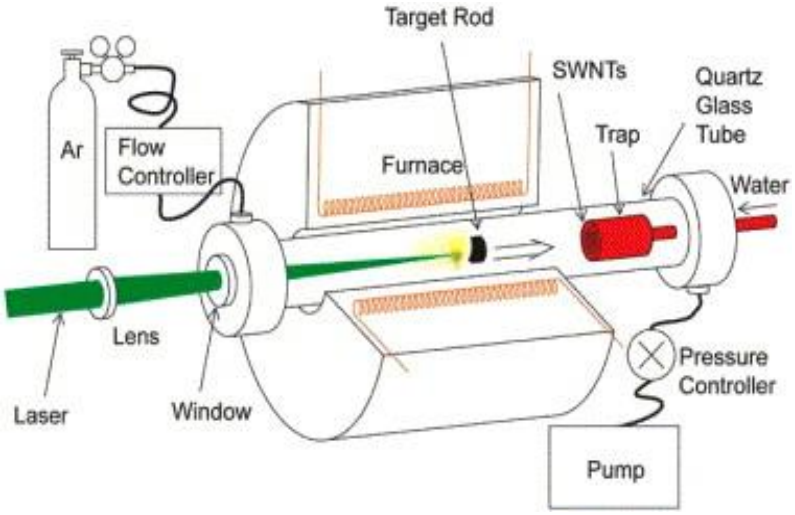

Figure 2.10. Schematic illustration of a laser-ablation apparatus
(Source: Ando, et al. 2004)

Although MWNT growth is not possible by using the laser-ablation method (Baddour and Briens 2005), it can synthesize SWNT with the highest purity (up to about 90% purity) in comparison with other techniques (Makita, et al. 2005).

The laser-ablation method is performed nearly at 1200 ^{o}C in an argon or helium gas environment kept at 500 Torr pressure (Baddour and Briens 2005) in a temperature controlled furnace in which a graphite target is placed in the middle of a quartz tube (Harris 2007). In comparison with the other vaporization devices, the energy density of the lasers used in this technique is much higher than those, so the laser has an appropriate usage for materials with a high melting temperature, such as graphite (Ando, et al. 2004).

The basic principle of this method is as follows: a powerful laser beam is introduced to the system through the window and focused onto the target located in the center of the furnace. The target consists of a mixture of graphite and metal catalysts, such as Co or Ni. After the target is vaporized by laser local heating, the vaporized carbon is carried to the copper collector and it deposits on the top surface of this collector (Harris 2007). When the system cools to low temperature by a water cooling system, this process finishes (Baddour and Briens 2005).

As a conclusion, CNTs with high quality have been synthesized by the laser-ablation method. However, this method has some drawbacks. Firstly, it produces a small amount of clean CNTs, whereas arc-discharge methods produce large quantities of impure material, in general. Secondly, this method costs a lot because of the laser, therefore, scale-up is not possible with this method. Additionally, this is a slow and expensive process by its nature (Wolf 2006).

2.3.3. Chemical Vapor Deposition Method

Chemical vapor deposition (CVD) technique has been used first for the production of carbon filaments more than 4 decades ago (Walker, et al. 1959), however, it was utilized to grow MWNTs till 1993 (Yacaman, et al. 1993). There are various CVD techniques for CNT growth such as plasma enhanced CVD, thermal CVD, alcohol catalytic CVD, laser assisted CVD and aero-gel supported CVD. Thermal CVD (TCVD) method used in this thesis study will be explained below in detail.

CNT growth includes two main parts which are the catalyst preparation also known as pretreatment and the CNT growth. To synthesis catalyst nano particles, a thin film layer can be used by annealing. As the growth process, some steps are followed: Firstly, the prepared substrate with catalyst is placed inside the quartz tube and the temperature is fixed for a selective point in an inert gas environment. While the temperature is increasing, an inert gas (in general, Ar) flows through the tube to prevent the oxidation contamination of samples. When the furnace reaches the desired temperature, etching gas such as hydrogen, nitrogen, or ammonium is started to be sent through the tube in order to form catalyst nano particles. In the second step, hydrocarbon gas flows into the system and decomposes on the catalyst surface. Acetylene (C_2H_2), ethylene (C_2H_4), methane (CH_4) are the most frequently used

hydrocarbons (Cui, et al. 2003) with the catalyst obtained over substrates (Moisala, et al. 2003), because of their high carbon content (Vesselényi, et al. 2001). Finally, CNTs grow over the catalyst and are collected upon cooling the system to room temperature (Merkoçi 2006). Figure 2.11 shows an illustration of the simplest set up used for CNT growth in CVD growth.

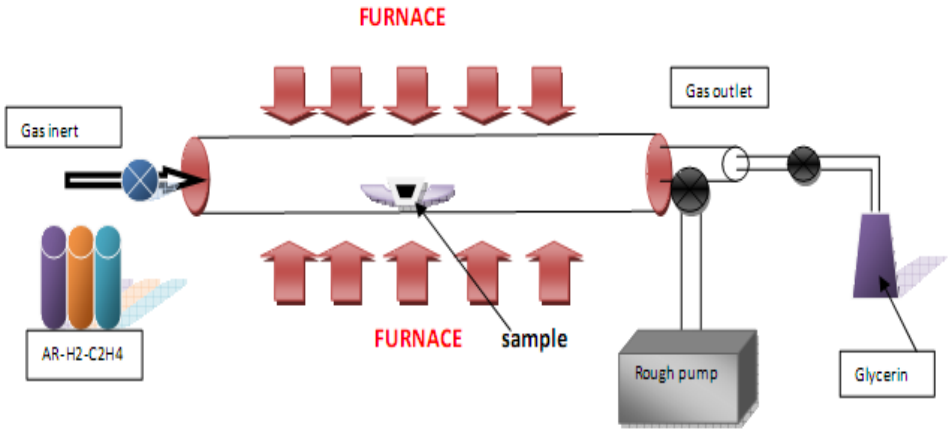

Figure 2.11. A schematic illustration of a CVD system
(Source: Journet and Bernier 1998)

This method is ideal to synthesize well-defined structures of CNT (Kong, et al. 1998). When it is compared with the other two methods, CVD has many advantages. The main advantage of this technique is that it exerts more control over the products with a large range and considering energy efficiency, less energy is required (Bonard 2006, Hornyak, et al. 2008). Second, it enables the use of various substrates (Ando, et al. 2004). The other superior property of this method is to provide directional growth of both SWNT and MWNTs. Moreover, this technique is a hot-wall system performing at relatively low temperature hence, does not require any cooling systems (Jung, et al. 2001, Meyyappan 2005). CVD is the best way to form CNT owing to its simplicity and most effectiveness for mass production (Hornyak, et al. 2008).

2.3.3.1. Key Parameters of Chemical Vapor Deposition Method

CNT growth mechanism has remained somewhat controversial despite being heavily investigated for years. In this part, the effects of important key parameters including catalyst thin films, thin film support layer, consideration of gases (hydrocarbons and flow rates), temperatures for both annealing and growth affecting the growth process of CNT are emphasized (Nessim 2010). In addition, the importance of oxidizers is mentioned in Chapter 3 in detail.

2.3.3.1.1. Catalyst Thin Film

One of the indispensible parameters affecting the CNT growth is catalyst material, whose size, density and also types have important effects on the CNT diameter (Bonard, et al. 2002, Chhowalla, et al. 2001), and the growth rate (Lee, et al. 2002). Furthermore, it affects the morphology of both SWNT and MWNTs grown with the tip-growth or base-growth mechanisms. In addition, the areal density of particles determines the spacing between CNTs (Chhowalla, et al. 2001, Kind, et al. 1999).

Ni, Co, Fe, Cr, Mn, Zn, Ti, Zr, Hf, Re, Sc, Y and Mo or a combination of them have been used to determine the most suitable metal catalyst in the growth of CNT. However, it has been observed that Co (Ivanov, et al. 1994), Fe (Hernadi, et al. 1996) and Ni (Yudasaka, et al. 1994) (transition metals) or alloys of them are the best catalyst choices among others due to having finite carbon solubility (0.5wt%-1.5wt%) at high temperatures (800-900 ^{o}C) (Ando, et al. 2004, Dai 2002, Deck and Vecchio 2006, Dresselhaus, et al. 2001) and catalytically decomposing gaseous carbon-containing molecules (Moisala, et al. 2003). Lee et al. showed that respective CNT growth rate and the best product are based on the catalyst type in the order of Fe>Co>Ni (Lee, et al. 2002). It has also been stated that growing both MWNT and SWNTs is possible by means of these three metals (Dupuis 2005). On the other hand, other elements such as Cu, Cr and Mn are used for only a limited amount of CNT growth (Vesselényi, et al. 2001).

The CNT diameter matches the catalyst size as observed by Cheung et al. (Cheung 2002). The catalyst does not necessarily need to be a nano particle, even a bulk metal can catalyze the CNT growth.

2.3.3.1.2. Thin Film Support Layer

Thin film support layer type may lead to different chemical or physical interactions between the catalyst metal and the supporting material. Additionally, the support layer have an important effect on mobility of catalyst nano particles (Dai 2002). Figure 2.12 shows that the catalyst orientation depending on the support layer differs during the growth process. It has been proven that the choice of underlayer is of critical importance for CNT growth.

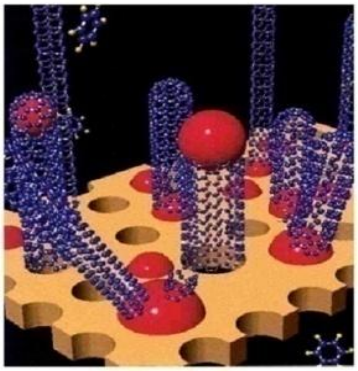

Figure 2.12. Schematic illustration of catalyst nano particles orientation
(Source: Dupuis 2005)

Quartz, silicon, silicon oxide (Zhang, et al. 2005), silica, alumina, alumina-silicate (zeolite), aluminium oxide (Hart and Slocum 2006, Hata, et al. 2004, Noda, et al. 2007), $CaCO_3$, magnesium oxide (Xiong, et al. 2005, Xiong, et al. 2006) are used as substrates in CVD. The most common buffer layers are silica (SiO_2) and alumina (Al_2O_3). Alumina materials are a better catalyst support layer than silica because of the fact that there is a stronger metal-support interaction in alumina materials. The thickness of the underlayer has been found to influence the CNT growth critically (Nessim 2010). Thin (thick) catalytic metal films break into smaller (larger) catalytic nano particles, which produce smaller (larger) CNTs, for this reason, thin catalytic metal films (~ 1 nm) are necessary to grow SWNTs, thicker metal films (for example 10 nm) are used for MWNT growth (Yamada, et al. 2006). CNTs have successfully been grown on insulating substrates by many scientific teams all over the world. In contrast to

insulating substrates, conductive layers have been used as an underlayer material by fewer teams in CNT growth (Nessim 2010).

2.3.3.1.3. Carbon Precursors

Most commonly used CNT precursors in CVD process are methane (CH_4) (Cassell, et al. 1999; Xiong, et al. 2005), ethylene (C_2H_4) (Futaba, et al. 2005, Futaba, et al. 2006, Hart and Slocum 2006, Hata, et al. 2004, Nessim, et al. 2008, Yamada, et al. 2006), acetylene (C_2H_2) (Patole, et al. 2008; Pint, et al. 2009a, Zhong, et al. 2009), benzene (C_6H_6) (Yang, et al. 2003) and carbon monoxide (CO) (Huang, et al. 2004). Each of them has a particular decomposition temperature, thereby resulting in a different CNT growth temperature.

There is a close relationship between the yield of CNTs and the injection time of the carbon source. The longer the injection time, the more molecules of hydrocarbon gases pass over the catalyst, with the result that the carbon yield of the deposits increases. Apart from the type of carbon precursor, its feed rate is also another important parameter for CNT growth. It is known that high feed rates can increase the growth rate. Cheung et al. explained that different carbon species can be produced with the same diameter catalyst nano particles using different flow rates of carbon precursor gas (Cheung 2002). When the flow rate of the carrier gas is higher, nano particles with larger diameter grow.

The reason why MWNT growth is easier than SWNT growth is that MWNT is possible to grow from most of the hydrocarbons, whereas SWNT grows from only selected hydrocarbons.

2.3.3.1.4. Temperature

CNTs are typically grown in a temperature range from 550 °C to 1000 °C (Moisala, et al. 2003). However, the reaction temperature may vary in terms of the catalyst-support material pair. In order to accelerate the catalytic decomposition of hydrocarbon molecules and to increase the diffusion rate of carbon in the metal particle, experiments are carried out with increased temperatures (Moisala, et al. 2003). Moreover, the temperature is a crucial agent in the pre-growth treatment of the catalyst.

2.4. Growth Mechanism of Carbon Nanotube

Two main growth models have been introduced for CNT growth whether the catalyst nano particles are at the tip of CNT or at the bottom side (Saito, et al. 1994). The former modelled by Hofmann et al. (Hofmann, et al. 2005) was called the tip-growth mechanism where the metal catalyst nano particle is lifted off from the support surface during the growth process owing to weak support-catalyst interaction (Moisala, et al. 2003, Nessim 2010). The latter is called base-growth mechanism which was modelled by Puretzky et al. (Puretzky, et al. 2005). In this growth, the catalyst particle stays in a pinned way at the support surface while the tube grows up, so that CNT nucleates and grows above the catalyst (Moisala, et al. 2003, Nessim 2010). For the base-growth mechanism, there is a strong interaction between the catalyst and substrate (Dresselhaus, et al. 2001). Figure 2.13 shows possible growth mechanisms of CNT explained by two groups.

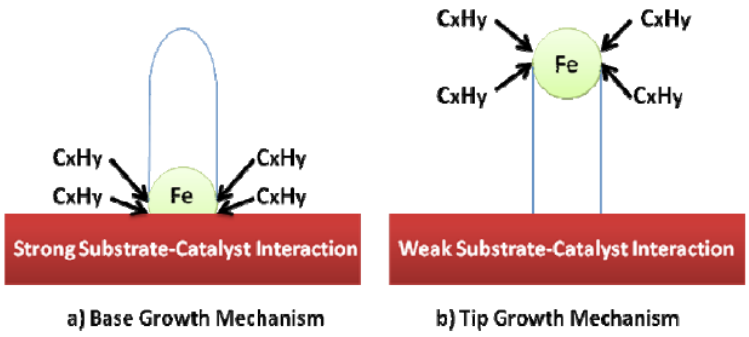

Figure 2.13. Schematic illustrations of CNT growth mechanisms a) Base-growth b) Tip-growth mechanism (Source: Ando, et al. 2004)

CHAPTER 3

OXIDIZERS

Although CNTs are of vital importance in terms of their unique properties in application areas today, their exact growth mechanism is not fully understood. It is commonly argued that mild oxidants (CO_2, O_2 and H_2O) play a significant role in CVD process. In this chapter, an extensive literature search done in order to investigate the growth mechanism and the role of oxidizers during CNT growth is given.

3.1. Importance of Oxidizers on Catalyst

Oxidizers keep catalyst particle functioning in the growth process by removing amorphous carbon coverage on them. Moreover, they can etch away amorphous carbon on the outer walls of CNTs. Hence, they keep catalyst particle functioning for a longer time during the growth and consequently increase the length, yield and quality of CNTs. They can also be utilized to control the size of catalyst particle during pretreatment time. The purpose of this study was to understand the role played by oxidizers during both pretreatment and growth time in the control of catalyst size, which consequently lead to the control of CNT diameters.

3.2. Literature Search

The CVD concept was expanded by the addition of a growth enhancer into the growth ambient of normal hydrocarbon CVD. As a result of the second ingredient, the growth efficiency increased to unprecedented levels (Hata, et al. 2004).

It is generally believed that water vapor cleans and reactivates the catalysts by removing amorphous carbon coverage, and as a result of this reactivation, it was seen that catalyst activity increased in a direct way (Yamada, et al. 2008, Hasegawa and Noda 2011a, Huang, et al. 2009), using water vapor can promote the synthesis of CNT forests, prolongs the catalyst particle lifetime, prevents the sintering of iron particles

(Amama, et al. 2009, Hata, et al. 2004, Yamada, et al. 2008), and also modulates both the morphology of the forest and the structure of the CNTs grown (Huang, et al. 2009). Consequently, the water-assisted method is called as 'Super Growth CVD Process'. SWNTs with good properties, such as high purity, long length and alignment can be grown by this process (Futaba, et al. 2009).

To understand how water modifies the diameter distribution of SWNTs, two aspects may be considered; the interaction between water and the growing CNTs, and the interaction between water and catalyst particle (Hu, et al. 2010).

There are two different views about the functional role of water for CNT growth. The first one proposed by Hata and co-workers (Hata, et al. 2004). In that opinion, CNT growth using CVD method can be dramatically enhanced by introducing small amount of water together with the carbon source. Moreover, there is a clear indication that water works as a protecting agent to extend the catalyst lifetime by etching the amorphous carbon deposit on the surface of the catalyst resulting in keeping the catalyst active during CNT growth. The other one was suggested by Amama et al. (Amama, et al. 2009). According to this view, CNT synthesis becoming more passive with Ostwald ripening can be reduced by surface hydroxylation of alumina support by means of water vapor. In Ostwald ripening, large particles are more preferred than small particles because of vertical fraction surface energy and in the end, more atoms are adsorbed from small particles (Wynblatt 1975), therefore, small catalyst particles disappears by atomic interdiffusion and the large ones get larger and less efficient (Hasegawa and Noda 2011b). Ultimately, if many more catalyst particles disappear, surface number density decreases, distribution range broadens and mean size shifts bigger values. If this event happens during CNT growth, it is very likely that it stops the growth. In parallel to this view, Hasegawa et al. showed that the number density of medium-sized particles decreased while that of both smaller and larger particles increased, thus the structural change was caused by Ostwald ripening (Hasegawa and Noda 2011b). Kim et al. also directly observed the Ostwald ripening behavior in two nearby Fe catalyst after the termination of MWNT growth and they found that a combination of both Ostwald ripening and subsequent subsurface diffusion caused loss of the Fe catalyst (Kim, et al. 2010). For a milimeter-tall SWNT forest, both Ostwald ripening of catalyst particles and growth termination of individual SWNTs through carbon byproduct formation on catalyst particles must be prevented and the rapid growth rate must be maintained (Hasegawa and Noda 2011b). In addition to these

different views, Futaba et al. put forward that highly efficient growth can be achieved not only using water but also other growth enhancers (alcohols, ethers, esters, ketones, aldehydes, and even CO_2) (Futaba, et al. 2009). Their extensive investigations showed two essential ingredients in the growth ambient: i) a growth enhancer containing oxygen and ii) a carbon source that does not contain oxygen (Futaba, et al. 2009).

Different levels of water had a significant effect on the catalyst lifetime: the reason of a drastic decrease in the catalyst lifetime is that even a small amount of water vapor in the reaction mixture can change the CNT growth kinetics (In, et al. 2011). When water is flown with the carbon source, during CVD growth process, the efficiency of the catalyst has been grown in a few minutes (Smajda, et al. 2009). However, the experiments of Hasegawa et al. showed that water addition stabilizes the growth of millimeter-tall SWNTs for various conditions. On the other hand, water addition disturbed SWNT growth using a thinner catalyst layer (Hasegawa and Noda 2011a) .

When compared to the SWNTs grown without water vapor, the intensities of large-diameter CNTs relative to small-diameter CNTs decrased by adding water from the beginning of CVD growth process in a few minutes (Hu, et al. 2010).

Although the growth mechanism and the role of water in CVD growth are still under debate, it has been accepted that a small amount of water leads to an enhancement in both growth height and nucleation density (Pint, et al. 2009b). Nonetheless, sudden decreases may occur in the growth characteristics as the optimum water level is exceeded resulting in the fact that both catalysts and CNTs are oxidized (Futaba, et al. 2005), the defect of CNTs increases (Liu, et al. 2010), the walls of SWNTs are damaged (Hasegawa and Noda 2011a).

No enhancing effects were observed when ammonia (NH_3) was selected as a growth enhancer. This result demonstrated that the fundamental requirement of the growth enhancer is to contain oxygen (Futaba, et al. 2009).

When compared with water; CO_2, a good weak oxidant, can be more easily controlled, and also promotes the growth of CNTs (Wen, et al. 2007). By introducing large amounts of CO_2 (to 30.4 mol %), clean and bare CNTs on the top surface of CNT forests can be formed, the wall numbers of CNTs can be decreased gradually, the diameter of CNTs can also be smaller, and the carbonaceous impurities can be eliminated (Huang, et al. 2009). In spite of large amounts of CO_2, Pint et al. pointed out

that the small amounts of CO_2 in the reaction gas mixture caused a significant enhancement of the CNT growth height (Pint, et al. 2009b).

As it was explained by Huang et al., the morphological variation due to increasing amounts of CO_2 is related to the change of CNT growth velocity and change of bonding force between CNT and support (Huang, et al. 2009).

Futaba et al. obtained vertically aligned CNT forests by using both acetone and CO_2 as growth enhancer with ethylene as a carbon source whereas forest growth from ethylene alone was very limited (Futaba, et al. 2009).

Although it was a previous common belief which the CNTs grown with water vapor had less defects, the Raman spectrum analysis has been shown that the SWNTs grown by adding water have the larger D-band intensity than those without water, as a result of which, the G/D peak ratio decreases (Hasegawa and Noda 2011a). Similarly, the decreasing of the G/D intensity ratio during the array growth has indicated the increasing concentration of amorphous carbon near the catalyst surface species (Stadermann, et al. 2009).

CHAPTER 4

EXPERIMENTAL PROCESS

This chapter involves experimental details about the thesis work and consists of three main parts. In the first part, the catalyst film deposition process by DC magnetron sputtering is discussed. The second part deals with the thermal CVD process in detail. The third part gives details of the characterization techniques of grown CNTs which are SEM, AFM and Raman Spectroscopy.

4.1. Catalyst Film Deposition by DC Magnetron Sputtering Process

In this work, deposition of very thin Fe catalyst film onto the $Al_2O_3/SiO_2/Si$ substrates was carried out by utilizing the DC magnetron sputtering method, which was the most popular technique used to fabricate the thin film materials from the point of good surface uniformity, growth on substrates, and its cost effectiveness. For this current work, AJA ATC Orion 5 UHV sputtering system was used (Figure 4.1).

(100) Si wafers with 2-inch diameter and a typical resistivity of 1-20 ohm-cm purchased to be used as support layer were cleaned chemically in methanol for 15 min in an ultrasonic bath and rinsed with ultra-pure water for 15 min prior to growth. The commercial silicon films were first oxidized by dry thermal oxidation system. 10-15 nm thick alumina (Al_2O_3-barrier) and than 0.5-3 nm thick iron (Fe catalyst) layers were deposited on a silicon dioxide (SiO_2) wafer by DC magnetron sputtering. At the end of this process, $Fe/Al_2O_3/SiO_2/Si$ substrates were ready for growing CNTs on them.

The magnetron sputtering process depended on the movement of electrons and ions in a magnetic field and the generation of ion-induced secondary electrons at the target takes place in an evacuated chamber. The chamber pressure was evacuated to a pressure of 10^{-6} Torr by means of turbomolecular pump and depositions were performed at a rate of 0.1 A^o/s and 20 W at a growth pressure of 0.5 mTorr under Ar ambient. This system was controlled by a computer.

Figure 4.1. The Magnetron Sputtering System in Physics Department, IYTE

In the basic sputtering process, a target (or cathode) plate is bombarded by energetic ions, so that collisions of ions with the target material remove electrons from the target. At the same time, secondary electrons are also emitted from the target surface. Magnetrons are utilized in the sputtering process to control the path of the displaced atoms which fly randomly around the vacuum chamber. As a consequence of the increased ionization efficiency of a magnetron resulting in a dense plasma in the target region, ion bombardment of the target is increased and sputtering rates become higher (Kelly and Arnell 2000).

4.2. Thermal Chemical Vapor Deposition Process

Thermal chemical vapor deposition (TCVD) apparatus used in this work was composed of a horizontally mounted quartz tube with outer diameter of 2.54 cm and length of 60 cm, equipped with various gas lines and mass flow controllers and an oven (Lindberg/Blue TF55035C Split Mini tube Furnace) (Figure 4.2). Because of the fact that melting point of quartz was higher than the experiment temperature performed, both quartz tube and quartz boat were used. The quartz boat and some Si-substrates with thin films grown on them used in CNT growth are displayed in Figure 4.3.

Figure 4.2. The TCVD System at CNL Lab at Physics Department, IYTE

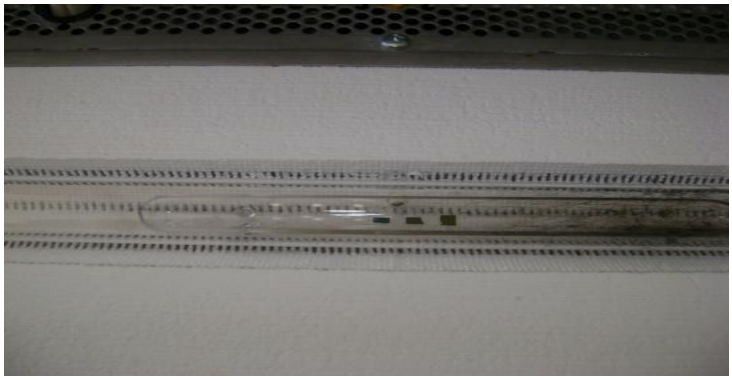

Figure 4.3. Some thin films used for CNT growth in the quartz boat

In the process, there is a matter not to be forgotten that the quartz boat and the samples placed are located in the middle of the furnace where a thermocouple is situated. Though the furnace temperature can reach to 1100 ^{o}C, the experiments were carried out at 750 ^{o}C, 760 ^{o}C and 770 ^{o}C in the work of the thesis. All CNT growth experiments were performed at atmospheric pressure.

The CVD process consisted of the following sequential steps: As a first step, before the CNT growth, argon, whose purpose was to remove the contamination before and after the CNT growth process and to prevent the oxidation of samples, flew through

the tube as the carrier gas. Second, prepared catalyst films (supported on a Si wafer) were placed in the quartz boat, and placed is in the furnace. After heating the furnace to the desired growth temperature, both etching gas (H_2) and oxidizer were started to be sent to do preannealing and form catalyst nano particles. Both H_2 and the oxidizer provided the reduction from metal oxide catalyst to metal catalyst. CO_2 was used as an oxidizer during all experiments. When the pretreatment time finished, CNT growth started with C_2H_4 flow through the tube for a predetermined time. When the growth time finished, firstly the hydrocarbon gas was turned off and then both the hydrogen gas and oxidizer were turned off. The temperature was set to 0 ^oC and the system was left for cooling in Ar gas environment.

Different gas flow rates and amount of oxidizer were investigated in this work. The flow rates of Ar, H_2, C_2H_4 (150 sccm, 140 sccm, 80 sccm) were constant during all experiments. In addition growth time was also another parameter for growing CNT, so the growth time was chosen as 15 minutes for all of the experiments in this study.

4.2.1. Growth with Oxidizers

The main parameters studied in the experiments carried out in presence of CO_2 were pretreatment time, oxidizer gas flows, sending moment and duration of oxidizer and rates of oxidizer in pretreatment and growth processes. As well as these main parameters, different growth temperatures were also tried to determine the optimum temperature value in presence of CO_2 as shown in Table 4.1.

Table 4.1. Studied parameters in the CNT growth with the oxidizing gas CO_2 during growth time; Pressure: 1 atm., Ar: 150 sccm, H_2: 140 sccm (sccm= standart cm^3/min.)

Sample Name	T (^oC)	Pretreatment				CNT growth		
		CO_2 (sccm)	H_2 (min.)	CO_2 (min.)	Time (min.)	C_2H_4 (sccm)	CO_2 (sccm)	Time (min.)
FeAlO9CNT762	760	10	15	10	15	80	2	15
FeAlO12CNT764	760	10	15	10	15	80	2	15
FeAlO15CNT766	760	10	15	10	15	80	2	15
FeAlO5CNT767	760	10	15	5	15	80	2	15
FeAlO9CNT768	760	10	15	5	15	80	2	15
FeAlO10CNT769	760	10	15	5	15	80	2	15
FeAlO12CNT770	760	10	15	5	15	80	2	15
FeAlO12CNT771	760	10	15	5	15	80	2	15
FeAlO14CNT772	760	10	15	5	15	80	2	15
FeAlO15CNT773	760	10	15	5	15	80	2	15
FeAlO12CNT777	760	8	15	10	15	80	2	15
FeAlO15CNT779	760	8	15	10	15	80	2	15
FeAlO9CNT780	760	8	15	5	15	80	2	15
FeAlO12CNT781	760	8	15	5	15	80	2	15
FeAlO14CNT782	760	8	15	5	15	80	2	15
FeAlO15CNT783	760	8	15	5	15	80	2	15
FeAlO12CNT785	750	8	15	5	15	80	2	15
FeAlO15CNT787	750	8	15	5	15	80	2	15
FeAlO12CNT789	770	8	15	5	15	80	2	15
FeAlO14CNT790	770	8	15	5	15	80	2	15
FeAlO15CNT791	770	8	15	5	15	80	2	15
FeAlO9CNT792	770	10	15	5	15	80	2	15
FeAlO12CNT793	770	10	15	5	15	80	2	15
FeAlO15CNT795	770	10	15	5	15	80	2	15
FeAlO12CNT799	760	10	15	10	15	80	2	15
FeAlO14CNT800	760	10	15	10	15	80	2	15
FeAlO15CNT801	760	10	15	10	15	80	2	15
FeAlO12CNT832	760	10	15	5	15	80	4	15
FeAlO15CNT834	760	10	15	5	15	80	4	15
FeAlO12CNT835	760	8	15	5	15	80	4	15
FeAlO14CNT836	760	8	15	5	15	80	4	15
FeAlO15CNT837	760	8	15	5	15	80	4	15
FeAlO12CNT838	750	10	15	5	15	80	2	15
FeAlO14CNT839	750	10	15	5	15	80	2	15

(cont. on next page)

Table 4.1 (cont.)

FeAlO15CNT840	750	10	15	5	15	80	2	15
FeAlO12CNT844	750	8	15	10	15	80	2	15
FeAlO14CNT845	750	8	15	10	15	80	2	15
FeAlO15CNT846	750	8	15	10	15	80	2	15
FeAlO12CNT850	760	8	15	5	15	80	6	15
FeAlO14CNT851	760	8	15	5	15	80	6	15
FeAlO15CNT852	760	8	15	5	15	80	6	15
FeAlO12CNT853	750	10	15	5	15	80	8	15
FeAlO14CNT854	750	10	15	5	15	80	8	15
FeAlO15CNT855	750	10	15	5	15	80	8	15
FeAlO12CNT856	760	10	15	5	15	80	8	15
FeAlO14CNT857	760	10	15	5	15	80	8	15
FeAlO15CNT858	760	10	15	5	15	80	8	15
FeAlO12CNT859	770	10	15	5	15	80	8	15
FeAlO14CNT860	770	10	15	5	15	80	8	15
FeAlO15CNT861	770	10	15	5	15	80	8	15
FeAlO16CNT862	760	8	15	5	15	80	6	15
FeAlO16CNT863	760	8	15	5	15	80	6	15
FeAlO12CNT864	760	10	15	10	15	80	8	15
FeAlO16CNT865	760	10	15	10	15	80	8	15
FeAlO16CNT866	760	8	15	10	15	80	8	15
FeAlO17CNT867	760	8	15	10	15	80	8	15
FeAlO17CNT868	760	8	15	10	15	80	8	15
FeAlO16CNT869	760	10	15	5	15	80	10	15
FeAlO17CNT870	760	10	15	5	15	80	10	15
FeAlO16CNT871	750	10	15	5	15	80	10	15
FeAlO17CNT872	750	10	15	5	15	80	10	15
FeAlO16CNT873	760	10	15	10	15	80	10	15
FeAlO17CNT874	760	10	15	10	15	80	10	15
FeAlO16CNT899	770	8	15	10	15	80	2	15
FeAlO17CNT900	770	8	15	10	15	80	2	15
FeAlO18CNT901	770	8	15	10	15	80	2	15
FeAlO16CNT911	750	10	15	10	15	80	2	15
FeAlO17CNT912	750	10	15	10	15	80	2	15
FeAlO18CNT913	750	10	15	10	15	80	2	15
FeAlO16CNT918	770	10	15	10	15	80	2	15
FeAlO17CNT919	770	10	15	10	15	80	2	15
FeAlO16CNT921	750	10	15	10	15	80	8	15
FeAlO17CNT922	750	10	15	10	15	80	8	15
FeAlO14CNT923	770	10	15	10	15	80	8	15

(cont. on next page)

Table 4.1 (cont.)

FeAlO16CNT924	770	10	15	10	15	80	8	15
FeAlO17CNT925	770	10	15	10	15	80	8	15
FeAlO16CNT926	750	10	15	10	15	80	10	15
FeAlO17CNT927	750	10	15	10	15	80	10	15
FeAlO18CNT928	750	10	15	10	15	80	10	15
FeAlO16CNT929	770	10	15	10	15	80	10	15
FeAlO18CNT931	770	10	15	10	15	80	10	15
FeAlO14CNT932	770	10	15	5	15	80	10	15
FeAlO16CNT933	770	10	15	5	15	80	10	15
FeAlO17CNT934	770	10	15	5	15	80	10	15
FeAlO18CNT935	770	10	15	5	15	80	10	15
FeAlO16CNT936	760	10	15	10	15	80	4	15
FeAlO17CNT937	760	10	15	10	15	80	4	15
FeAlO18CNT938	760	10	15	10	15	80	4	15
FeAlO16CNT939	760	8	15	10	15	80	4	15
FeAlO17CNT940	760	8	15	10	15	80	4	15
FeAlO16CNT941	760	8	15	10	15	80	6	15
FeAlO17CNT942	760	8	15	10	15	80	6	15
FeAlO18CNT943	760	8	15	10	15	80	6	15

4.3. Characterization Techniques

Characterization of the chemical and physical properties of CNTs is crucial in terms of qualifying them. In this study, different characterization techniques were used to examine the samples after pretreatment and growth. For catalyst characterization, AFM and EDX were used. In addition, CNT samples were analyzed with SEM, STEM and Raman Spectroscopy.

4.3.1. Scanning Electron Microscopy

Scanning Electron Microscopy (SEM) is one of the main methods to characterize CNTs in that it is the simplest technique with wider availability. Both CNT powder samples and individual tubes on a bulk substrate, Si wafer, can be observed by SEM (Jorio, et al. 2008). Although SEM gives information about morphology, dimensions, densities and orientations of CNTs (Thess, et al. 1996), it can only measure

their diameter roughly. The walls of SWNT and MWNTs cannot be examined with SEM because of the fact that its resolution is restricted (Jorio, et al. 2008).

As for its working principle, SEM images the sample morphology by scanning the surface with a high energy beam of electrons instead of light. When the beam of electrons strikes the surface of the specimen, the interaction occurs between the atoms of the sample and the electrons, then several signals in the form of secondary electrons (SE), back scattered electrons (BSE) and characteristic X-rays containing information about the surface topography and composition of the samples can be detected (Joshi 2008). Back scattered electrons coming from the flat and polished sample provides contrast, so that they give the elemental composition of the sample depending on the composition and orientation between the electron beam and surface.

SEM pictures were taken with Quanta FEG 250, at IYTE for this thesis work. In addition, energy dispersive X-ray (EDX) analyses were also used to analyze near surface (about 2 microns in depth) elements and estimate their proportion at different position by Oxford Aztec X-Act detector. Furthermore, scanning transmission electron microscopy detector (STEM) providing a complementary method for image acquisition of the transmitted electrons was utilized.

4.3.2. Atomic Force Microscopy

It is known that the diameters of CNTs are directly related to the diameters of catalyst nanoparticles. Because of the low resolution of SEM, AFM (Atomic Force Microscopy) was used to determine the catalyst particles and measure their diameters roughly. AFM is a relatively compact instrument providing a 3D profile with very high resolution of thin films (topography) on a nanoscale by measuring the forces between the probe and surface at very short distance (0.2-10 nm probe-sample separation). The AFM probe has a very sharp tip, often less than 100 Å diameter to obtain information about the surface of the sample. AFM consists of a sharp tip, a cantilever, piezoelectric scanner, photodiode, detector and feedback electronics.

The basic operation mode is common to all the scanning probe techniques: a very sharp tip is attached to a cantilever spring moving over a sample surface. When the

tip is moved near the surface, Van der Waals, electrostatic, frictional or magnetic forces can occur among them.

According to the applications, AFM can be performed in three modes: tapping mode, contact mode and non-contact mode. The tapping mode is generally preferable in that it does not touch the sample surface and not damage the surface. Additionally, it allows high resolution of samples that are easily damaged and/or loosely held to a surface. In the contact mode, the interaction between the tip and the surface atoms gives rise to removing the atoms from their places and scratch the surface of the material although it supplies fast scanning. In view of the fact that the non-contact mode generally gives lower resolution, it is not usually used.

The AFM utilized for analyzing the catalyst particles in this work was Digital Instruments-MMSPM Nanoscope IV, IYTE.

4.3.3. Raman Spectroscopy

Raman Spectroscopy is a spectroscopic technique to study vibrational, rotational, and other low frequency modes in a system. Since CNTs have distinctive Raman spectra, Raman spectroscopy is used in qualitative and quantitative analysis of CNTs including their type and structure of them as well as the diameter distribution of CNT bundles (Zhao and Wagner 2004).

For this work, Raman spectra of CNTs grown were collected with a Raman spectrometer at IYTE with a 488 nm wavelength laser (Figure 4.4).

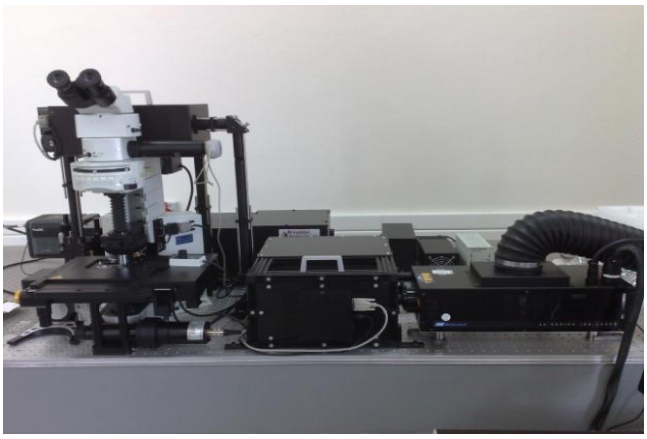

Figure 4.4. The Raman Spectroscopy in Physics Department, IYTE

The principle of Raman spectroscopy depends upon an inelastic scattering, or Raman scattering of monochromatic laser light. When the molecule under excitation radiation is excited from the ground state to a virtual state and followed by relaxation to a vibrational level by emitting a photon, a difference in energy between the original state and this new state which brings about a shift in the frequency of the emitted photon away from the excitation wavelength occurs. This is the Raman effect which is a form of light scattering. When the spontaneous Raman effect considered, if the molecule is already in an elevated vibrational energy state, the Raman scattering is called anti-stokes Raman scattering. However, in stokes Raman scattering, the molecule will be excited from the ground state to a virtual state.

The characteristic Raman spectrum of SWNT includes three main zones (Figure 4.5). These zones are at low (100-250 cm^{-1}), intermediate (300-1300 cm^{-1}) and high (1500-1620 cm^{-1}) frequencies (Journet and Bernier 1998).

There are two main first order peaks for carbon-based materials. The first one, which is due to amorphous carbon, is the disorder-induced, which is called D peak. It is observed around 1300 cm^{-1} for excitation He-Ne laser, or at 1350 cm^{-1} for an Ar^{+} ion laser. The D band reveals the presence of defects. D line resonance is effected by the electronic nature of the tubes (Dresselhaus, et al. 2002). It has also been shown that the D line and its second harmonic, the G line, vary both in value and amplitude with laser excitation frequency (Matthews, et al. 1999). The other one is the tangential G peak and observed at about 1580 cm^{-1}, which originates from the C=C stretching mode in graphene, an optical phonon mode.

There might be several reasons for the existence of the strong D band peak (Li, et al. 1997, Xiea, et al. 1999). The first one is a presence of highly compacted arrays. The other one is the relatively low crystallization degree of the CNT arrays along with turbostratic structures formed in some carbon sheets. The deposition rate and the growth time along with the carbon concentration of the carbon precursor are of vital importance for reducing the D band (Shanov, et al. 2006).

For SWNTs, the G mode can be decomposed in one main peak with a shoulder (Dresselhaus, et al. 2002). As it is shown in Figure 4.5, the G peak is doubly split into higher and lower sides of the 1582 cm^{-1} line, G^{+} (frequency) and G^{-} (frequency). The differences between the G band spectra for metallic and semiconducting CNT give significant information about SWNT. G^{-} component at lower frequencies determines metallic character of the CNT, G^{+} component at higher frequencies determines their

semiconductor behavior (Dresselhaus, et al. 2002). In semiconducting tube bundles the frequency of G^+ line is determined by bundle size. For semiconducting SWNT in bundles, the linewidths are determined by the intertube interactions and the diameter distribution. In metallic tubes, the G^- line feature is broadened. This broadening is related to the presence of free electrons in nanotubes with metallic character.

The ratio of the D-band to G-band intensity, I_D/I_G, is used as a measure of the defect density of a particular CNT and can provide information on the crystalline quality of the CNTs. A small I_D/I_G ratio suggests reasonable crystalline quality and a perfect graphite structure. In other words, if there is a high ratio between the G band and D band peak intensities, it shows that the CNTs are of high purity (Dresselhaus, et al. 2002).

In the lower frequency region, the spectrum is dominated by the in-phase mode known as the radial breathing mode (RBM) appearing between 120 cm^{-1} and 250 cm^{-1} for SWNT. The RBM also provides information on chirality and thus the electronic properties of CNTs (Thess, et al. 1996). The RBM frequency is associated with the symmetric movement of carbon atoms in the radial direction (Figure 4.6). The RBM frequency is inversely proportional to the reciprocal diameter of the SWNT with the relationship below (Jorio, et al. 2003).

$$W(cm^{-1})=224(cm^{-1})/d_t(nm) \quad (4.1)$$

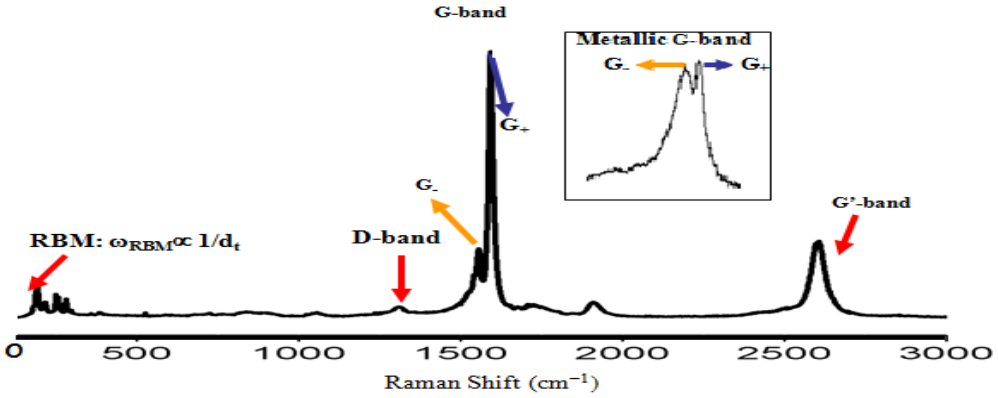

Figure 4.5. Raman spectra showing the main peaks of SWNTs
(Source: Dresselhaus, et al. 2002)

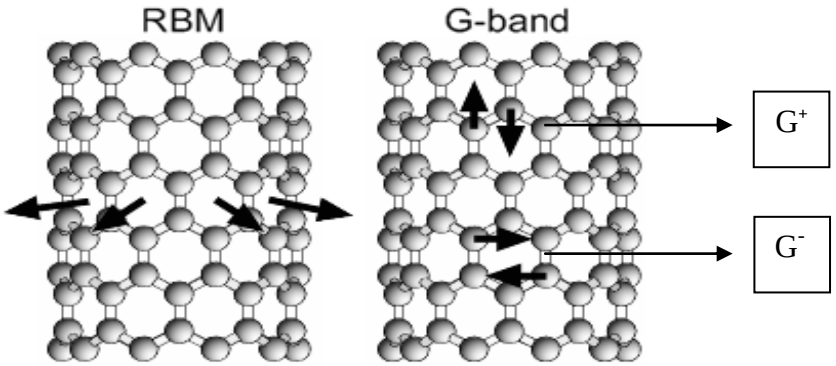

Figure 4.6. Schematic picture showing the atomic vibrations for a) the RBM and b) the G band modes (Source: Jorio, et al. 2003)

CHAPTER 5

RESULTS AND DISCUSSION

This chapter focuses on the results and discussions of the experiments. The first section of this chapter focuses on catalyst characterization by using the results of AFM and SEM. In the second section of the chapter, growth results are analyzed to determine for optimal parameters for CNT growth. Different parameters were studied for the purpose of the optimal growth conditions. In this section, the effects of temperature on the CNT growth, CNT formations at different CO_2 flow rates and different pretreatment times are analyzed, respectively. For CNT characterization discussions, SEM, STEM and Raman Spectroscopy techniques were utilized. The third section of the chapter includes analyzing the dependence of mean diameters of all samples on pretreatment duration and CO_2 flow rates. To draw conclusion, an extensive statistical analysis of all samples are given in the last section.

5.1. Catalyst Characterization

Catalyst material is an important parameter for CNT growth process. The diameter of a CNT is directly proportional to the size of nano particles. As explained before, only transition metals give better results for effective CNT growth as a catalytic material, and Fe, Co, Ni are the most common ones. In this thesis, Fe catalyst material was utilized. The following AFM and SEM analyses give information about the catalyst obtained and used for CNT growth in this study.

5.1.1. AFM Results

There exists a positive correlation between the diameters of CNTs and the sizes of catalyst nano particles. To determine the sizes of catalyst particles, Fe catalyst thin films were deposited on $Al_2O_3/SiO_2/Si$ substrates. CNT growth was not performed onto these substrates since the purpose was to analyze the catalyst particles prior to growth. However, the growth gases (except C containing C_2H_4) were used since they would continually be exposed to them during growth. CO_2 was also utilized in these pretreatments with various amounts and duration analyzed with the AFM. Table 5.1 shows the growth parameters and the heights of catalyst nano particles. The morphology of catalysts revealed by AFM is given in Figure 5.1 and Figure 5.2.

Table 5.1. Growth parameters of Fe catalyst nano particles;
Pressure: 1 atm, Ar: 150 sccm

Sample Name	T (^oC)	Pretreatment				Growth			Height (nm)
		H_2		CO_2		C_2H_4	CO_2		
		(sccm)	(min.)	(sccm)	(min.)	(sccm)	(sccm)	(min.)	
FeAlO16 CNT891	750	140	15	8	5	-	2	15	2.2
FeAlO16 CNT880	760	140	15	8	5	-	2	15	2.0
FeAlO16 CNT888	770	140	15	8	5	-	2	15	4.8
FeAlO17 CNT906	750	140	15	10	5	-	10	15	5.3
FeAlO17 CNT915	760	140	15	10	5	-	10	15	2.6
FeAlO17 CNT947	770	140	15	10	5	-	10	15	6.7

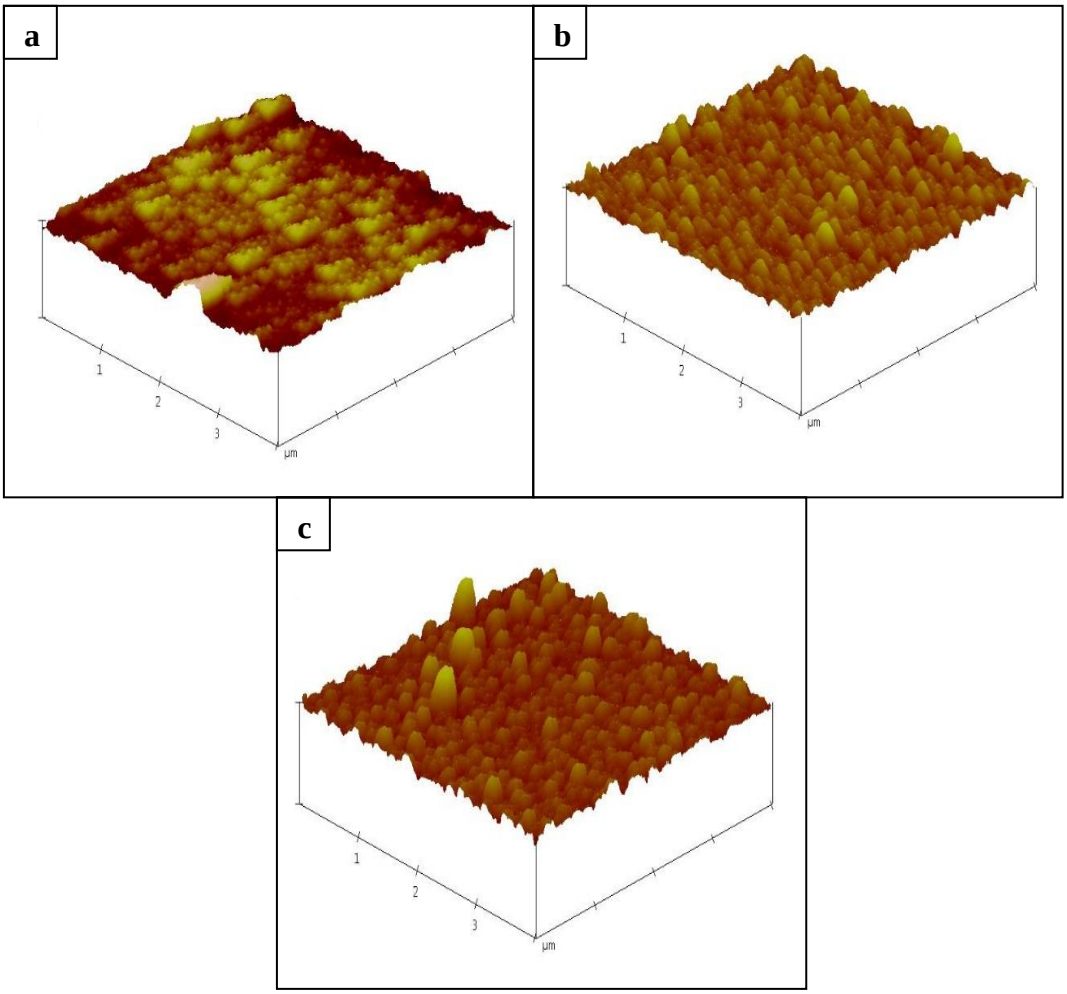

Figure 5.1. AFM micrographs of a) FeAlO16 CNT891 at 750 °C, b) FeAlO16 CNT880 at 760 °C, c) FeAlO16 CNT888 at 770 °C

AFM images in Figure 5.1 illustrate that Fe nano particles are not exactly occurred at 750 ^{o}C, the lighter parts on Fe surface show the catalyst nano particles and they do not have a smooth shape. Unlike the Fe particles at 750 ^{o}C, the orientation of the particles is clearly seen with the smooth shape at 760 ^{o}C and 770 ^{o}C. There are not any big particles for the nano particle at 760 ^{o}C although there are only a few particles for the Fe nano particles at 770 ^{o}C. The temperature increasing from 750 ^{o}C to 760 ^{o}C decreases the height of the catalyst nano particles. Further 10 ^{o}C raise in temperature from 760 ^{o}C to 770 ^{o}C results in increasing the height of them.

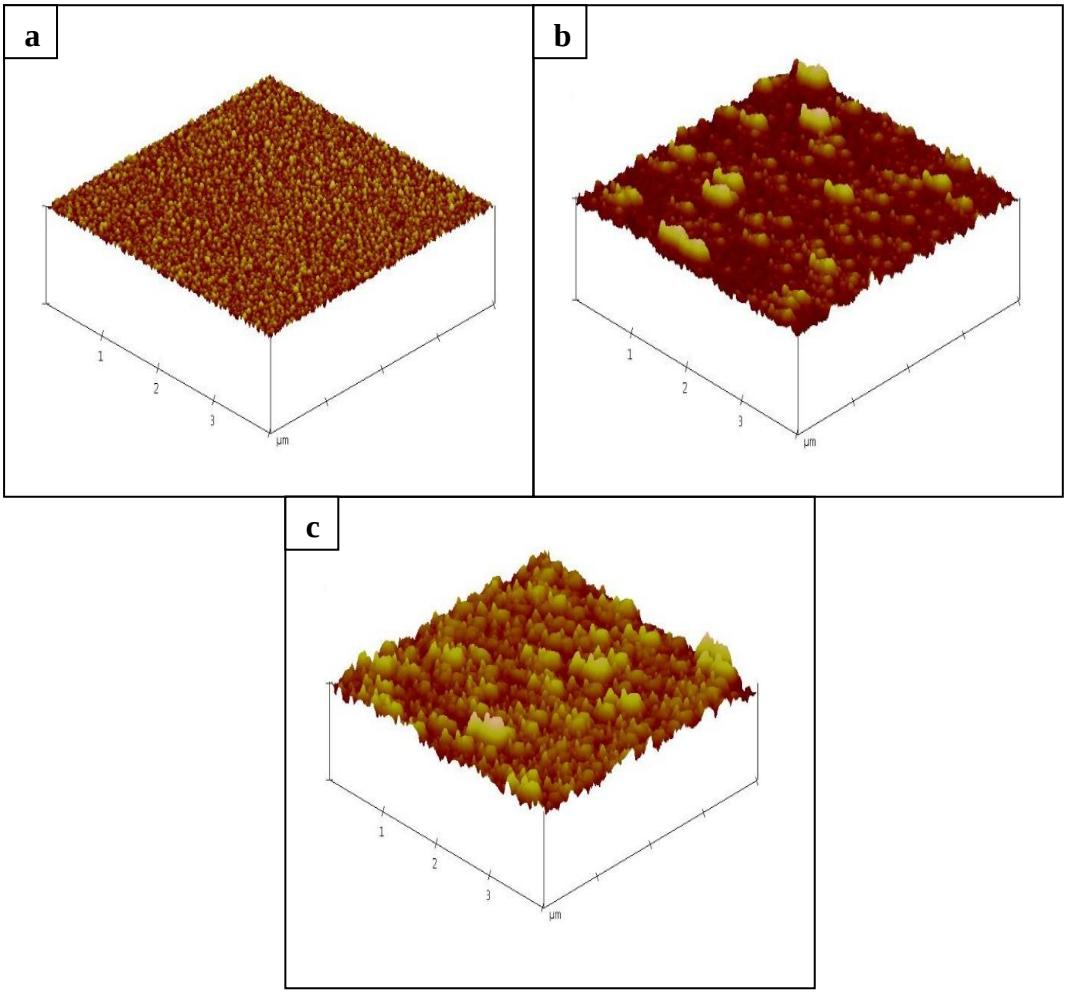

Figure 5.2. AFM micrographs of a) FeAlO17 CNT906 at 750 °C, b) FeAlO17 CNT915 at 760 °C, c) FeAlO17 CNT947 at 770 °C

For FeAlO17 substrate, the catalyst nano particles can be seen in AFM images in Figure 5.2. When the differences of three temperatures are compared, it can be seen that the size of the catalyst particles increases and the number of them decreases with the increased temperature. The height of the samples decreased from 5.3 nm at 750 ^{o}C to 2.6 nm at 760 ^{o}C and then increased to 6.7 nm at 770 ^{o}C.

When Figure 5.1 and Figure 5.2 are analyzed, it can be concluded that temperature plays a significant role on the sizes of catalyst particles. The catalyst morphology changes with the temperature.

5.1.2. EDX Results

In this section, three SEM pictures of Fe catalyst thin films deposited on $Al_2O_3/SiO_2/Si$ taken with EDX detector in order to analyze near surface elements and their proportion at different position are given below (Figure 5.3).

a

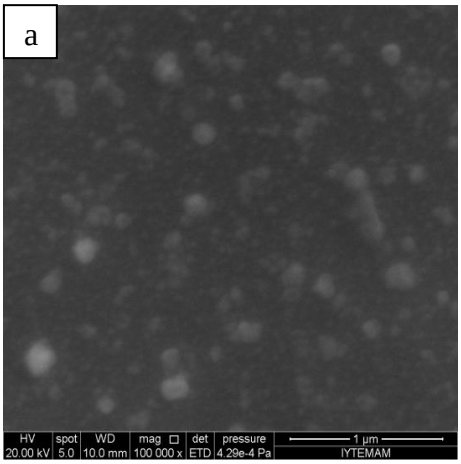

Element	Wt %	Atomic %
C	2.9	2.77
O	54.02	66.53
Al	0.07	0.05
Si	1.09	0.38
Fe	43.12	30.25
Total	100.00	100.00

b

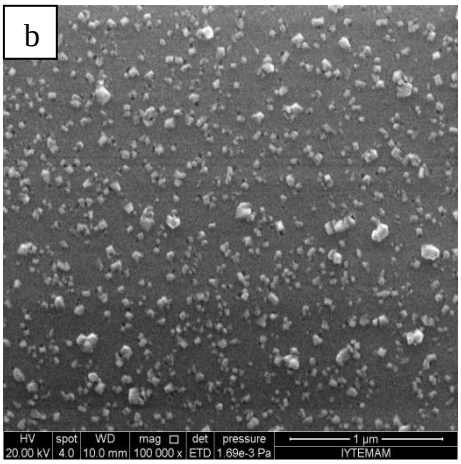

Element	Wt %	Atomic %
C	7.76	13.49
O	48.59	63.47
Al	0.13	0.10
Si	17.99	13.39
Fe	25.53	9.55
Total	100.00	100.00

Figure 5.3. SEM micrographs of nano particles a) FeAlO16 CNT885 at 770 ºC, $CO_2(p)/CO_2(g)$: 10/10, 5 min., b) FeAlO17 CNT915 at 760 ºC, $CO_2(p)/CO_2(g)$: 10/10, 5 min., c) FeAlO17 CNT894 at 770 ºC, $CO_2(p)/CO_2(g)$: 8/2, 10 min.

(cont. on next page)

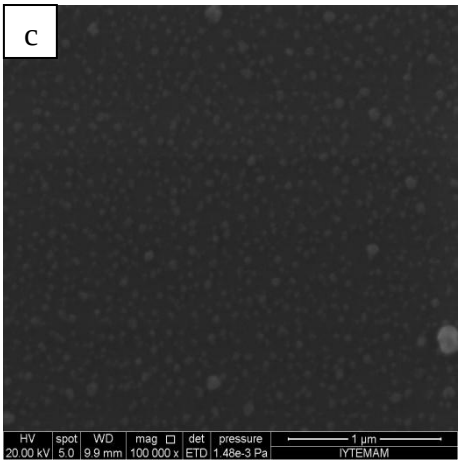

Element	Wt %	Atomic %
C	2.14	3.67
O	50.79	65.40
Al	0.43	0.33
Si	36.76	26.96
Fe	9.88	3.64
Total	100.00	100.00

Figure 5.3. (cont.)

The signals are transmitted from substrate and environment during the EDX measurements intensively. Although the quantitative values are not considered, it is possible to see from the data analysis that the direct relation between the C amount and CNT surface density has been determined. The signals taken from the materials are Si: from Si substrate and SiO_2 buffer; O_2: from Al_2O_3 and SiO_2 buffer; Al: from Al_2O_3 buffer, C: from contamination either from growth chamber contamination from the previous CNT growth or from exposure to air, CO_2, CO or oil from finger prints.

5.2. CNT Characterization

5.2.1. SEM Results

Several parameters including growth temperature, pretreatment time, amount of oxidizers, the ratio of oxidizer in pretreatment to that of in growth were important for the effective CNT growth. In order to obtain the average diameters and related diameter distributions, the SEM images of CNTs grown with different growth parameters were evaluated.

In this study, all parameters mentioned in previous paragraph, were tried in nearly one hundred experiments to obtain high quality of CNTs. For this work, ethylene (C_2H_4) showing a good harmony with Fe catalyst under proper conditions, was used as

the carbon source. CO_2 with different amounts was utilized as the catalyst enhancer and preserver. H_2 used as the carrier gas provided reduction of Fe catalyst particles and preventing amorphous carbon formation at growth. In addition, growth conditions were Ar: 150 sccm, H_2: 140 sccm, C_2H_4: 80sccm (sccm=standart cm^3/min.). All CNTs were grown in both CO_2 and H_2 environment to transform the catalyst in the metal-oxide form to elemental form by removing the oxide with the help of H_2. The mean diameters of each growth conditions are given in Table 5.2.

Table 5.2. Growth conditions and the mean diameters of CNTs obtained as a result

Sample Name	T(^{o}C)	Pretreatment(min.) H_2/CO_2		CO_2(p)/CO_2(g) (sccm)	Mean Diameter (nm)
FeAlO12CNT785	750	15	5	8/2	8.8
FeAlO15CNT787	750	15	5	8/2	8.2
FeAlO12CNT844	750	15	10	8/2	8.3
FeAlO14CNT845	750	15	10	8/2	8.9
FeAlO15CNT846	750	15	10	8/2	10.4
FeAlO9CNT780	760	15	5	8/2	9.8
FeAlO12CNT781	760	15	5	8/2	8.2
FeAlO14CNT782	760	15	5	8/2	8.5
FeAlO15CNT783	760	15	5	8/2	9.3
FeAlO12CNT777	760	15	10	8/2	8.3
FeAlO15CNT779	760	15	10	8/2	8.3
FeAlO12CNT789	770	15	5	8/2	8.9
FeAlO14CNT790	770	15	5	8/2	12.0
FeAlO15CNT791	770	15	5	8/2	10.1
FeAlO16CNT899	770	15	10	8/2	8.9
FeAlO17CNT900	770	15	10	8/2	8.8
FeAlO18CNT901	770	15	10	8/2	9.3
FeAlO12CNT838	750	15	5	10/2	9.6
FeAlO14CNT839	750	15	5	10/2	11.1
FeAlO15CNT840	750	15	5	10/2	9.7
FeAlO16CNT911	750	15	10	10/2	9.5
FeAlO17CNT912	750	15	10	10/2	9.0
FeAlO18CNT913	750	15	10	10/2	10.0
FeAlO5CNT767	760	15	5	10/2	9.1
FeAlO9CNT768	760	15	5	10/2	8.7
FeAlO10CNT769	760	15	5	10/2	8.7
FeAlO12CNT770	760	15	5	10/2	8.5

(cont. on next page)

Table 5.2. (cont.)

FeAlO12CNT771	760	15	5	10/2	8.9
FeAlO14CNT772	760	15	5	10/2	10.5
FeAlO15CNT773	760	15	5	10/2	8.7
FeAlO9CNT762	760	15	10	10/2	7.6
FeAlO12CNT764	760	15	10	10/2	8.2
FeAlO15CNT766	760	15	10	10/2	8.8
FeAlO12CNT799	760	15	10	10/2	10.5
FeAlO14CNT800	760	15	10	10/2	9.8
FeAlO15CNT801	760	15	10	10/2	9.4
FeAlO9CNT792	770	15	5	10/2	9.1
FeAlO12CNT793	770	15	5	10/2	8.4
FeAlO15CNT795	770	15	5	10/2	9.2
FeAlO16CNT918	770	15	5	10/2	8.0
FeAlO17CNT919	770	15	10	10/2	8.3
FeAlO12CNT853	750	15	5	10/8	9.3
FeAlO14CNT854	750	15	5	10/8	8.6
FeAlO15CNT855	750	15	5	10/8	9.5
FeAlO16CNT921	750	15	10	10/8	9.9
FeAlO17CNT922	750	15	10	10/8	9.9
FeAlO12CNT856	760	15	5	10/8	8.3
FeAlO14CNT857	760	15	5	10/8	9.3
FeAlO15CNT858	760	15	5	10/8	10.4
FeAlO12CNT864	760	15	10	10/8	9.1
FeAlO16CNT865	760	15	10	10/8	8.7
FeAlO12CNT859	770	15	5	10/8	9.5
FeAlO14CNT860	770	15	5	10/8	9.5
FeAlO15CNT861	770	15	5	10/8	9.6
FeAlO14CNT923	770	15	10	10/8	7.9
FeAlO16CNT924	770	15	10	10/8	7.3
FeAlO17CNT925	770	15	10	10/8	9.1
FeAlO16CNT871	750	15	5	10/10	9.4
FeAlO17CNT872	750	15	5	10/10	11.4
FeAlO16CNT926	750	15	10	10/10	8.9
FeAlO17CNT927	750	15	10	10/10	9.7
FeAlO18CNT928	750	15	10	10/10	8.6
FeAlO16CNT869	760	15	5	10/10	9.9
FeAlO17CNT870	760	15	5	10/10	8.6
FeAlO16CNT873	760	15	10	10/10	9.3
FeAlO17CNT874	760	15	10	10/10	7.6
FeAlO14CNT932	770	15	5	10/10	8.7

(cont. on next page)

Table 5.2. (cont.)

FeAlO16CNT933	770	15	5	10/10	8.7
FeAlO17CNT934	770	15	5	10/10	8.5
FeAlO18CNT935	770	15	5	10/10	8.4
FeAlO16CNT929	770	15	10	10/10	7.9
FeAlO18CNT931	770	15	10	10/10	9.1

5.2.1.1. CNT Formation at Different Growth Temperatures

In order to examine the temperature effects in CO_2-assisted CVD, three different growth temperatures (750 ^oC, 760 ^oC and 770 ^oC) were studied on the thin Fe films sputtered on different $Al_2O_3/SiO_2/Si$ substrates (FeAlO12, FeAlO14, FeAlO15, FeAlO16, FeAlO17).

Studied growth conditions and obtained the mean diameters of CNTs including all substrates are given in Table 5.3 – Table 5.7. SEM pictures of as grown samples grown using all growth parameters are shown in Figure 5.4, Figure 5.6, Figure 5.8, Figure 5.10 and Figure 5.12 and diameter distributions of them are depicted in Figure 5.5, Figure 5.7, Figure 5.9, Figure 5.11 and Figure 5.13.

Table 5.3. Growth conditions and the mean diameters of CNTs used FeAlO12 substrate obtained as a result

Sample Name	T(^oC)	Pretreatment(min.) H_2/CO_2		CO_2(p)/CO_2(g) (sccm)	Mean Diameter (nm)
FeAlO12CNT785	750	15	5	8/2	8.8
FeAlO12CNT781	760	15	5	8/2	8.2
FeAlO12CNT789	770	15	5	8/2	8.9
FeAlO12CNT838	750	15	5	10/2	9.6
FeAlO12CNT770	760	15	5	10/2	8.5
FeAlO12CNT793	770	15	5	10/2	8.4
FeAlO12CNT853	750	15	5	10/8	9.3
FeAlO12CNT856	760	15	5	10/8	8.3
FeAlO12CNT859	770	15	5	10/8	9.5

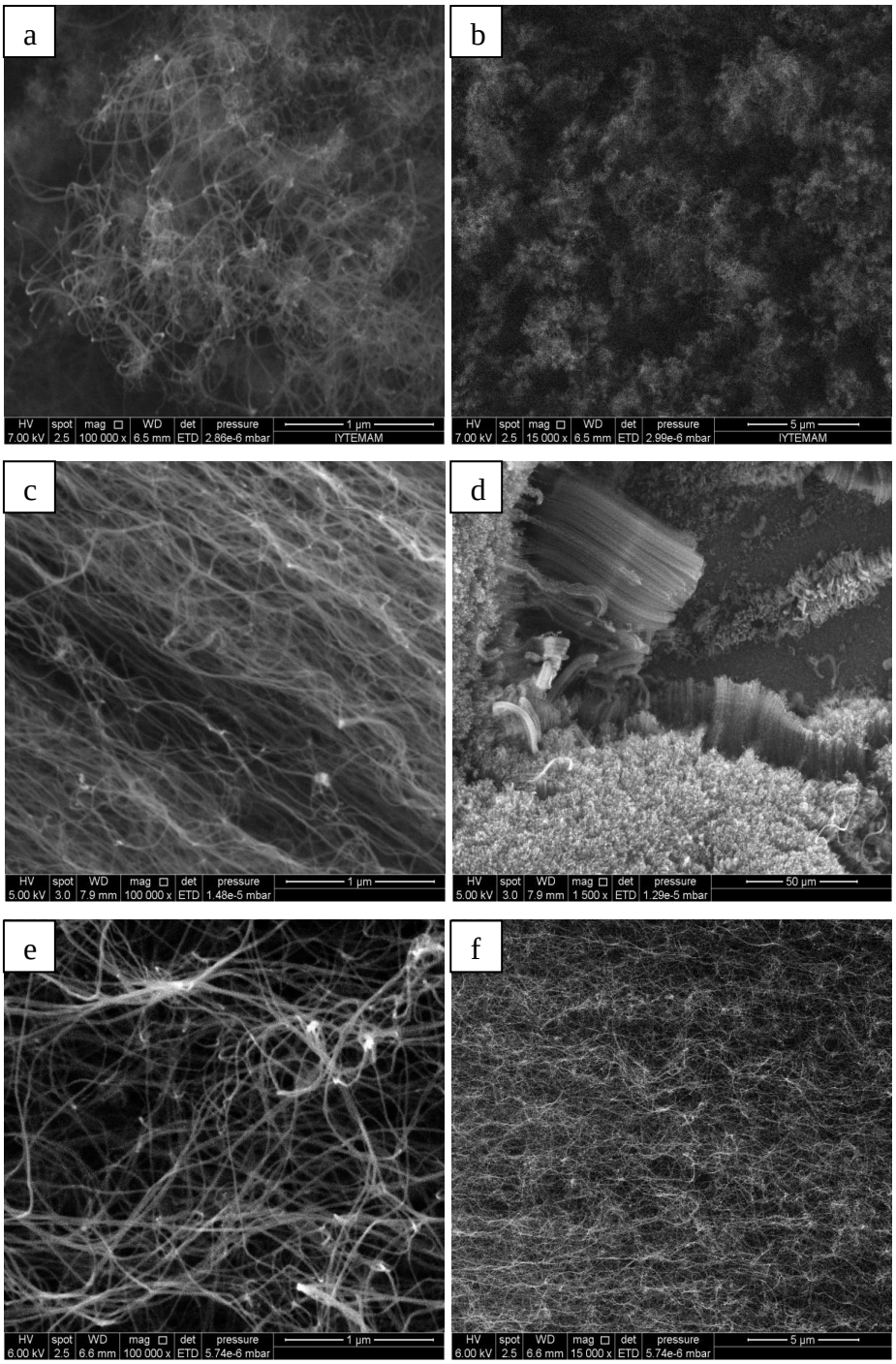

Figure 5.4. The growths with CO_2 (CO_2(p)/CO_2(g): 8/2) at 750 ºC, 760 ºC and 770 ºC: a), b) 750 ºC, FeAlO12 CNT785, 5 min. c), d) 760 ºC, FeAlO12 CNT781, 5 min. e), f) 770 ºC, FeAlO12 CNT789, 5 min.

Table 5.3 shows that the mean diameters of CNTs grown on FeAlO12 substrate obtained with 10/2 sccm CO_2 decrease when the temperature increases. However, when 8/2 and 10/2 sccm CO_2 are sent to the system, at first the mean diameters of CNTs decrease, afterwards ascend with increasing temperature. By regarding the last two flow rates (8/2 and 10/2 sccm CO_2), the same characteristics of diameters (decreasing and increasing successively) are shown, but the diameters coming from 8/2 sccm CO_2 are smaller than 10/2 sccm as required. Additionally, the diameters coming from 8/2 sccm have the same properties with previous catalyst diameters results in Table 5.1.

Since the diameters results at 8/2 sccm are chosen for best results in this experiment Sides and angled views of CNTs grown with 8/2 sccm CO_2 are given in Figure 5.4. SEM images show those samples grown at 750 ºC and 770 ºC are less densely populated than those grown at 760 ºC. In addition, CNTs grown at 760 ºC are vertical aligned. According to Figure 5.5, the numbers of CNTs at the mean diameters (8.8, 8.2 and 8.9 nm) at 8/2 sccm and at 750 ºC, 760 ºC and 770 ºC are 26 out of 58, 31 out of 61, 34 out of 69, respectively.

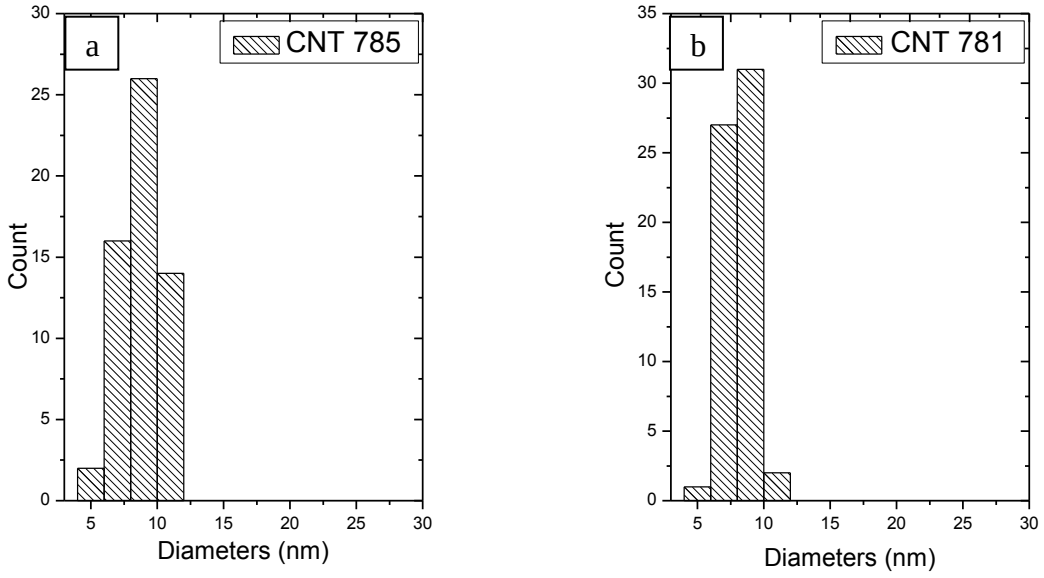

Figure 5.5. The diameter distributions of CNTs at different growth temperatures: 750 ºC, 5 min. b) 760 ºC, 5 min. c) 770 ºC, 5 min. (CO_2(p)/CO_2(g): 8/2)

(cont. on next page)

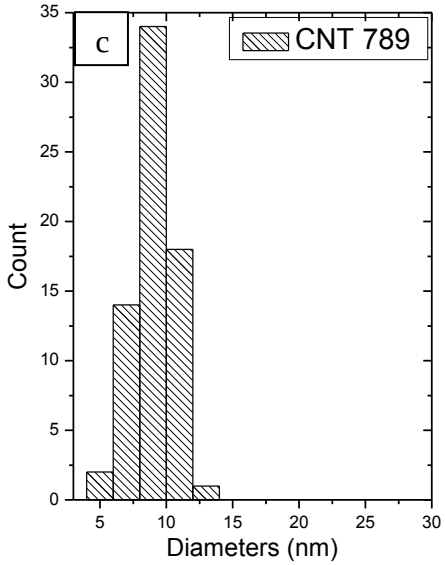

Figure 5.5. (cont.)

Table 5.4. Growth conditions and the mean diameters of CNTs used FeAlO14 substrate obtained as a result

Sample Name	T(^{o}C)	Pretreatment(min.) H_2/CO_2		CO_2(p)/CO_2(g) (sccm)	Mean Diameter (nm)
FeAlO14CNT782	760	15	5	8/2	8.5
FeAlO14CNT790	770	15	5	8/2	12.0
FeAlO14CNT839	750	15	5	10/2	11.1
FeAlO14CNT772	760	15	5	10/2	10.5
FeAlO14CNT854	750	15	5	10/8	8.6
FeAlO14CNT857	760	15	5	10/8	9.3
FeAlO14CNT860	770	15	5	10/8	9.5

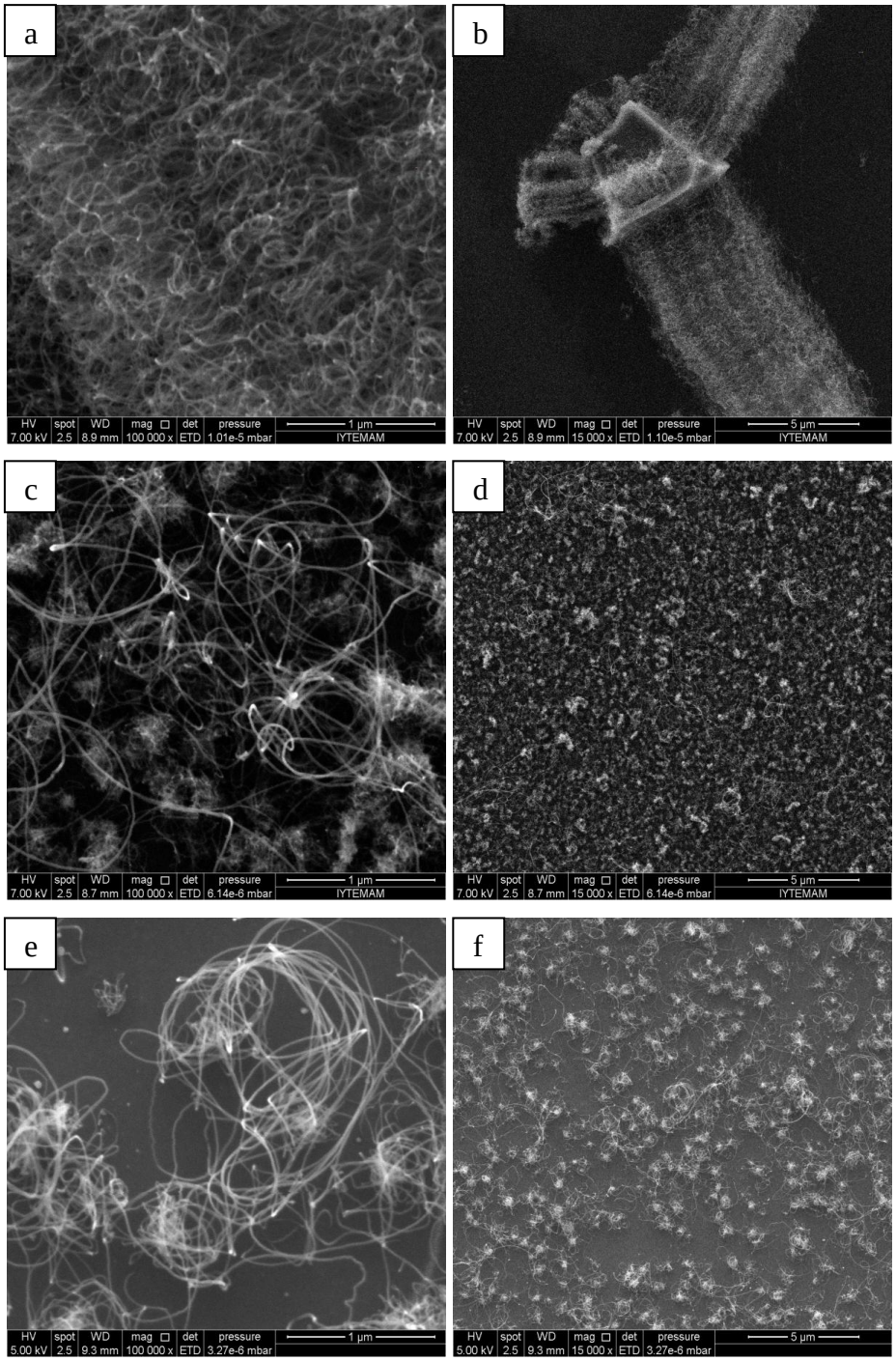

Figure 5.6. The growths with CO_2 (CO_2(p)/CO_2(g) 10/8) at 750 ºC, 760 ºC and 770 ºC: a), b) 750 ºC, FeAlO14 CNT854, 5 min. c), d) 760 ºC, FeAlO14 CNT857, 5 min. e), f) 770 ºC, FeAlO14 CNT860, 5 min.

Due to the lack of FeAlO14 substrates at the studied parameters 8/2 and 10/2 sccm CO_2, all the three growth temperatures (750 ºC, 760 ºC and 770 ºC) have been studied at the same time only at the parameters of 10/8 sccm CO_2 (Table 5.4). But the characteristics of these results (increasing diameters with rising temperatures) come from this experiment are not matched with the results (first decreasing and increasing diameters with rising temperatures) coming from FeAlO12 substrates 10/8 sccm.

SEM results of CNTs grown with 10/8 sccm CO_2 are given in Figure 5.6. SEM images show those samples grown at 760 ºC and 770 ºC are less densely populated than those grown at 750 ºC. As it is shown in Figure 5.7, the numbers of CNTs at the mean diameters (8.6, 9.3 and 9.5 nm) at 10/8 sccm and at 750 ºC, 760 ºC and 770 ºC are 20 out of 40, 22 out of 65, 32 out of 63, respectively.

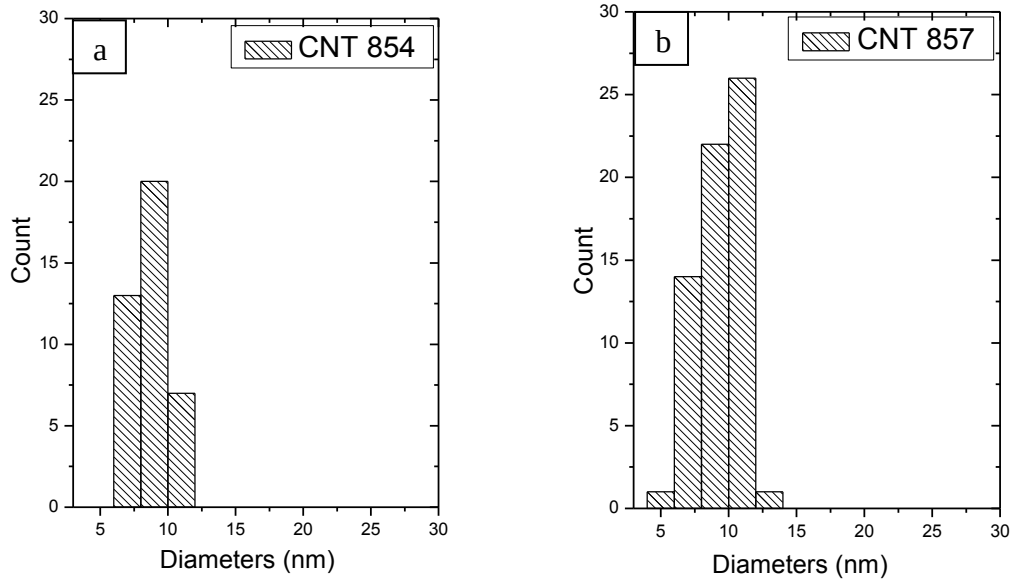

Figure 5.7. The diameter distributions of CNTs at different growth temperatures:
a) 750 ºC, 5 min. b) 760 ºC, 5 min. c) 770 ºC, 5 min. (CO_2(p)/CO_2(g): 10/8)

(cont. on next page)

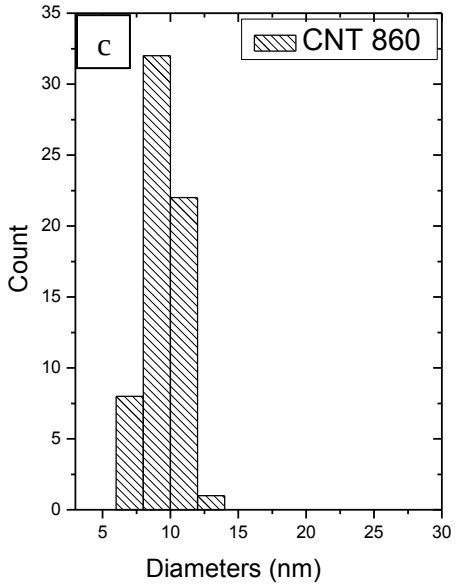

Figure 5.7. (cont.)

Table 5.5. Growth conditions and the mean diameters of CNTs used FeAlO15 substrate obtained as a result

Sample Name	T(^{o}C)	Pretreatment(min.) H_2/CO_2		CO_2(p)/CO_2(g) (sccm)	Mean Diameter (nm)
FeAlO15CNT787	750	15	5	8/2	8.2
FeAlO15CNT783	760	15	5	8/2	9.3
FeAlO15CNT791	770	15	5	8/2	10.1
FeAlO15CNT840	750	15	5	10/2	9.7
FeAlO15CNT773	760	15	5	10/2	8.7
FeAlO15CNT795	770	15	5	10/2	9.2
FeAlO15CNT855	750	15	5	10/8	9.5
FeAlO15CNT858	760	15	5	10/8	10.4
FeAlO15CNT861	770	15	5	10/8	9.6

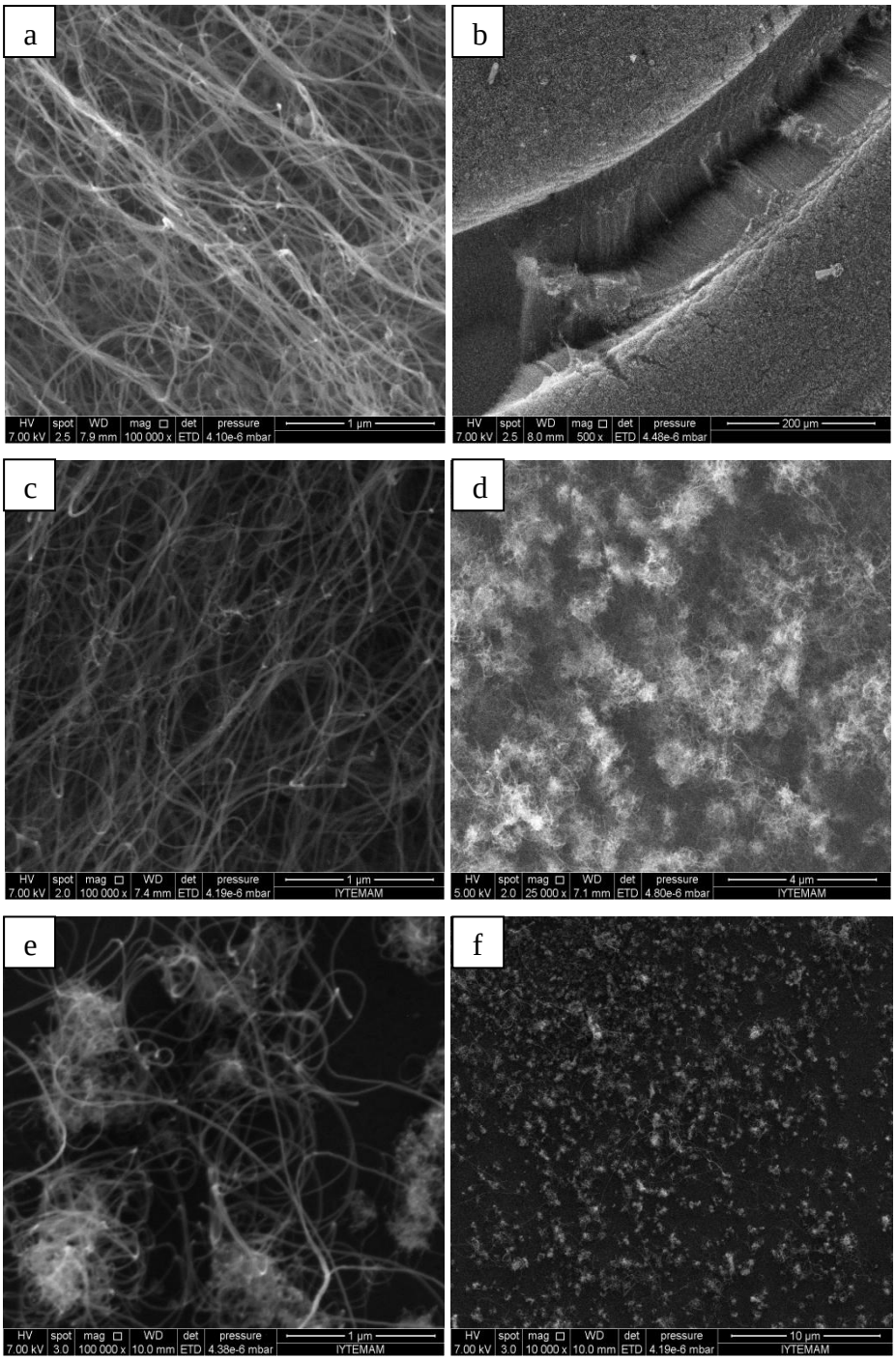

Figure 5.8. The growths with CO_2 (CO_2(p)/CO_2(g):10/2)at 750 ºC, 760 ºC and 770 ºC : a), b) 750 ºC, FeAlO15 CNT840, 5 min. c), d) 760 ºC, FeAlO15 CNT773, 5 min, e), f) 770 ºC, FeAlO15 CNT795, 5 min.

How the CNT mean diameters obtained using FeAlO15 substrate change with three different growth temperatures can be seen in Table 5.4. The diameters obtained from 8/2 and 10/8 sccm are not valuable by regarding the expected trend of diameter values. On the other hand, the diameter decreases from 9.7 nm at 750 ºC to 8.7 nm at 760 ºC and then increases to 9.2 nm at 770 ºC for CO_2 10/2 flow rate. SEM images of the CNTs for 10/2 sccm are depicted in Figure 5.8. According to Figure 5.9, the numbers of CNTs at the mean diameters (9.7, 8.7 and 8.2 nm) at 10/2 sccm and at 750 ºC, 760 ºC and 770 ºC are 42 out of 81, 31 out of 69, 40 out of 56, respectively.

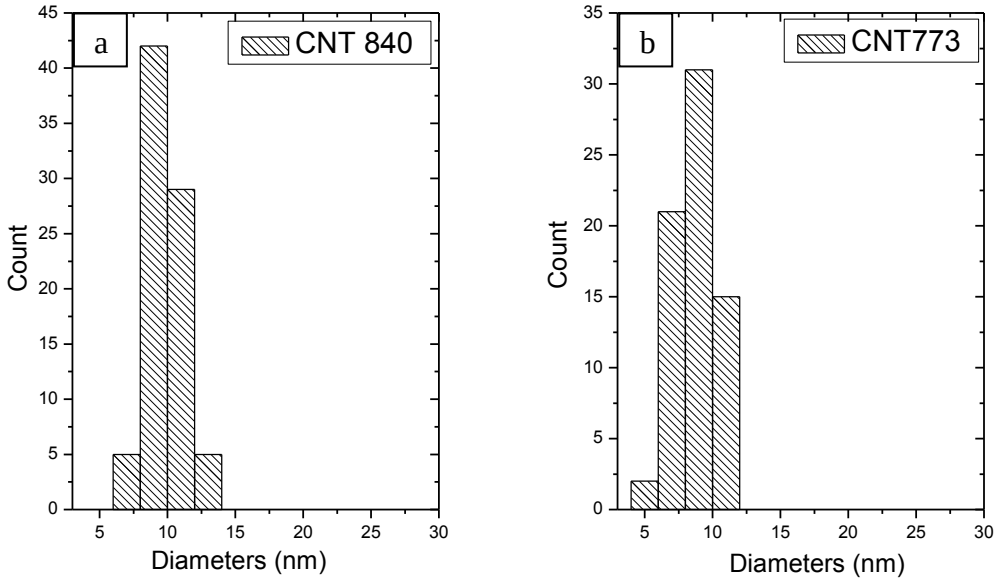

Figure 5.9. The diameter distributions of CNTs at different growth temperatures:
a) 750 ºC, 5 min., b) 760 ºC, 5 min., c) 770 ºC, 5 min (CO_2(p)/CO_2(g):10/2)

(cont. on next page)

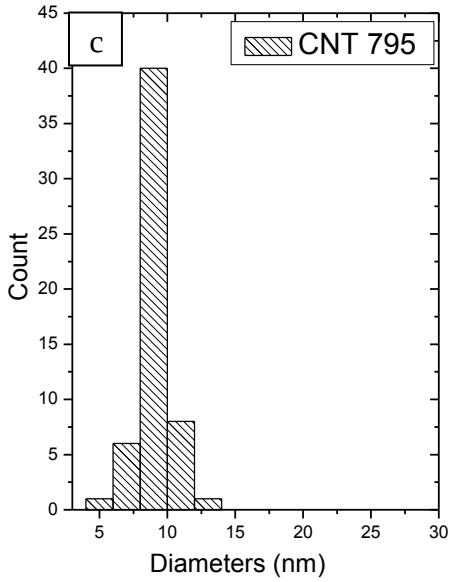

Figure 5.9. (cont.)

Table 5.6. Growth conditions and the mean diameters of CNTs used FeAlO16 substrate obtained as a result

Sample Name	T(^{o}C)	Pretreatment(min.) H_2/CO_2		CO_2(p)/CO_2(g) (sccm)	Mean Diameter (nm)
FeAlO16CNT921	750	15	10	10/8	9.9
FeAlO16CNT865	760	15	10	10/8	8.7
FeAlO16CNT924	770	15	10	10/8	7.3
FeAlO16CNT926	750	15	10	10/10	8.9
FeAlO16CNT873	760	15	10	10/10	9.3
FeAlO16CNT929	770	15	10	10/10	7.9

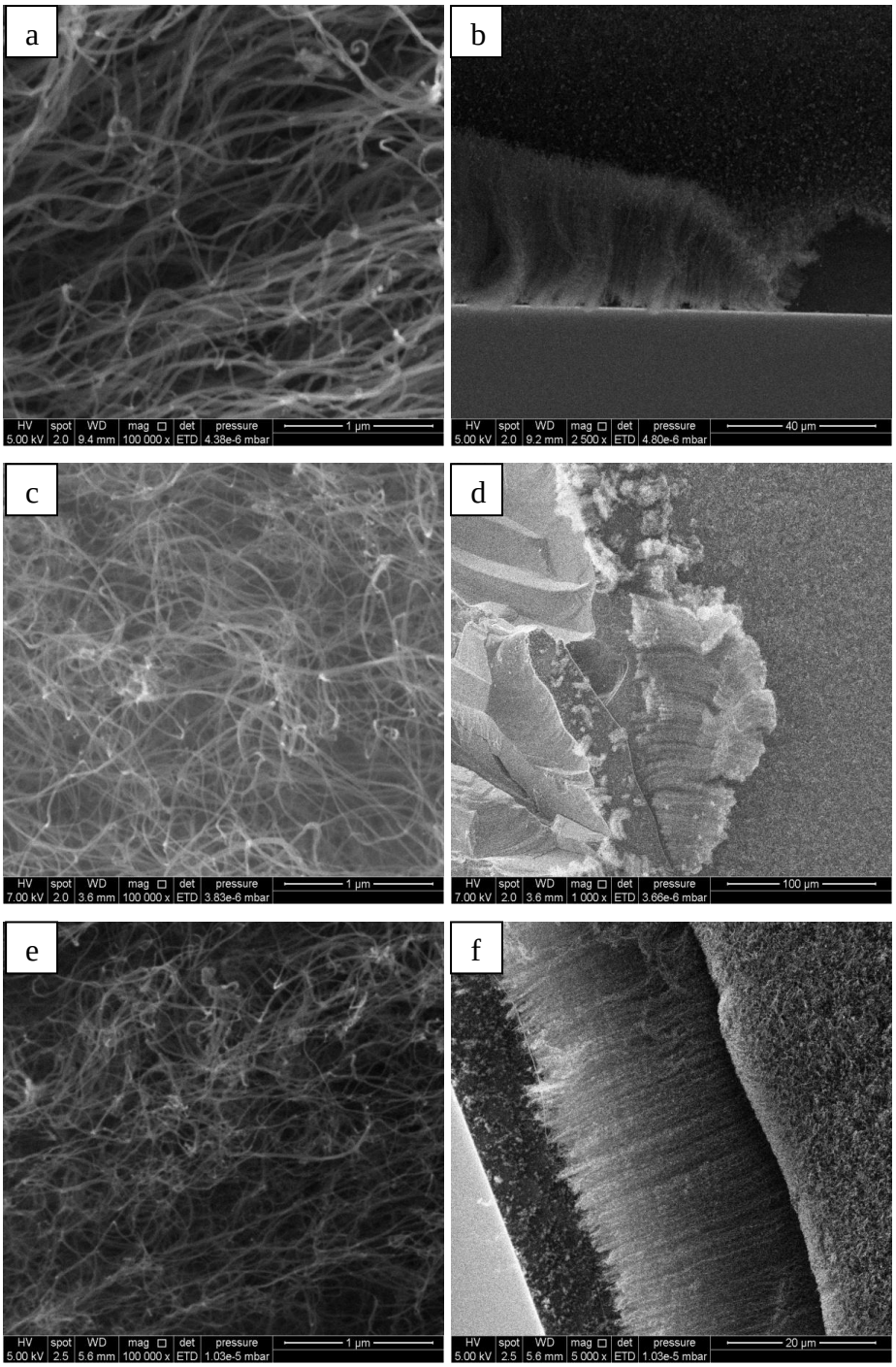

Figure 5.10. The growths with CO_2 (CO_2(p)/CO_2(g): 10/8) at 750 °C, 760 °C and 770 ºC: a), b) 750 °C, FeAlO16 CNT921, 10 min. c), d) 760 °C, FeAlO16 CNT865, 10 min. e), f) 770 °C, FeAlO16 CNT924, 10 min.

Table 5.6 shows that the shorter mean diameters come from 10/8 sccm, which is the reason why the mean diameters of 10/8 sccm are deeply analyzed on the following side and the angled views of SEM images for CNTs grown on FeAlO16 substrate (Figure 5.10). As the CO_2 is sent to the system with 10/10 sccm, it is observed that the temperature that the diameters of CNTs increase first and then decrease. If the CO_2 is sent with 10/8 sccm, the diameters decrease continuously with the temperature. This situation is different from the change of the characteristics of CNT diameters (first increasing and then decreasing) with the temperature in that the use of different substrates such as FeAlO12, FeAlO14, FeAlO15 chosen for CNT growth.

SEM results of CNTs grown with 10/8 sccm CO_2 are given in Figure 5.10. It can be easily seen that the diameters of CNTs at 750 ºC are bigger than those at 760 ºC and 770 ºC. Additionally, the diameters of CNTs at 770 ºC are the smallest values. With this comparision, the truth that higher temperatures give smaller diameters can be proven. According to Figure 5.11, the numbers of CNTs at the mean diameters (9.9, 8.7 and 7.3 nm) at 10/8 sccm and at 750 ºC, 760 ºC and 770 ºC are 17 out of 37, 56 out of 91, 31 out of 57, respectively.

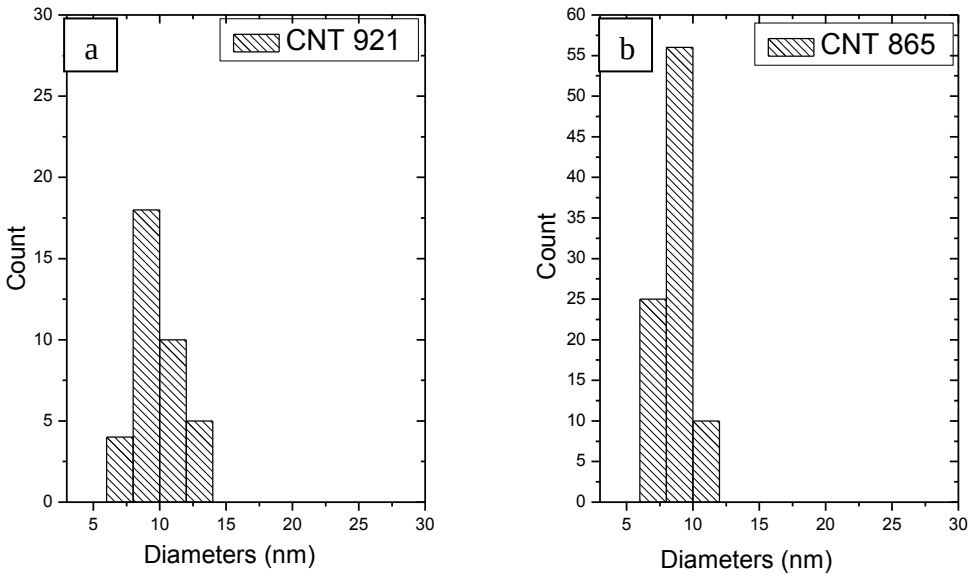

Figure 5.11. The diameter distributions of CNTs at different growth temperatures: a) 750 ºC, 10 min. b) 760 ºC, 10 min. c) 770 ºC, 10 min. (CO_2(p)/CO_2(g): 10/8)

(cont. on next page)

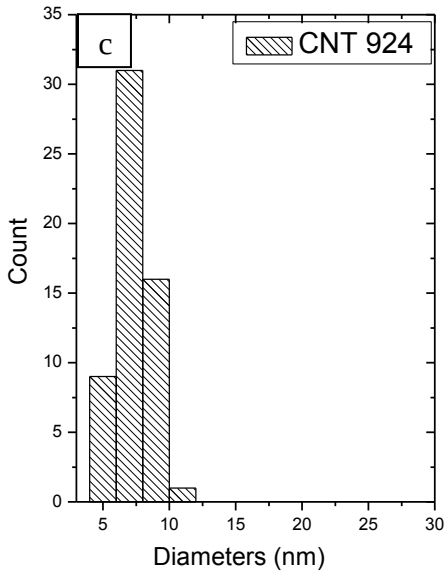

Figure 5.11. (cont.)

Table 5.7. Growth conditions and the mean diameters of CNTs used FeAlO17 substrate obtained as a result

Sample Name	T(^{o}C)	Pretreatment(min.) H_2/CO_2		CO_2(p)/CO_2(g) (sccm)	Mean Diameter (nm)
FeAlO17CNT872	750	15	5	10/10	11.4
FeAlO17CNT870	760	15	5	10/10	8.6
FeAlO17CNT934	770	15	5	10/10	8.5

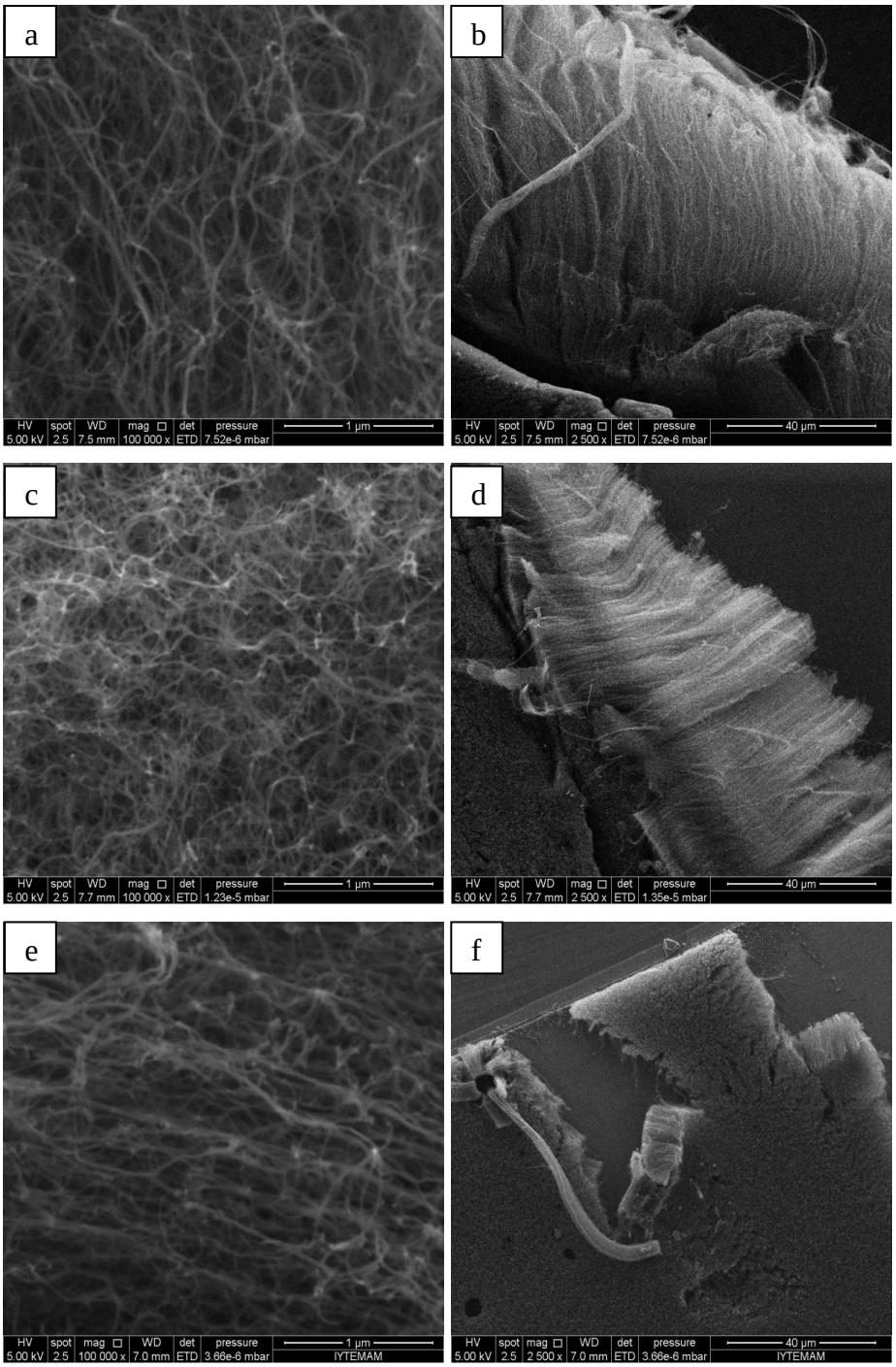

Figure 5.12. The growths with CO_2 (CO_2(p)/CO_2(g): 10/10) at 750 ºC, 760 ºC and 770 ºC: a), b) 750 ºC, FeAlO17 CNT872, 5 min. c), d) 760 ºC, FeAlO17 CNT870, 5 min. e), f)770 ºC, FeAlO17 CNT934, 5 min.

Due to the lack of FeAlO17 substrates for studying other parameters, the three growth temperatures (750 ºC, 760 ºC and 770 ºC) have been studied at the same time only at the parameters of 10/10 sccm CO_2. Table 5.7 displays when the temperature rises from 750 ºC to 760 ºC, approximately 3nm decrease in CNT diameters is seen clearly. Though, the decrease is lower (0.1 nm) when the temperature increases from 760 ºC to 770 ºC. These results show that 750 is the critical temperature for this substrate. SEM results of CNTs grown with 10/10 sccm CO_2 are given in Figure 5.12. SEM images obviously show that those samples grown at 750 ºC are less densely populated than those grown at 770 ºC. According to Figure 5.13, the numbers of CNTs at the mean diameters (11.4, 8.6 and 8.5 nm) at 10/10 sccm and at 750 ºC, 760 ºC and 770 ºC are 25 out of 28, 22 out of 39, 44 out of 77, respectively.

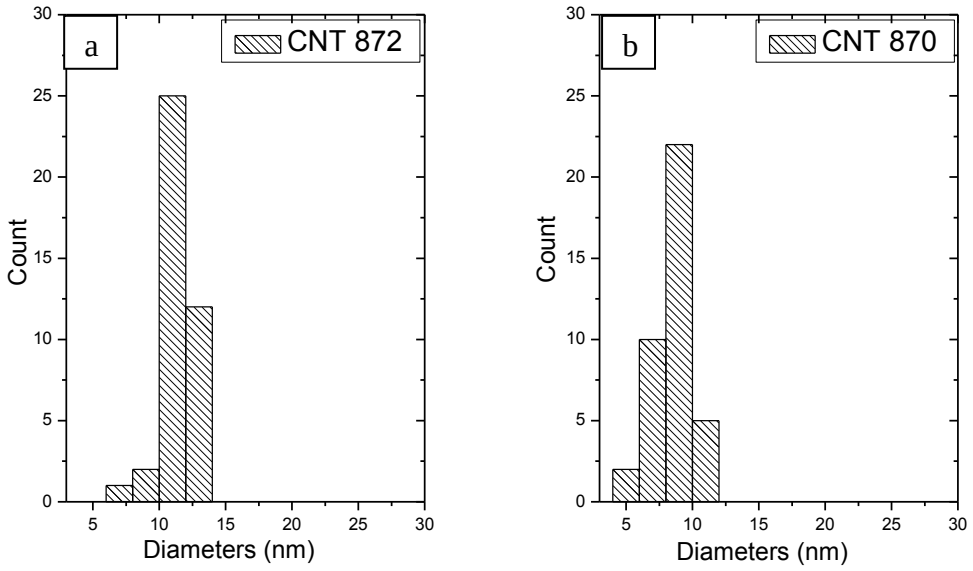

Figure 5.13. The diameter distributions of CNTs at different growth temperatures:
a) 750 ºC, 5 min. b) 760 ºC, 5 min. c) 770 ºC, 5 min.
(CO_2(p)/CO_2(g): 10/10)

(cont. on next page)

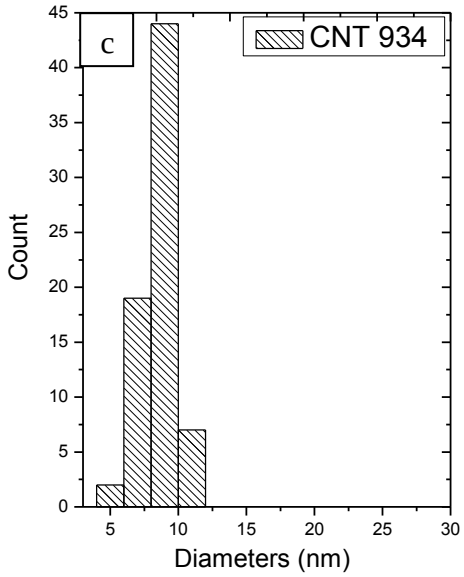

Figure 5.13. (cont.)

5.2.1.2. CNT Formation at Different CO_2 Flow Rates

Weak oxidizers are widely used to remove amorphous carbon to prevent the poisoning of the catalyst particle and to obtain pure CNT during the growth period. Some studies also suggest that oxidizers functionalize the substrate surface which inhibits catalyst particle mobility and deter them from joining and forming larger particles. In the pretreatment process, they are used to control the size of catalyst particle and in the growth process to keep catalyst particle functioning throughout the growth time and to prevent amorphous carbon formation on the outer walls of CNTs.

In order to investigate the influence of CO_2 on effective CNT growth, it is focused on how diameters of CNTs varied with the amount of CO_2 at a fixed growth temperature. CO_2 gas flow ratios in pretreatment and growth stages were studied as 8:2, 10:2, 10:8 and 10:10. SEM images of CNTs were characterized in order to see effects of CO_2 under growth conditions. According to the results obtained, the mean diameters are given in Table 5.8 - Table 5.11. In addition, SEM images are given in Figure 5.14, Figure 5.16 and Figure 5.18 and diameter distributions of CNTs with CO_2 are shown in Figure 5.15, Figure 5.17 and Figure 5.19.

Table 5.8. The amounts of CO_2 used during pretreatment and growth processes and the mean diameters of CNTs used FeAlO12 substrate obtained as a result

Sample Name	T(^oC)	Pretreatment(min.) H_2/CO_2		$CO_2(p)/CO_2(g)$ (sccm)	Mean Diameter (nm)
FeAlO12CNT838	750	15	5	10/2	9.6
FeAlO12CNT853	750	15	5	10/8	9.3
FeAlO12CNT770	760	15	5	10/2	8.5
FeAlO12CNT856	760	15	5	10/8	8.3
FeAlO12CNT793	770	15	5	10/2	8.4
FeAlO12CNT859	770	15	5	10/8	9.5

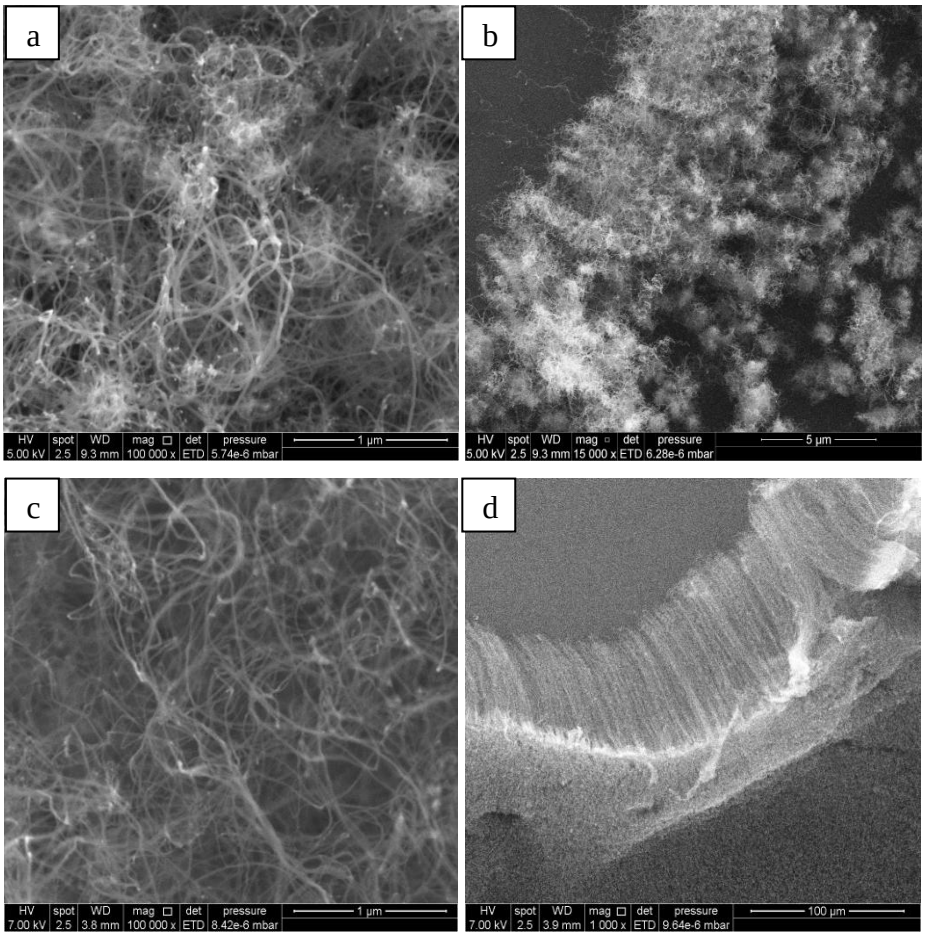

Figure 5.14. The growths with CO_2 at 750 ºC: a), b) $CO_2(p)/CO_2(g)$: 10/2, FeAlO12 CNT838, 5 min. c), d) $CO_2(p)/CO_2(g)$: 10/8, FeAlO12 CNT853, 5 min.

In this part, for the first substrate, FeAlO12, two different CO_2 flow rates (10/2 and 10/8) are studied at fixed growth temperatures (750 ºC, 760 ºC and 770 ºC). According to Table 5.8, when CO_2 flow rate decreases, the CNT mean diameter decreases nearly 0.2-0.3 nm at 750 ºC and 760 ºC. On the other hand, for 770 ºC, the CNT mean diameter increases nearly 1 nm while CO_2 flow rate decreases. Figure 5.14 illustrates that when CO_2 is sent with 10/2 sccm into the system at 750 ºC, CNT diameters can be selected individually whereas they form groups when the the CO_2 is sent with 10/8 sccm. According to Figure 5.15, the numbers of CNTs at the mean diameters (9.6 and 9.3 nm) at 10/2 sccm and 10/8 sccm at 750 ºC are 26 out of 49 and 34 out of 72, respectively.

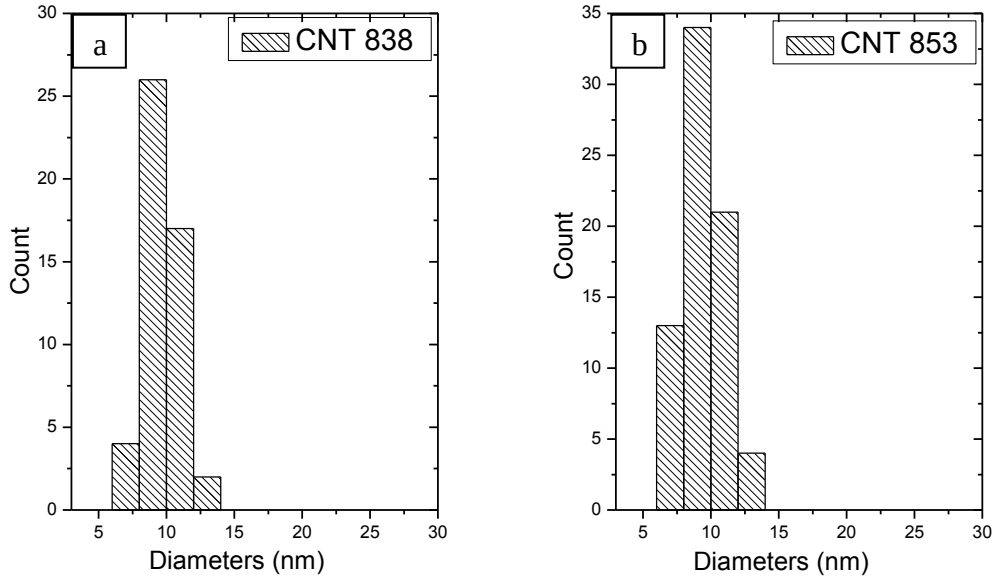

Figure 5.15. The diameter distributions of CNTs at different CO_2 flow rates at 750 ºC: a) CO_2(p)/CO_2(g): 10/2, 5 min. b) CO_2(p)/CO_2(g): 10/8, 5 min.

Table 5.9. The amounts of CO_2 used during pretreatment and growth processes and the mean diameters of CNTs used FeAlO15 substrate obtained as a result

Sample Name	T(^oC)	Pretreatment(min.) H_2/CO_2		$CO_2(p)/CO_2(g)$ (sccm)	Mean Diameter (nm)
FeAlO15CNT840	750	15	5	10/2	9.7
FeAlO15CNT855	750	15	5	10/8	9.5
FeAlO15CNT773	760	15	5	10/2	8.7
FeAlO15CNT858	760	15	5	10/8	10.4
FeAlO15CNT795	770	15	5	10/2	9.2
FeAlO15CNT861	770	15	5	10/8	9.6

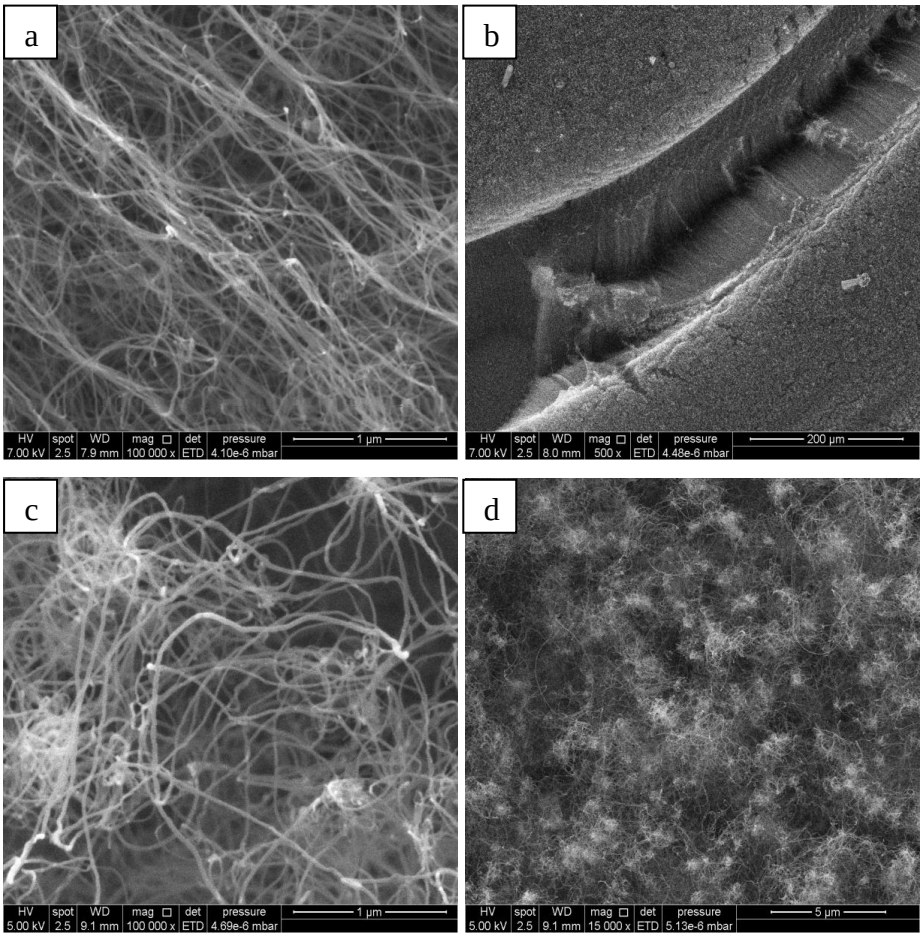

Figure 5.16. The growths with CO_2 at 750 ºC: a), b) $CO_2(p)/CO_2(g)$: 10/2, FeAlO15 CNT840, 5 min. c), d) $CO_2(p)/CO_2(g)$: 10/8, FeAlO15 CNT855, 5 min.

For FeAlO15 substrate, two different CO_2 flow rates (10/2 and 10/8) are studied at fixed growth temperatures (750 ºC, 760 ºC and 770 ºC) again. Table 5.9 shows that when CO_2 flow rate decreases, the CNT mean diameter increases at 760 ºC and 770 ºC. However, the CNT mean diameter decreases 0.2 nm while CO_2 flow rate decreases at 750 ºC. Figure 5.16 illustrates that CNTs grown at 10/2 sccm are vertical aligned. According to Figure 5.17, the numbers of CNTs at the mean diameters (9.7 and 9.5 nm) at 10/2 sccm and 10/8 sccm at 750 ºC are 42 out of 81 and 46 out of 89, respectively.

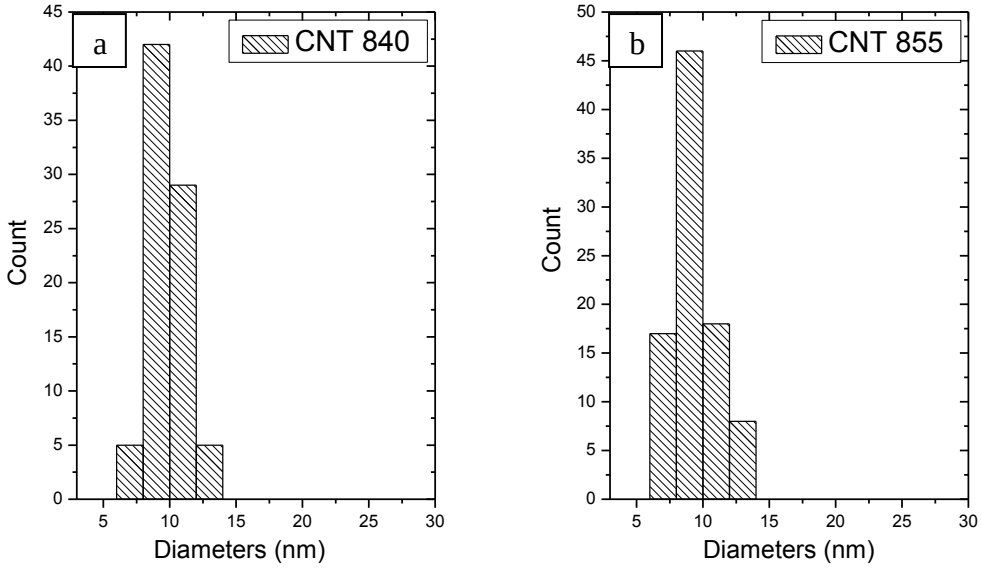

Figure 5.17. The diameter distributions of CNTs at different CO_2 flow rates at 750 ºC: a) CO_2(p)/CO_2(g): 10/2, 5 min. b) CO_2(p)/CO_2(g): 10/8, 5 min.

Table 5.10. The amounts of CO_2 used during pretreatment and growth processes and the mean diameters of CNTs used FeAlO16 substrate obtained as a result

Sample Name	T(^{o}C)	Pretreatment(min.) H_2/CO_2		CO_2(p)/CO_2(g) (sccm)	Mean Diameter (nm)
FeAlO16CNT921	750	15	10	10/8	9.9
FeAlO16CNT926	750	15	10	10/10	8.9
FeAlO16CNT865	760	15	10	10/8	8.7
FeAlO16CNT873	760	15	10	10/10	9.3
FeAlO16CNT924	770	15	10	10/8	7.3
FeAlO16CNT929	770	15	10	10/10	7.9

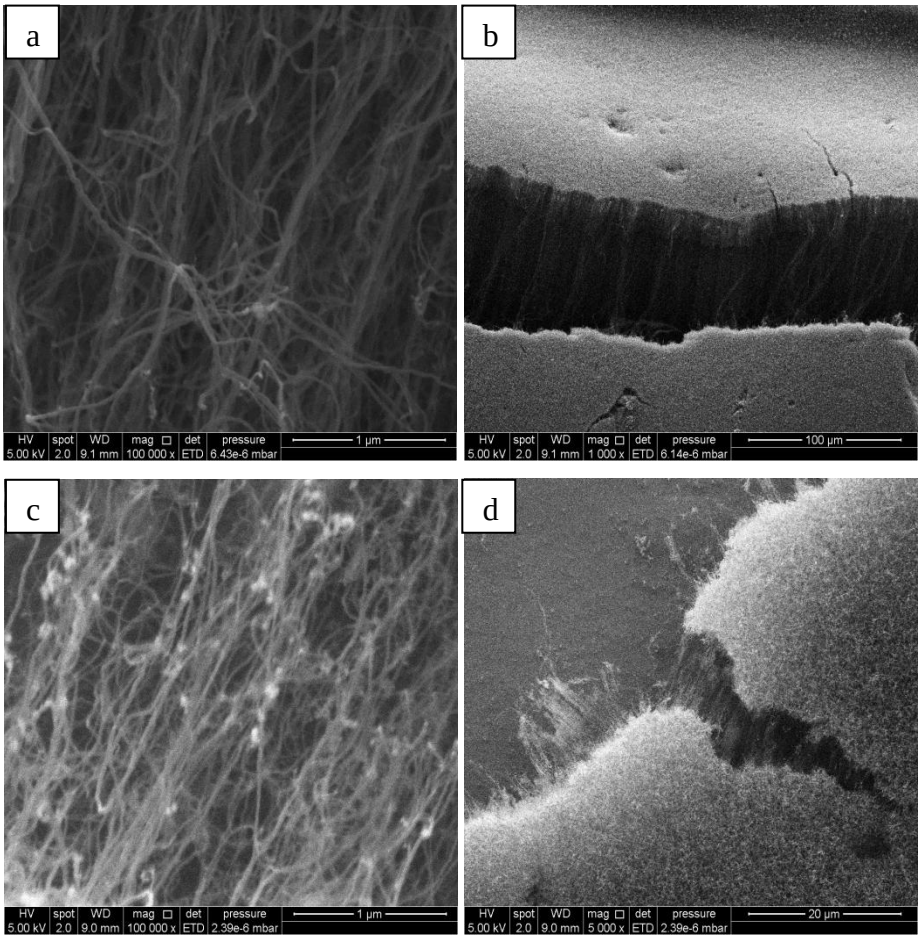

Figure 5.18. The growths with CO_2 at 750 ºC: a), b) CO_2(p)/CO_2(g): 10/8, FeAlO16 CNT921, 10 min. c), d) CO_2(p)/CO_2(g): 10/10, FeAlO16 CNT926, 10 min.

For FeAlO16 substrate, two different CO_2 flow rates (10/8 and 10/10) are studied at fixed growth temperatures (750 ºC, 760 ºC and 770 ºC) again. Table 5.10 shows that when CO_2 flow rate decreases (from 10/8 to 10/10), the CNT mean diameter increases at 760 ºC and 770 ºC. However, the CNT mean diameter decreases nearly 1 nm while CO_2 flow rate decreases at 750 ºC. When Figure 5.18 is analyzed, it is clearly seen that the CNT diameters grown at 10/8 sccm are big. According to Figure 5.19, the numbers of CNTs at the mean diameters (9.9 and 8.9 nm) at 10/8 sccm and 10/10 sccm at 750 ºC are 18 out of 37 and 23 out of 39, respectively.

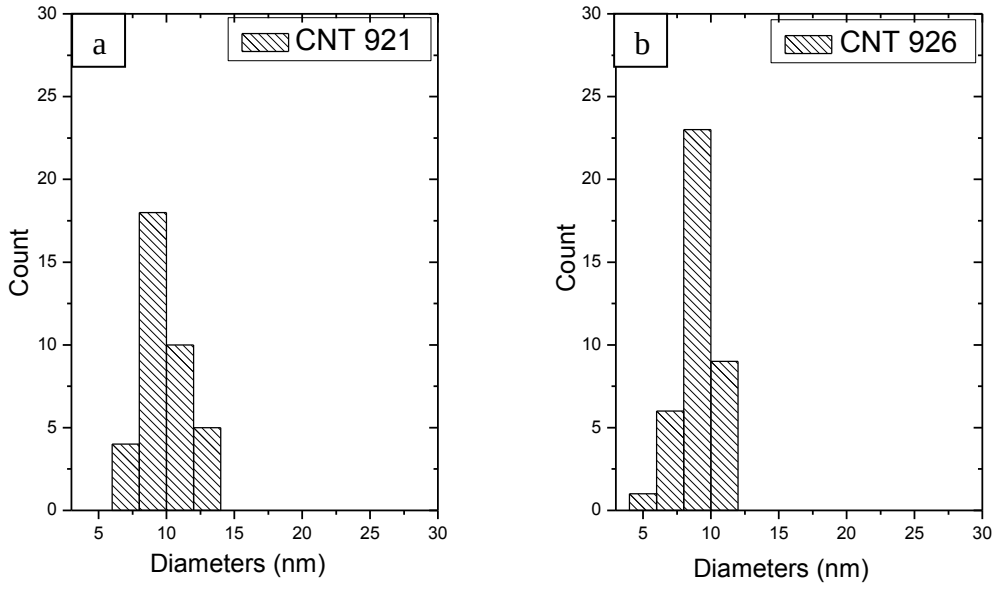

Figure 5.19. The diameter distributions of CNTs at different CO_2 flow rates at 750 ºC: a) CO_2(p)/CO_2(g): 10/8, 10 min. b) CO_2(p)/CO_2(g): 10/10, 10 min.

Table 5.11. The amounts of CO_2 used during pretreatment and growth processes and the mean diameters of CNTs used FeAlO17 substrate obtained as a result

Sample Name	T(^oC)	Pretreatment(min.) H_2/CO_2		$CO_2(p)/CO_2(g)$ (sccm)	Mean Diameter (nm)
FeAlO17CNT912	750	15	10	10/2	9.0
FeAlO17CNT922	750	15	10	10/8	9.9
FeAlO17CNT927	750	15	10	10/10	9.7

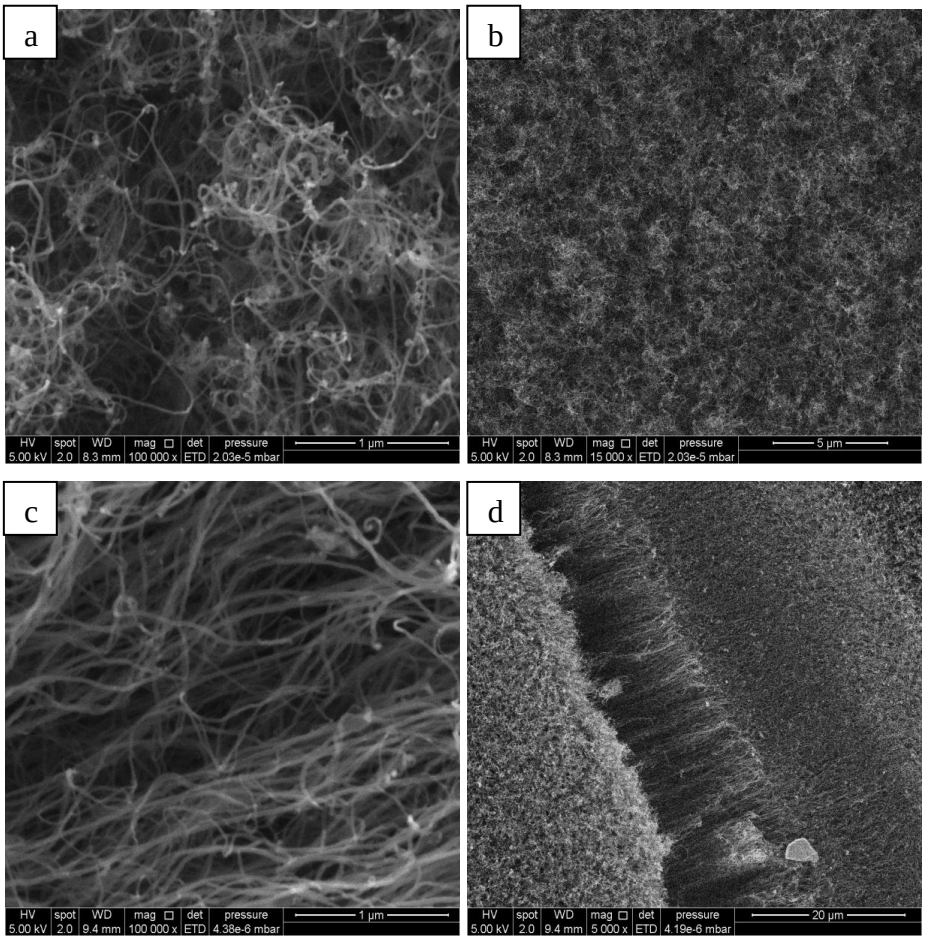

Figure 5.20. The growths with CO_2 at 750 ºC: a), b) $CO_2(p)/CO_2(g)$: 10/2, FeAlO17 CNT912, 10 min. c), d) $CO_2(p)/CO_2(g)$: 10/8, FeAlO17 CNT922, 10 min. e), f) $CO_2(p)/CO_2(g)$: 10/10, FeAlO17 CNT927, 10 min.

(cont. on next page)

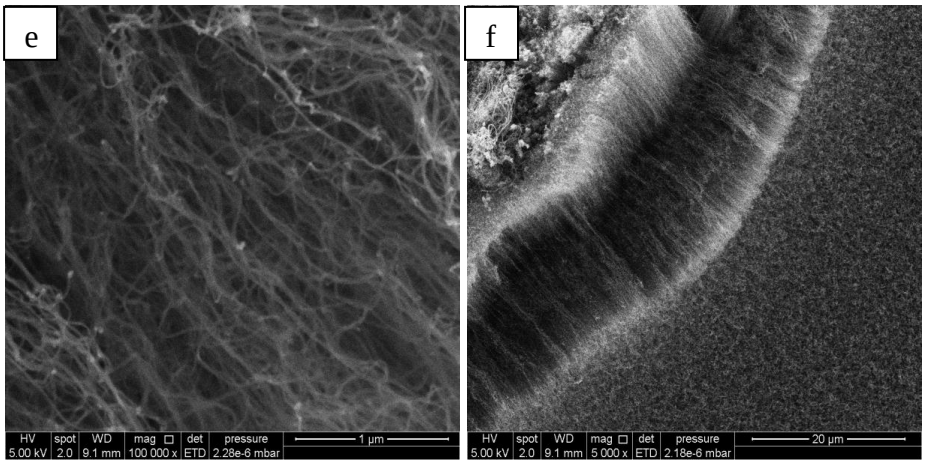

Figure 5.20. (cont.)

Due to the lack of FeAlO17 substrates for studying other parameters, only 750 ºC has been studied at the same time at the parameters of 10/2, 10/8 and 10/10 sccm CO_2. Table 5.11 shows that the diameters increase and then decrease with decreasing the ratio of CO_2 in pretreatment to that of in growth. Sides and angled views of SEM images of CNTs are depicted in Figure 5.20. It can be clearly seen in SEM images that when CO_2 is sent with 10/2 sccm into the system, CNT diameters reach the minimum value. Additionally, when CO_2 is sent with 10/8 sccm, the maximum CNT diameter is observed. According to Figure 5.21, the numbers of CNTs at the mean diameters (9.0, 9.9 and 9.7 nm) at 10/2 sccm, 10/8 sccm and 10/10 sccm at 750 ºC are 36 out of 78, 20 out of 52 and 22 out of 40, respectively.

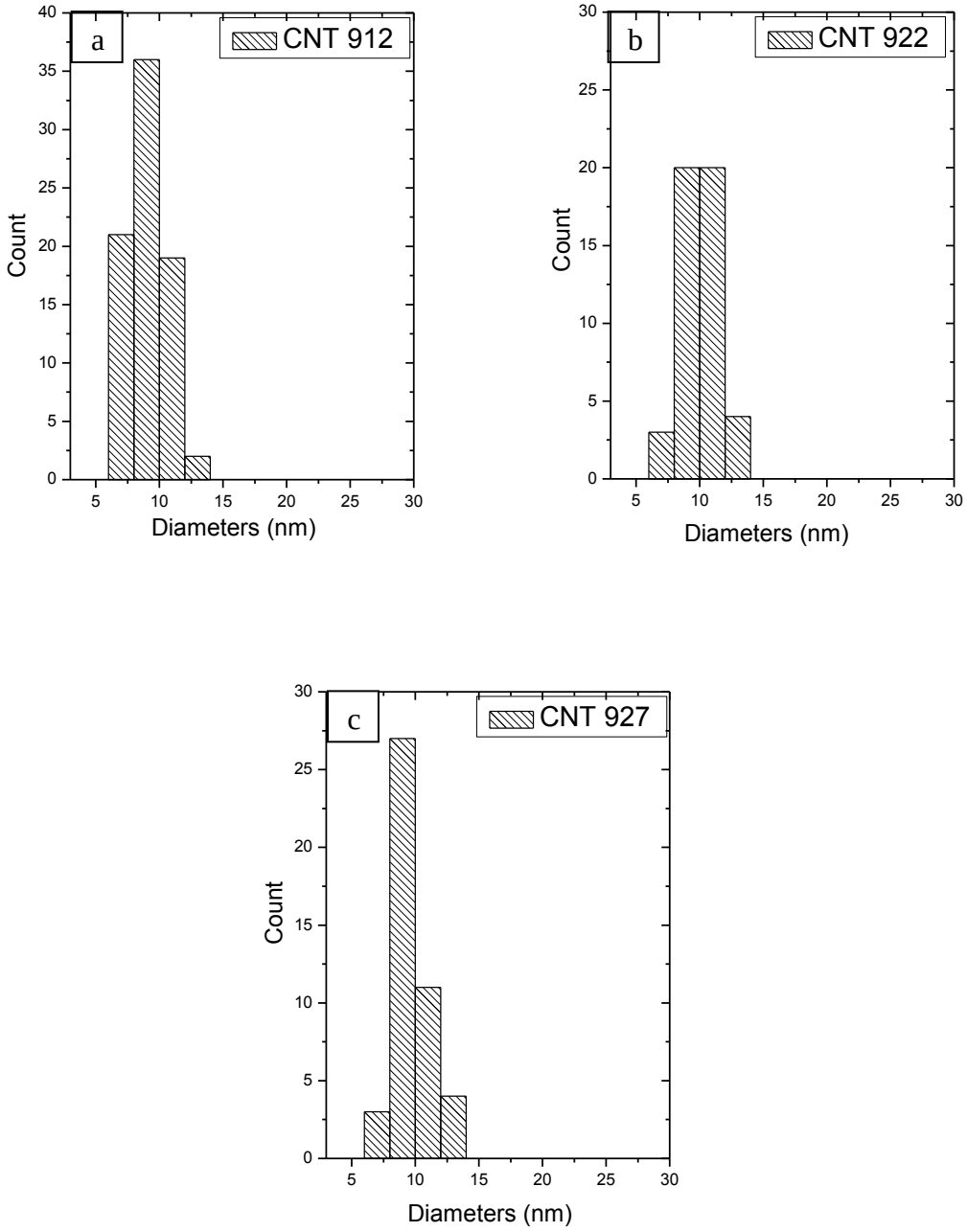

Figure 5.21. The diameter distributions of CNTs at different CO_2 flow rates at 750 ºC: a) CO_2(p)/CO_2(g): 10/2, 5 min. b) CO_2(p)/CO_2(g): 10/8, 5 min. c) CO_2(p)/CO_2(g): 10/10, 5 min.

5.2.1.3. CNT Formation at Different Pretreatment Time of CO_2

The influence of CO_2 on CNT growth was investigated by sending CO_2 later or earlier than H_2 in pretreatment process. During the experiments, CO_2 flow rates were 8:2, 10:2, 10:8 and 10:10 sccm and pretreatment time was kept at the constant value of 15 min. and weak oxidizer, CO_2, introduced 5 and 10 min. prior to the CNT growth.

How mean diameters depended on pretreatment times are shown in Table 5.12 – Table 5.16. SEM images of the growths with during different pretreatment times of CO_2 are illustrated in Figure 5.22, Figure 5.24, Figure 5.26, Figure 5.28 and Figure 5.30 and the diameter distributions of CNTs are illustrated in Figure 5.23, Figure 5.25, Figure 5.27, Figure 5.29 and Figure 5.31.

Table 5.12. The amounts of CO_2 used during various pretreatment and growth times and the mean diameters of CNTs used FeAlO12 substrate obtained as a result

Sample Name	T(^{o}C)	Pretreatment(min.) H_2/CO_2		CO_2(p)/CO_2(g) (sccm)	Mean Diameter (nm)
FeAlO12CNT785	750	15	5	8/2	8.8
FeAlO12CNT844	750	15	10	8/2	8.3
FeAlO12CNT781	760	15	5	8/2	8.2
FeAlO12CNT777	760	15	10	8/2	8.3
FeAlO12CNT771	760	15	5	10/2	8.9
FeAlO12CNT764	760	15	10	10/2	8.2

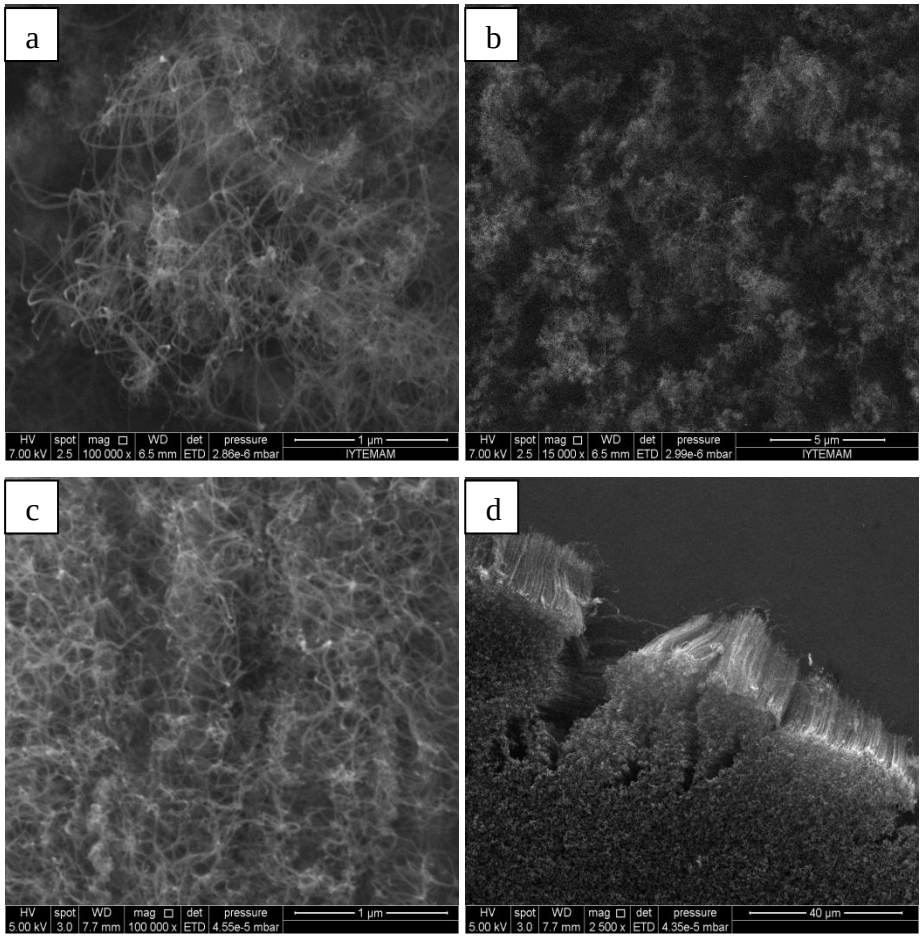

Figure 5.22. The growths with CO_2 (CO_2(p)/CO_2(g): 8/2) at 750 ºC: a), b) FeAlO12 CNT785, 5min. c), d) FeAlO12 CNT844, 10 min.

Due to the lack of FeAlO12 substrates for different pretreatment durations (5 and 10 min.) of CO_2, the values of 8/2 sccm at 750 ºC and 760 ºC; single value of 10/2 sccm at 760 ºC are examined. Table 5.13 shows that when CO_2 is kept longer than that of H_2 at 8/2 sccm at 750 ºC and 10/2 sccm at 760 ºC, CNT diameters decrease under these conditions. However, when CO_2 is kept longer than that of H_2 at 8/2 sccm at 760 ºC, it can be seen that there is no effect of CO_2 duration. According to Figure 5.23, the numbers of CNTs at the mean diameters (8.8 and 8.3 nm) at 8/2 at 750 ºC with the duration of 5 and 10 min. are 26 out of 58 and 15 out of 42, respectively.

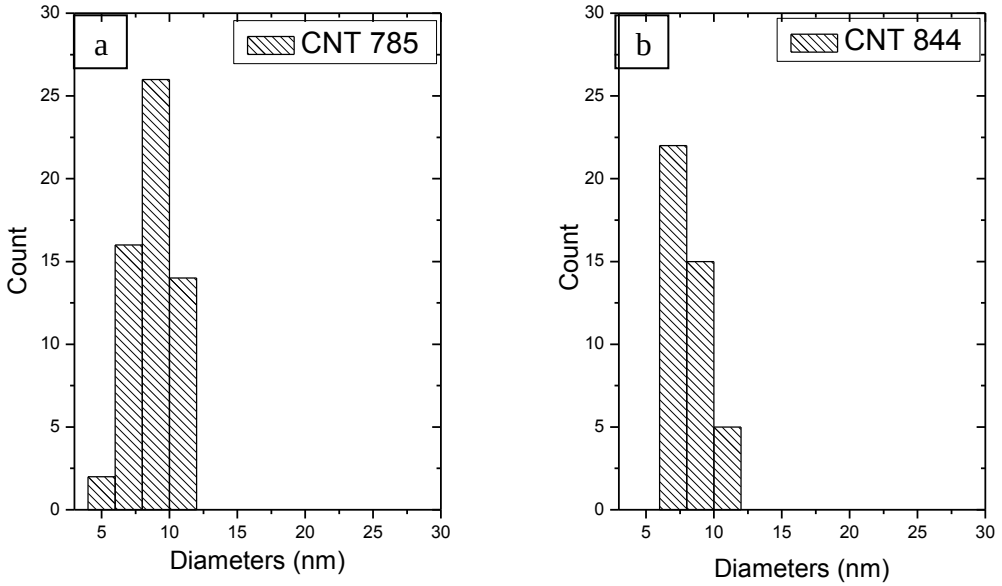

Figure 5.23. The diameter distributions of CNTs at different pretreatment time of CO_2 at 750 ºC: a) CO_2(p)/CO_2(g): 8/2, 5 min. b) CO_2(p)/CO_2(g): 8/2, 10 min.

Table 5.13. The amounts of CO_2 used during various pretreatment and growth times and the mean diameters of CNTs used FeAlO14 substrate obtained as a result

Sample Name	T(^{o}C)	Pretreatment(min.) H_2/CO_2		CO_2(p)/CO_2(g) (sccm)	Mean Diameter (nm)
FeAlO14CNT772	760	15	5	10/2	10.5
FeAlO14CNT800	760	15	10	10/2	9.8
FeAlO14CNT860	770	15	5	10/8	9.5
FeAlO14CNT923	770	15	10	10/8	7.9

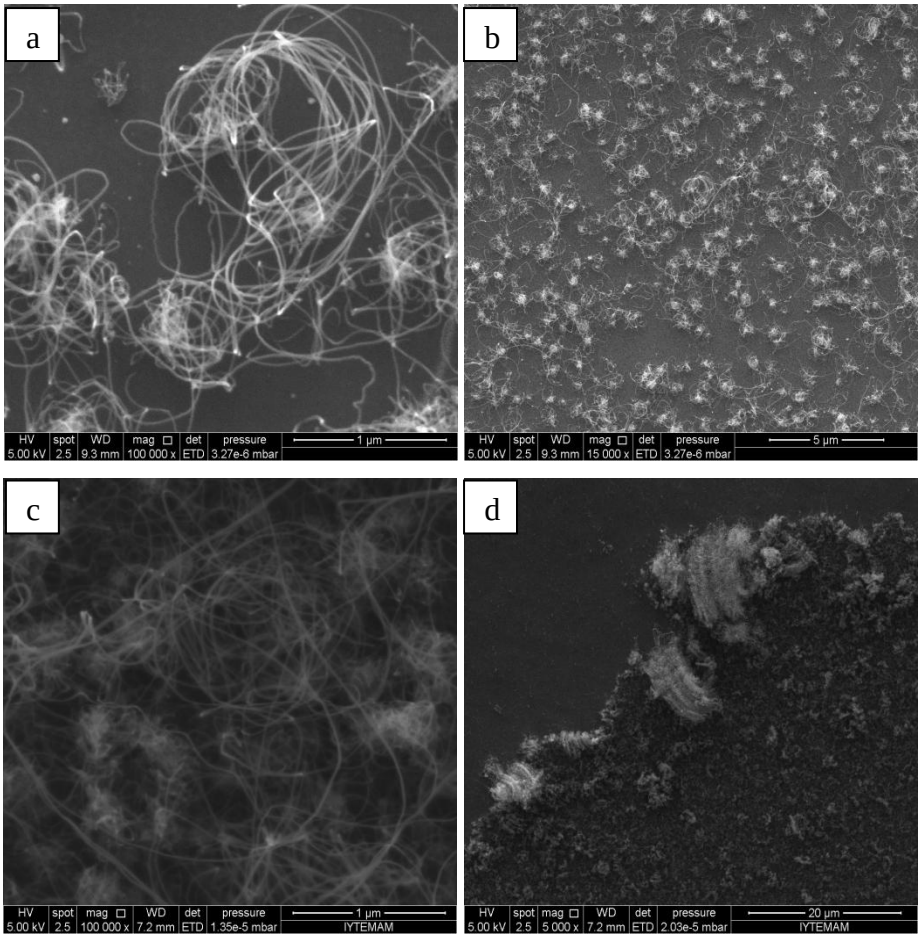

Figure 5.24. The growths with CO_2 (CO_2(p)/CO_2(g): 10/8) at 770 ºC: a), b) FeAlO14 CNT860, 5min. c), d) FeAlO14 CNT923, 10 min.

Due to the lack of FeAlO14 substrates for different pretreatment durations (5 and 10 min.) of CO_2, single value of 10/2 sccm at 760 ºC and single value of 10/8 sccm at 770 ºC are analyzed. Under these conditions, it can be seen that the mean diameter decreases while the duration increases (Table 5.13). For the related SEM results, the different durations at 770 ºC are chosen due to the smaller mean diameters. The SEM results in Figure 5.24 show that if CO_2 is kept longer than that of H_2, the sample becomes more densely populated. According to Figure 5.25, the numbers of CNTs at the mean diameters (9.5 and 7.9 nm) at 10/8 sccm at 770 ºC with the duration of 5 and 10 min. are 32 out of 63 and 24 out of 76, respectively.

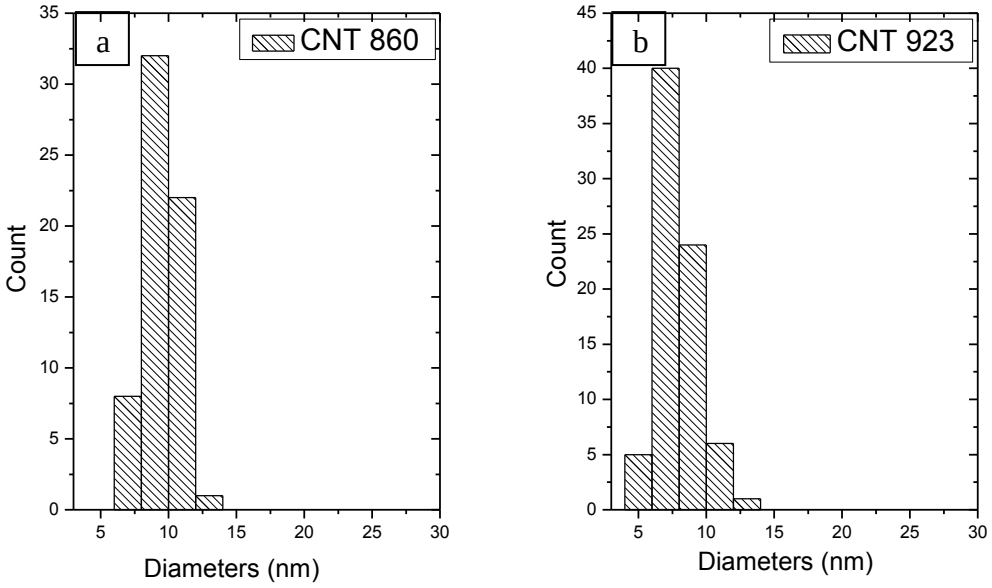

Figure 5.25. The diameter distributions of CNTs at different pretreatment time of CO_2 at 770 ºC: a) CO_2(p)/CO_2(g): 10/8, 5 min. b) CO_2(p)/CO_2(g): 10/8, 10 min.

Table 5.14. The amounts of CO_2 used during various pretreatment and growth times and the mean diameters of CNTs used FeAlO15 substrate obtained as a result

Sample Name	T(^{o}C)	Pretreatment(min.) H_2/CO_2		CO_2(p)/CO_2(g) (sccm)	Mean Diameter (nm)
FeAlO15CNT787	750	15	5	8/2	8.2
FeAlO15CNT846	750	15	10	8/2	10.4
FeAlO15CNT783	760	15	5	8/2	9.3
FeAlO15CNT779	760	15	10	8/2	8.3
FeAlO15CNT773	760	15	5	10/2	8.7
FeAlO15CNT801	760	15	10	10/2	9.4

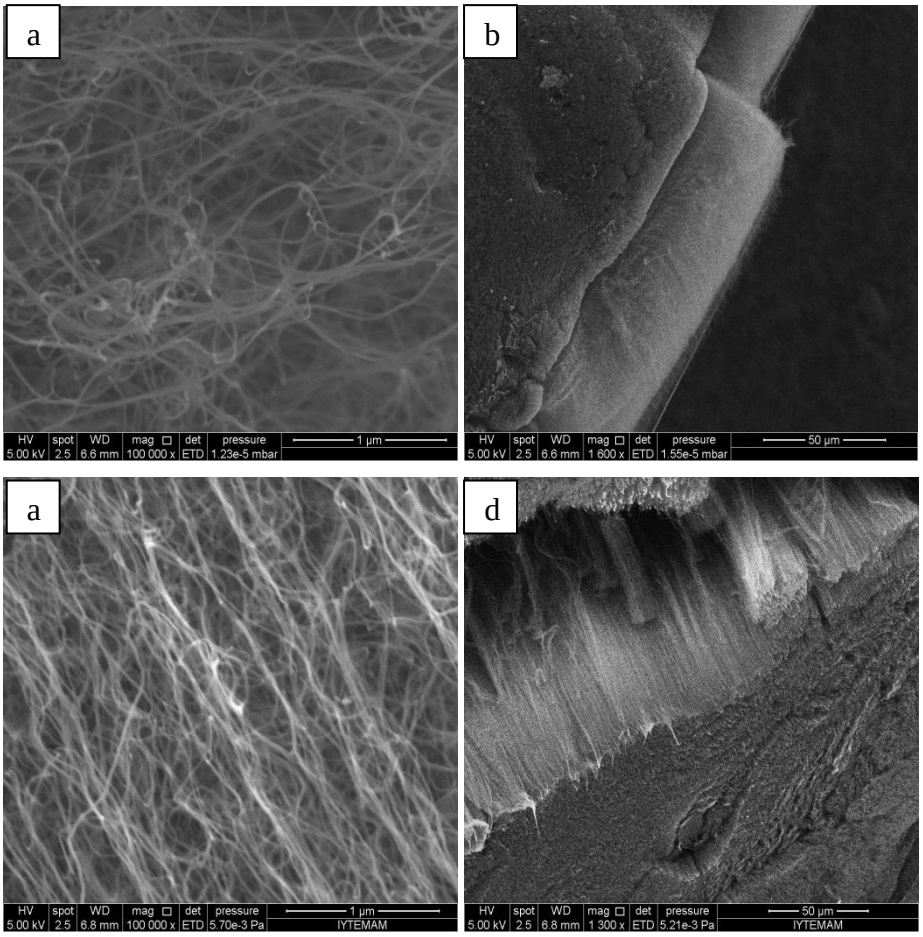

Figure 5.26. The growths with CO_2 (CO_2(p)/CO_2(g): 8/2) at 760 ºC: a), b) FeAlO15 CNT783, 5min. c), d) FeAlO15 CNT779, 10 min.

Due to the lack of FeAlO15 substrates for different pretreatment durations (5 and 10 min.) of CO_2, single value of 8/2 sccm at 750 ºC; the values of 8/2 sccm and 10/2 sccm at 760 ºC are examined. Under these conditions, the changes in diameters are given in Table 5.13. The SEM results in Figure 5.26 indicate that when CO_2 is kept longer than that of H_2 at 8/2 sccm at 760 ºC, CNTs become vertical aligned. According to Figure 5.27, the numbers of CNTs at the mean diameters (9.3 and 8.3 nm) at 8/2 sccm at 760 ºC with the duration of 5 and 10 min. are 37 out of 59 and 39 out of 82, respectively.

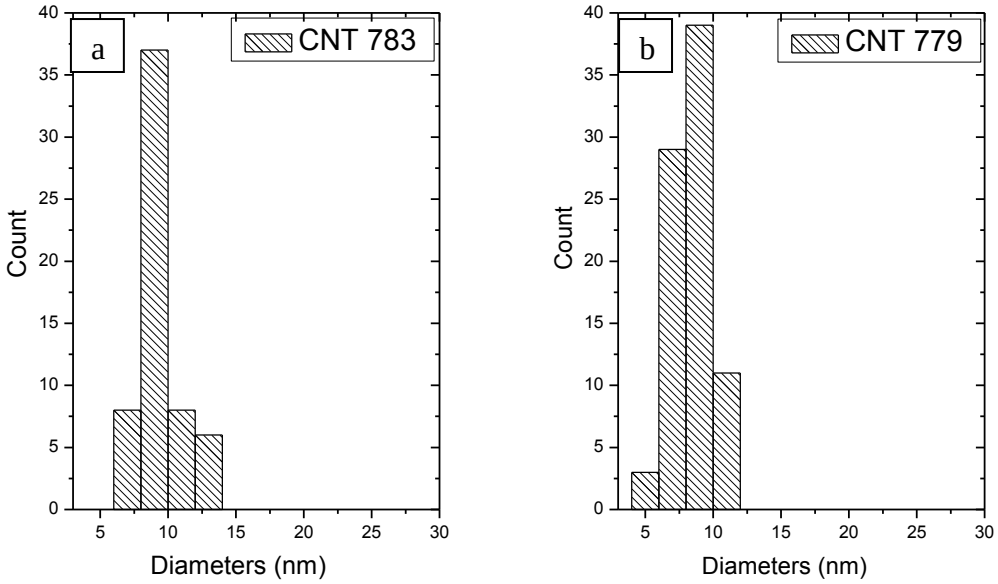

Figure 5.27. The diameter distributions of CNTs at different pretreatment time of CO_2 at 760 ºC: a) CO_2(p)/CO_2(g): 8/2, 5 min. b) CO_2(p)/CO_2(g): 10/8, 10 min.

Table 5.15. The amounts of CO_2 used during various pretreatment and growth times and the mean diameters of CNTs used FeAlO16 substrate obtained as a result

Sample Name	T(^{o}C)	Pretreatment(min.) H_2/CO_2		CO_2(p)/CO_2(g) (sccm)	Mean Diameter (nm)
FeAlO16CNT871	750	15	5	10/10	9.4
FeAlO16CNT926	750	15	10	10/10	8.9
FeAlO16CNT869	760	15	5	10/10	9.9
FeAlO16CNT873	760	15	10	10/10	9.3
FeAlO16CNT933	770	15	5	10/10	8.7
FeAlO16CNT929	770	15	10	10/10	7.9

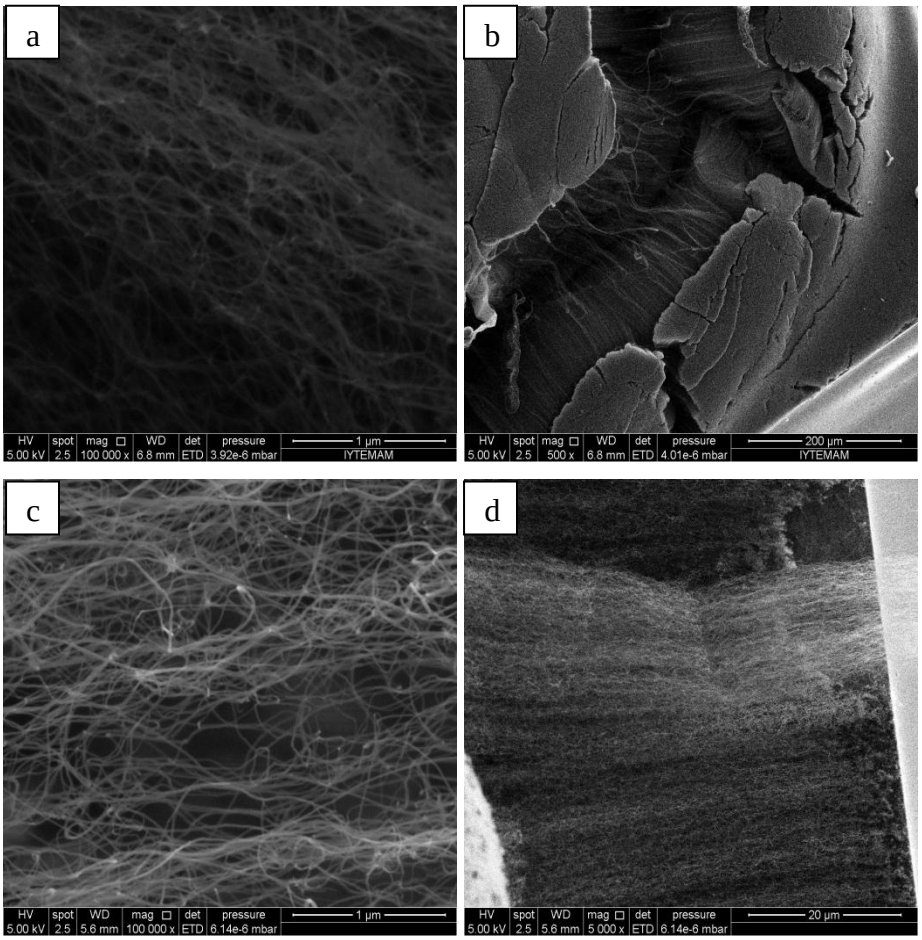

Figure 5.28. The growths with CO_2 (CO_2(p)/CO_2(g): 10/10) at 770 ºC: a), b) FeAlO16 CNT933, 5min. c), d) FeAlO16 CNT929, 10 min.

Table 5.15 displays that if the duration of CO_2 is kept longer than that of H_2 at the pretreatment stage for 10/10 sccm CO_2, the mean diameters of CNTs using FeAlO16 substrate decrease at all the three growth temperatures. For the related SEM results, the different durations at 770 ºC are chosen due to the smaller mean diameters. When the SEM results given in Figure 5.28 are analyzed, if CO_2 is kept longer than that of H_2, the CNTs become more densely populated. According to Figure 5.29, the numbers of CNTs at the mean diameters (8.7 and 7.9 nm) at 10/10 sccm at 770 ºC with the duration of 5 and 10 min. are 40 out of 70 and 44 out of 86, respectively.

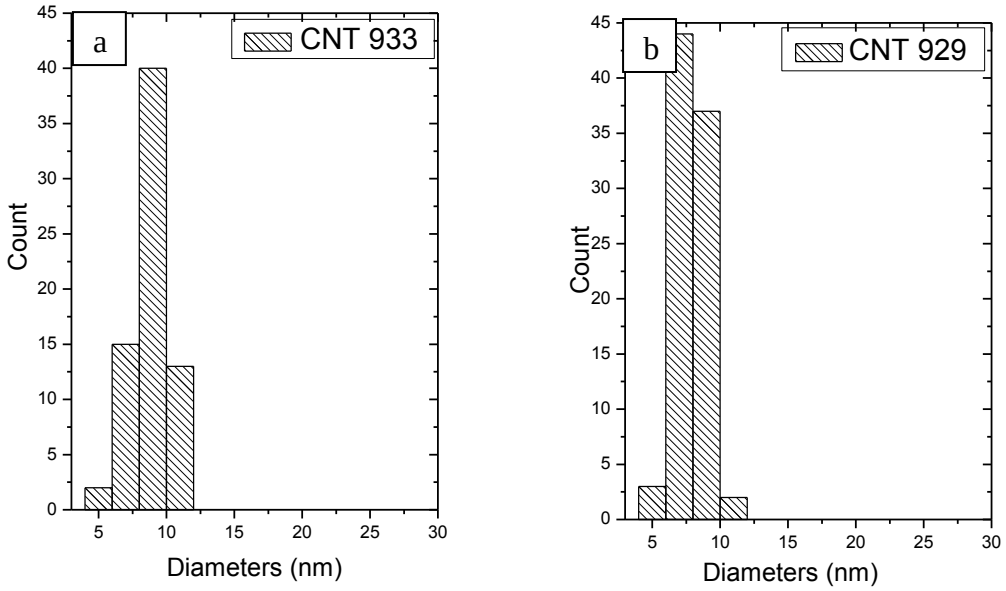

Figure 5.29. The diameter distributions of CNTs at different pretreatment time of CO_2 at 770 ºC: a) CO_2(p)/CO_2(g): 10/10, 5 min. b) CO_2(p)/CO_2(g): 10/10, 10 min.

Table 5.16. The amounts of CO_2 used during various pretreatment and growth times and the mean diameters of CNTs used FeAlO17 substrate obtained as a result

Sample Name	T(^{o}C)	Pretreatment(min.) H_2/CO_2		CO_2(p)/CO_2(g) (sccm)	Mean Diameter (nm)
FeAlO17CNT872	750	15	5	10/10	11.4
FeAlO17CNT927	750	15	10	10/10	9.7
FeAlO17CNT870	760	15	5	10/10	8.6
FeAlO17CNT874	760	15	10	10/10	7.6

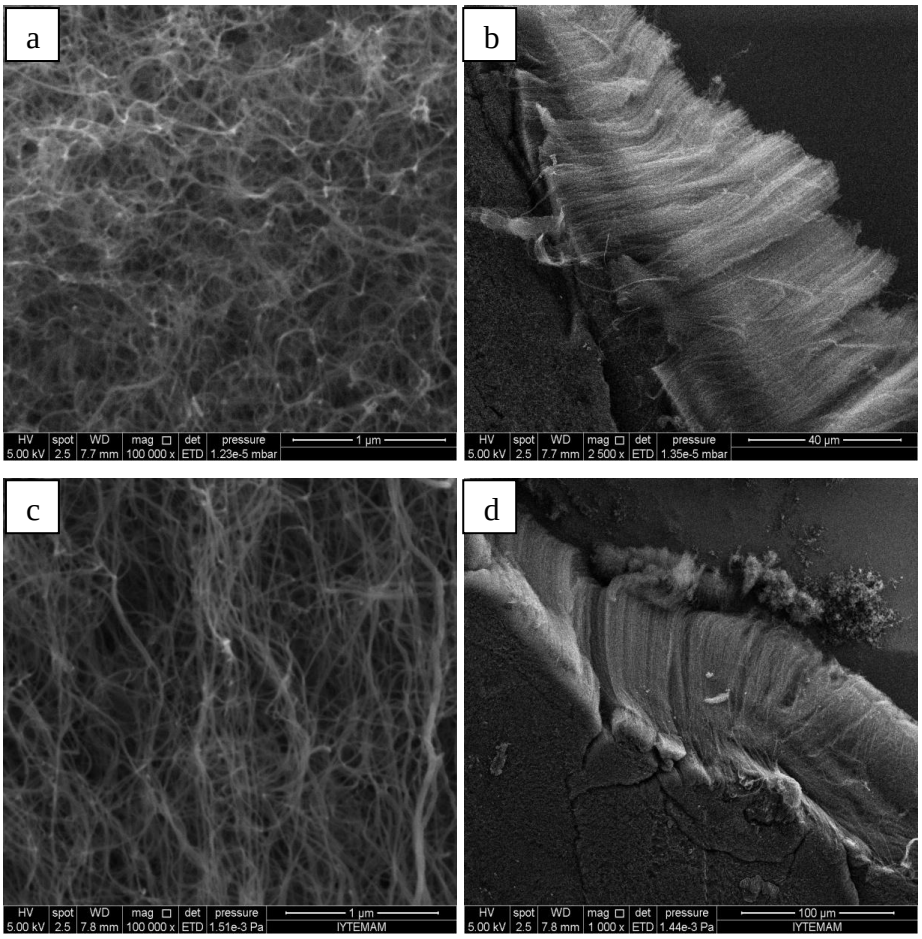

Figure 5.30. The growths with CO_2 (CO_2(p)/CO_2(g): 10/10) at 760 °C: a), b) FeAlO17 CNT870, 5min. c), d) FeAlO17 CNT874, 10 min.

The results of experiments using FeAlO17 substrate indicate the decreasing of the mean diameter with the increasing of 10/10 sccm CO_2 duration than that of H_2 at the pretreatment process at 750 °C and 760 °C (Table 5.16). For the related SEM results, the different durations at 760 ºC are chosen due to the smaller mean diameters. SEM results are displayed in Figure 5.30. If CO_2 is kept longer than that of H_2, the CNTs become more densely populated. According to Figure 5.31, the numbers of CNTs at the mean diameters (8.6 and 7.6 nm) at 10/10 sccm at 760 ºC with the duration of 5 and 10 min. are 22 out of 39 and 29 out of 73, respectively.

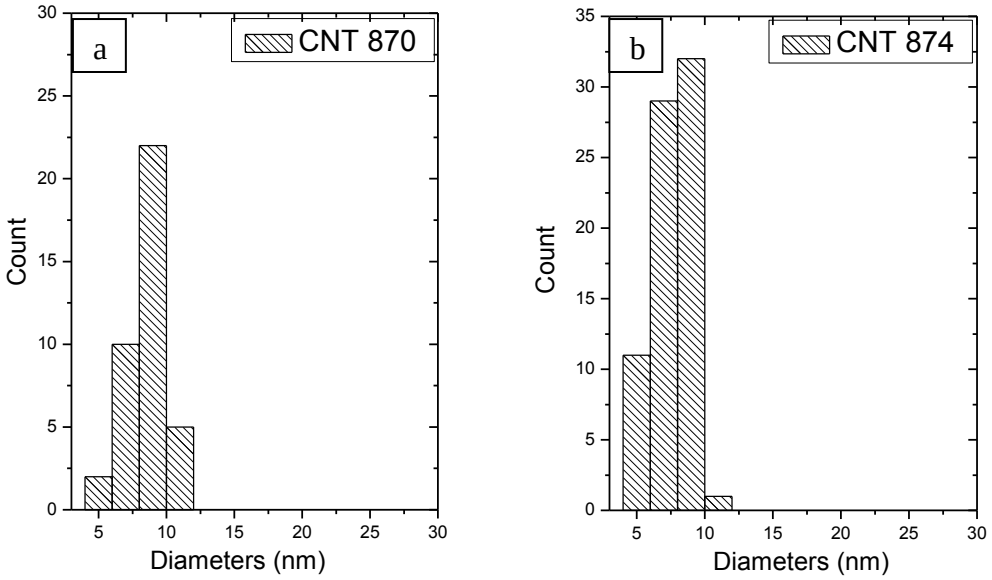

Figure 5.31. The diameter distributions of CNTs at different pretreatment time of CO_2 at 760 °C: a) CO_2(p)/CO_2(g): 10/10, 5 min. b) CO_2(p)/CO_2(g): 10/10, 10 min.

5.2.2. STEM Results

STEM detector was used to measure outer and inner radius of the CNT grown and determine the diameter of SWNTs and MWNTs.

The CNT shown in Figure 5.32 is MWNT. However, this is not a general result because there is only limited number of SEM results with the STEM detector.

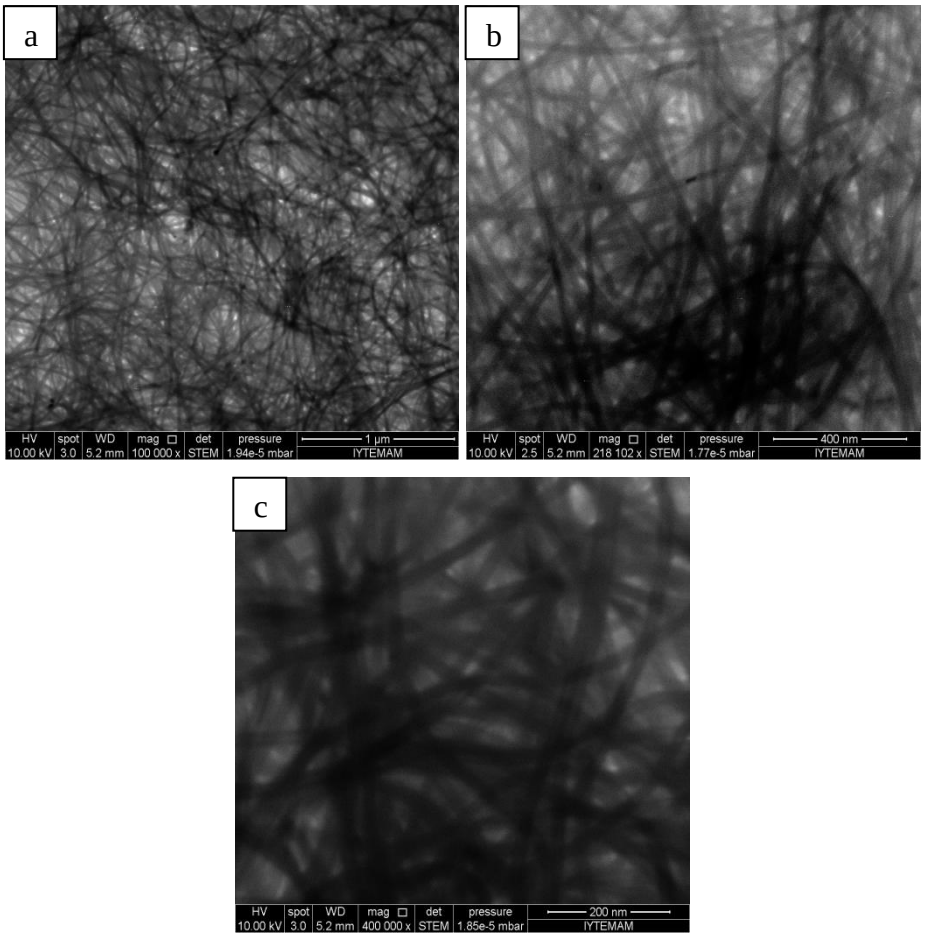

Figure 5.32. SEM micrographs taken by STEM detector of FeAlO12 CNT771 produced at 760 °C, CO_2(p)/CO_2(g):10/2, 5 min. a) 1 µm scale, b) 400 nm scale, c) 200 nm scale

The STEM images of the CNT in Figure 5.32.b show that the mean diameter was measured as 10.11 nm. For the same CNT evaluated from SEM image, the mean diameter was found as 8.9 nm (Table 5.2).

5.2.3. Raman Spectroscopy Results

Raman Spectroscopy with Ar^+ ion laser with the excitation wavelength of 488 nm was used to examine the quality and type of the CNTs grown in the experiments.

The disorder-induced D peak, which is a sign of the presence of defects, is at nearly 1350 cm^{-1}. The other one, tangential G peak, is at nearly 1580 cm^{-1}. Moreover,

for SWNTs, there is a third mode, which is called RBM, is related to the diameter of them.

The ratio of D line to G line intensity provides a good index for showing the presence of defects and also the quality of the CNTs. Figure 5.33 - Figure 5.36 demonstrate Raman signals coming from the sample. When the Raman spectras of the samples are analyzed, the intensity of D peak is always smaller compared with that of G peak. This intensity ratio shows that CNTs have small amount of defects in their structure. Hence, to have similar intensity of the two peaks indicate that CNTs have high structural quality.

The relationship between relative intensity ratio of the D band to G band and the growth conditions is given in Table 5.17.

Table 5.17. The growth conditions and intensity ratio of the D band to the G band

Sample Name	T(^{o}C)	Pretreatment (min.) H_2/CO_2	CO_2(p)/ CO_2(g) (sccm)	Deconvolated Raman Peaks		Quality of Fits (R^2)	Intensity D/G
				Center	Height		
FeAlO15 CNT846	750	15/10	8/2	1347.2	2045	0.996	0.817
				1574.4	2500.2		
				1618.3	630		
FeAlO16 CNT911			10/2	1358.9	2057.6	0.997	0.575
				1582	3576.4		
				1618.1	481		
FeAlO17 CNT912				1358	1492.4	0.996	0.727
				1582.3	2050.8		
				1617.8	378		
FeAlO18 CNT913				1357.7	1302.9	0.996	0.629
				1581.1	2069.1		
				1617.1	314.4		
FeAlO16 CNT921			10/8	1348.5	1108.3	0.995	0.631
				1573.2	1755.6		
				1617.8	320.5		
FeAlO17 CNT922				1353	2682.2	0.996	0.562
				1575.6	4772.2		
				1611.4	555.3		

(cont. on next page)

Table 5.17. (cont.)

FeAlO18 CNT928	750	15/10	10/10	1349.4	1561	0.996	0.699
				1576	2230.4		
				1620.9	409.7		
FeAlO15 CNT840		15/5	10/2	1347.6	1697.6	0.995	0.802
				1573.3	2116		
				1616.7	514.1		
FeAlO15 CNT855			10/8	1348.5	1792.8	0.996	0.514
				1572.4	3481.5		
				1616.1	678.9		
FeAlO16 CNT871			10/10	1355.5	1905.8	0.995	0.758
				1580.6	2512		
				1616.3	439.7		
FeAlO17 CNT872				1354.3	1627.4	0.994	0.854
				1579.9	1905.2		
				1615.3	388.5		
FeAlO15 CNT779	760	15/10	8/2	1348.6	2011.5	0.998	0.849
				1572	2366.9		
				1609.2	398.5		
FeAlO16 CNT865			10/8	1351.6	659.5	0.99	0.894
				1576.4	737.1		
				1607.5	187.97		
FeAlO17 CNT874			10/10	1356.9	2487.6	0.995	0.709
				1580.7	3507.7		
				1617.2	681.9		
FeAlO16 CNT873				1358	2263.9	0.997	0.689
				1581.9	3282.3		
				1619.1	485.2		
FeAlO12 CNT781		15/5	8/2	1346.6	1252.7	0.996	0.634
				1570.6	1974.5		
				1614.4	427.5		
FeAlO14 CNT782				1350.5	1494.7	0.997	0.741
				1573.8	2014.7		
				1608.2	478.1		
FeAlO15 CNT783				1347.6	1390.8	0.994	0.907
				1572.6	1532.1		
				1614.5	403.1		

(cont. on next page)

Table 5.17. (cont.)

FeAlO15 CNT773	760	15/5	10/2	1347.5	2077	0.996	0.63
				1572.5	3296.4		
				1616.1	811.4		
FeAlO12 CNT771				1355.3	341.6	0,994	0.59
				1577.3	578.9		
				1606.2	122.9		
FeAlO15 CNT858			10/8	1347.5	1485.6	0.997	0.8
				1571.2	1854.9		
				1606.8	289.8		
FeAlO14 CNT857				1352.9	3390.9	0.997	0.465
				1575.8	7284.8		
				1610	913.3		
FeAlO16 CNT869			10/10	1353.39	1005.84	0.994	0.751
				1577.34	1338.38		
				1610.49	241.936		
FeAlO18 CNT901	770	15/10	8/2	1353.9	1392.8	0.995	0.61
				1577.3	2282.3		
				1609.5	403,4		
FeAlO17 CNT919			10/2	1355.61	1902.06	0.993	0.794
				1580.75	2393.77		
				1614.12	450.745		
FeAlO16 CNT924			10/8	1348.08	1132.19	0.994	0.742
				1573.22	1524.14		
				1605.28	308.788		
FeAlO16 CNT929			10/10	1352.5	1149	0.994	0.591
				1576.7	1942.6		
				1619.7	388.4		
FeAlO14 CNT860		15/5	10/8	1357.9	1253.3	0.996	0.93
				1579.7	1347.5		
				1609.8	445.4		
FeAlO15 CNT861				1355.8	1601.2	0.996	0.674
				1579.5	2374.9		
				1614.6	373.8		
FeAlO16 CNT933			10/10	1349.3	1496.9	0.997	0.565
				1571.7	2645.8		
				1606.6	296.9		

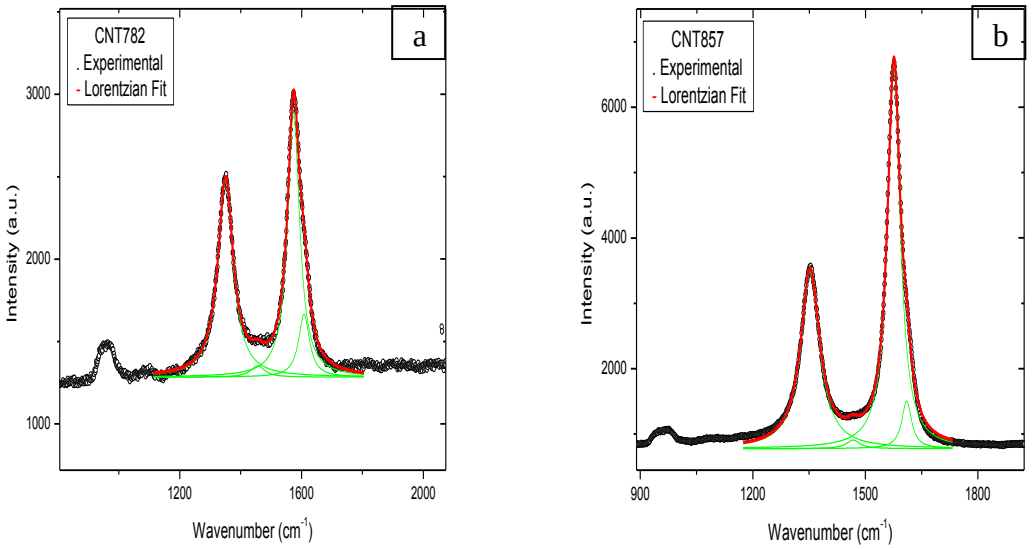

Figure 5.33. Raman spectra of CNTs grown at 760 °C: a) FeAlO14 CNT782, CO_2(p)/CO_2(g): 8/2, 5 min. b) FeAlO14 CNT857, CO_2(p)/CO_2(g): 10/8, 5 min.

For FeAlO14 substrate, Raman spectra of CNTs grown at 760 ºC with two different CO_2 flow rates (8/2 and 10/8) during 5 min. are given in Figure 5.33. In Raman spectra of CNT782, the D peak and G peak are observed at 1350 cm^{-1} and 1573 cm^{-1}, respectively. However, in Raman spectra of CNT857, the D peak and G peak are observed at 1352 cm^{-1} and 1575 cm^{-1}, respectively. When CO_2 flow rate decreases from 8/2 to 10/8, intensity ratio of the D band to G band decreases from 0.7 to 0.4. In addition, it can be said that D peak and G peak are shifted to right.

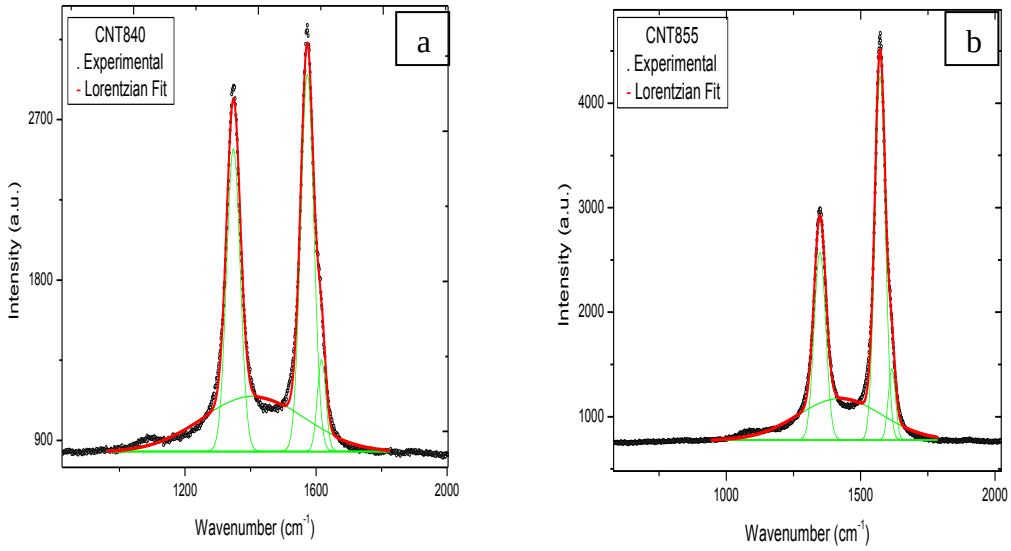

Figure 5.34. Raman spectra of CNTs grown at 750 °C: a) FeAlO15 CNT840, CO_2(p)/CO_2(g): 10/2, 5 min. b) FeAlO15 CNT855, CO_2(p)/CO_2(g): 10/8, 5 min.

For FeAlO15 substrate, Raman spectra of CNTs grown at 750 ºC with two different CO_2 flow rates (10/2 and 10/8) during 5 min. are displayed in Figure 5.34. In Raman spectra of CNT840, the D peak and G peak are observed at 1347 cm^{-1} and 1573 cm^{-1}, respectively. However, in Raman spectra of CNT855, the D peak and G peak are observed at 1348 cm^{-1} and 1572 cm^{-1}, respectively. When CO_2 flow rate decreases from 10/2 to 8/2, intensity ratio of the D band to G band decreases from 0.8 to 0.5. In addition, it can be said that D peak and G peak are not shifted, they are observed at the same point.

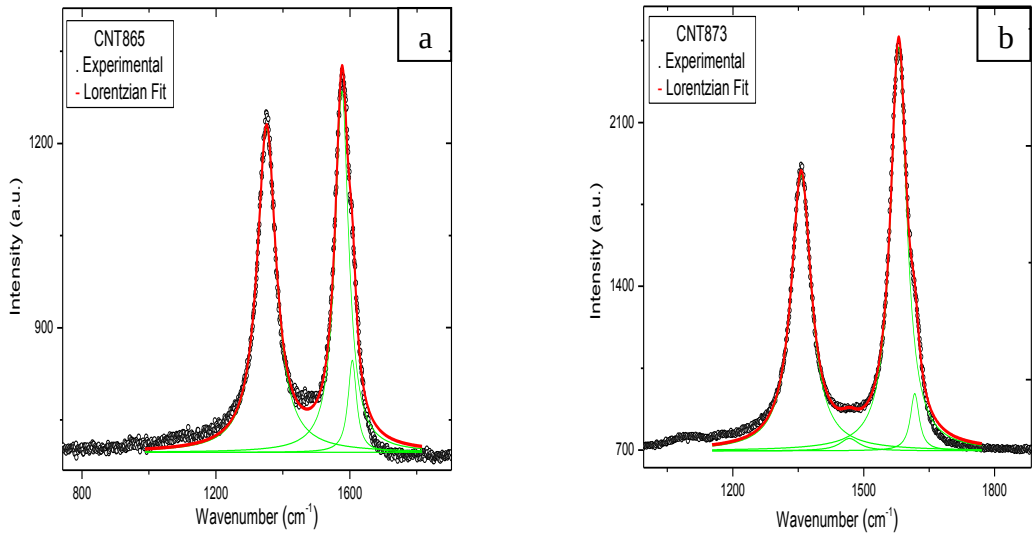

Figure 5.35. Raman spectra of CNTs grown at 760 °C: a) FeAlO16 CNT865, CO_2(p)/CO_2(g): 10/8, 10 min. b) FeAlO16 CNT873, CO_2(p)/CO_2(g): 10/10, 10 min.

For FeAlO16 substrate, Raman spectra of CNTs grown at 760 ºC with two different CO_2 flow rates (10/8 and 10/10) during 10 min. are given in Figure 5.35. In Raman spectra of CNT865, the D peak and G peak are observed at 1351 cm^{-1} and 1576 cm^{-1}, respectively. However, in Raman spectra of CNT873, the D peak and G peak are observed at 1358 cm^{-1} and 1581 cm^{-1}, respectively. When CO_2 flow rate decreases from 10/8 to 10/10, intensity ratio of the D band to G band decreases from 0.8 to 0.6. In addition, it can be said D peak and G peak are shifted to right.

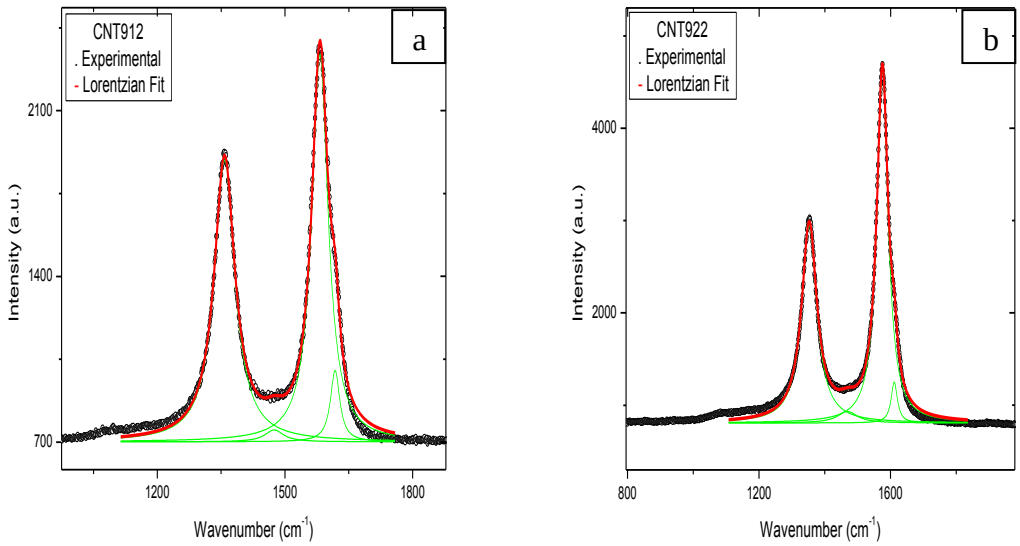

Figure 5.36. Raman spectra of CNTs grown at 750 °C: a) FeAlO17 CNT912, CO_2(p)/CO_2(g): 10/2, 10 min. b) FeAlO17 CNT922, CO_2(p)/CO_2(g): 10/8, 10 min.

For FeAlO17 substrate, Raman spectra of CNT912 and CNT922 grown at 750 ºC with two different CO_2 flow rates (10/2 and 10/8) during 10 min. are given in Figure 5.36. In Raman spectra of CNT912, the D peak and G peak are observed at 1358 cm^{-1} and 1582 cm^{-1}, respectively. However, in Raman spectra of CNT922, the D peak and G peak are observed at 1353 cm^{-1} and 1576 cm^{-1}, respectively. When CO_2 flow rate decreases from 10/2 to 10/8, intensity ratio of the D band to G band decreases from 0.7 to 0.5. In addition, it can be said D peak and G peak are shifted to left.

All the Raman analysis of CNTs given above reveal that when CO_2 flow rate decreases in growth, intensity of D band and G band increase, as a result of which the D/G peak ratio decreases and the concentration of amorphous carbon near the catalyst surface increases.

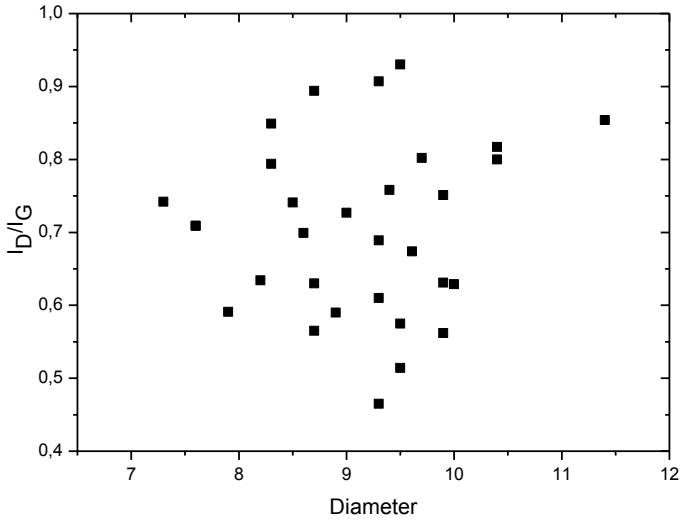

Figure 5.37. The variation of CNT diameters as a function of I_D/I_G

Figure 5.37 shows that the D/G peak ratio is proportional to the diameter of CNTs, roughly.

5.3. Dependence of Diameters of CNTs on Growth Temperature, Pretreatment Time and CO_2 Flow Rates

The role of CO_2 in the CNT growth with TCVD technique by ethylene decomposition has been investigated by changing growth temperature, pretreatment time, amount of CO_2, the ratio of CO_2 in pretreatment to that of in growth using the thin Fe film sputtered on SiO_2/Si substrates (FeAlO12, FeAlO14, FeAlO15, FeAlO16, FeAlO17). Figure 5.38 – Figure 5.42 indicate the variation of mean diameters of CNTs of all substrates used in the experiments as a function of pretreatment time-growth temperature and CO_2 amount-growth temperature.

It is estimated that C reacts with O_2 to form CO because of metal-oxide form of catalyst particle. If proper pretreatment and growth parameters are not used for metal catalyst particle, amorphous carbon forms instead of CNT growth on the catalyst surface. The catalyst particle loses its functionality due to the amorphous carbon coverage. It is expected that the catalyst film easily coalescences to form nano particles with the effect of temperature and H_2 and these particles uniformly spread over the

whole face. The formed catalyst particles are mobile and can form larger clusters with the effect of high temperature when they are in the elemental form and they occur very fast especially on SiO_2 layer.

It is required that the catalyst particles have small size and narrower distribution for an effective CNT growth. Large nano particles are not very effective for CNT growth, and at the same time decrease the density of CNTs per unit area. The amounts of H_2 and CO_2 play significant roles in this process.

The coalescence happens after metal-oxide film converts to metal film. The function of CO_2 in pretreatment stage is to adjust the reduction rate of already oxidized Fe (due to exposure to the air) and reduce mobility of the reduced Fe nano particles on the surface to prevent larger particle formation. In addition, CO_2 keeps catalyst particle functioning in the growth process by removing amorphous carbon coverage on them.

If the duration of CO_2 is kept longer than that of H_2 at the pretreatment stage, the CNT mean diameter decreases and diameter distribution becomes narrower. This decreasing in the CNT density can be explained by catalyst particles' forming smaller particles.

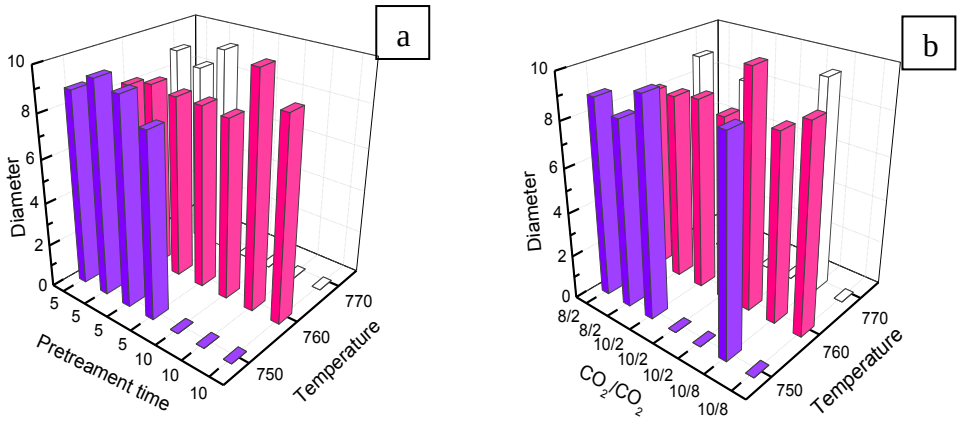

Figure 5.38. The variation of mean diameters of CNTs used FeAlO12 substrate as a function of a) pretreatment time and growth temperature, b) CO_2 amount and growth temperature

According to Figure 5.38a, at 750 ºC and 770 ºC, the minimum diameters are obtained as 8.35 nm and 8.48 nm, respectively at the end of 5 min. pretreatment time while the minimum diameter is obtained as 8.2 nm at the end of 10 min. pretreatment time at 760 ºC.

According to Figure 5.38b, the minimum diameter is obtained as 8.35 nm at 750 ºC at the rate of 8/2; while the minimum diameters are obtained as 8.2 nm at 760 ºC and 8.48 nm at 770 ºC at the rate of 10/2.

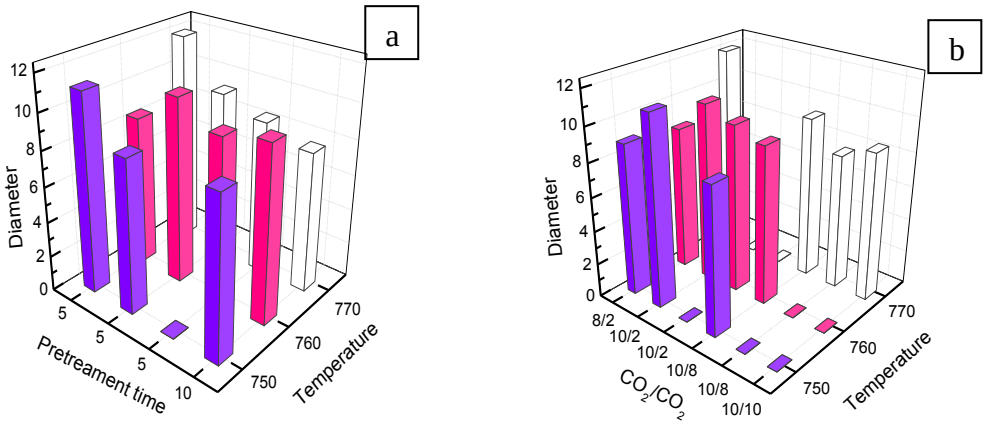

Figure 5.39. The variation of mean diameters of CNTs used FeAlO14 substrate as a function of a) pretreatment time and growth temperature, b) CO_2 amount and growth temperature

According to Figure 5.39a, at 750 ºC and 760 ºC, the minimum diameters are obtained as 8.65 nm and 8.56 nm, respectively at the end of 5 min. pretreatment time; while the minimum diameter is obtained as 7.97 nm at the end of 10 min. pretreatment time at 770 ºC.

According to Figure 5.39b, the minimum diameters are obtained as 8.65 nm at 750 ºC and 7.97 nm at 770 ºC at the rate of 10/8; while the minimum diameter is obtained as 8.56 nm at the rate of 8/2 at 760 ºC.

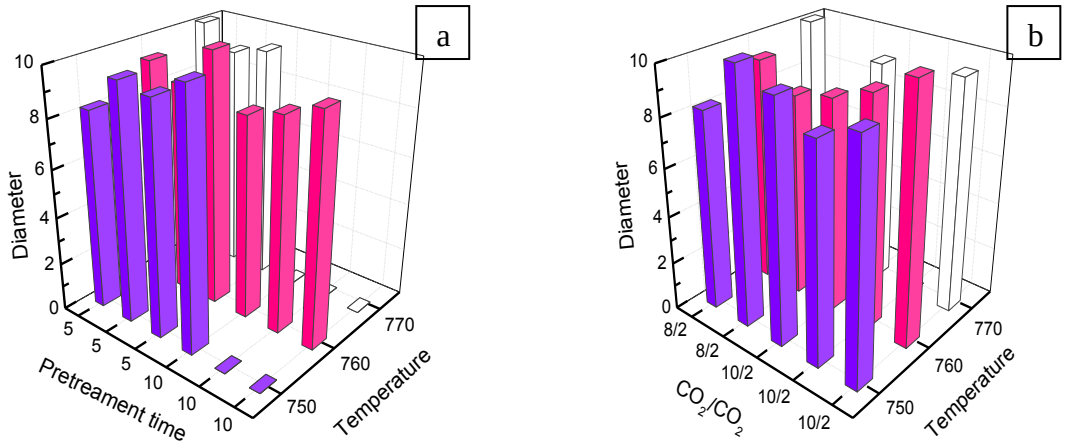

Figure 5.40. The variation of mean diameters of CNTs used FeAlO15 substrate as a function of a) pretreatment time and growth temperature, b) CO_2 amount and growth temperature

According to Figure 5.40a, at 750 ºC and 770 ºC, the minimum diameters are obtained as 8.27 nm and 9.24 nm, respectively at the end of 5 min. pretreatment time; while the minimum diameter is obtained as 8.39 nm at the end of 10 min. pretreatment time at 760 ºC.

According to Figure 5.40b, the minimum diameters are obtained as 8.27 nm, 8.39 nm and 10.14 nm at 750 ºC, 760 ºC and 770 ºC, respectively at the rate of 8/2.

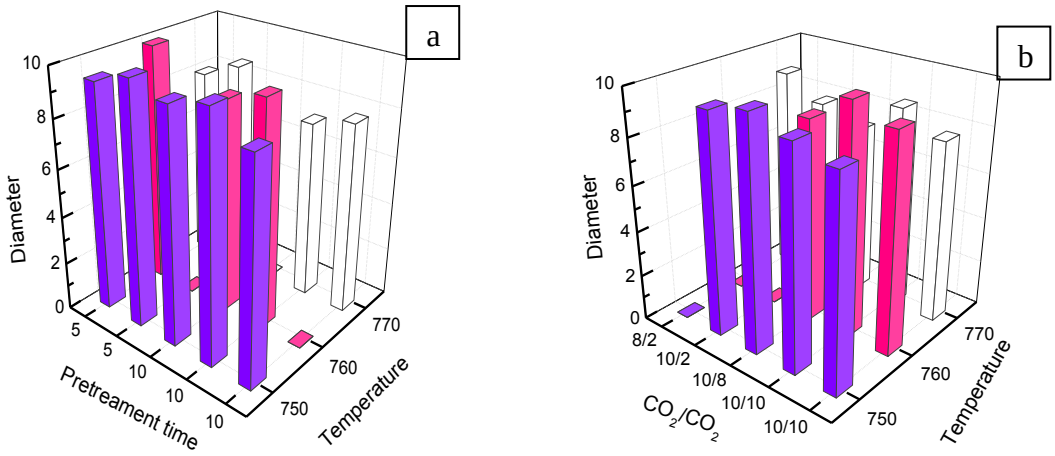

Figure 5.41. The variation of mean diameters of CNTs used FeAlO16 substrate as a function of a) pretreatment time and growth temperature, b) CO_2 amount and growth temperature

According to Figure 5.41a, at 750 ºC, 760 ºC and 770 ºC, the minimum diameters are obtained as 8.96 nm, 8.78 nm and 7.39 nm, respectively at the end of 10 min. pretreatment time.

According to Figure 5.41b, the minimum diameter is obtained as 8.96 nm 750 ºC at the rate of 10/10; while the minimum diameters are obtained as 8.78 nm and 7.39 nm at 760 ºC and 770 ºC, respectively at the rate of 10/8.

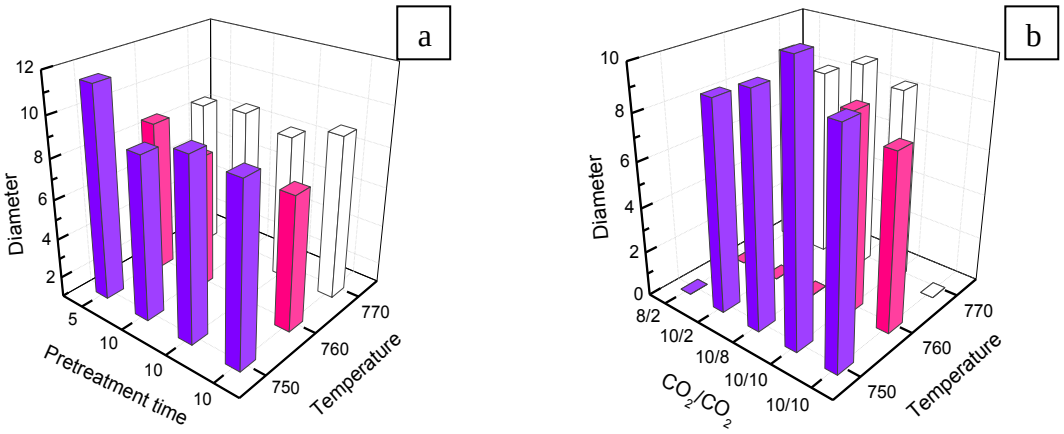

Figure 5.42. The variation of mean diameters of CNTs used FeAlO17 substrate as a function of a) pretreatment time and growth temperature, b) CO_2 amount and growth temperature

According to Figure 5.42a, at 750 ºC, 760 ºC and 770 ºC, the minimum diameters are obtained as 9.08 nm, 7.67 nm and 8.32 nm, respectively at the end of 10 min. pretreatment time.

According to Figure 5.42b, the minimum diameters are obtained as 9.08 nm at 750 ºC and 8.32 nm at 770 ºC at the rate of 10/2; while the minimum diameter is obtained as 7.67 nm at 750 ºC at the rate of 10/10.

5.4. Statistical Analysis Results

As a final step, all data have been analyzed through a statistical analysis, including standard deviation, standard error, kurtosis variations and skewness variations of the samples grown by utilizing CO_2. The so-called analysis results are represented in Figure 5.43a, b and Figure 5.44a, b.

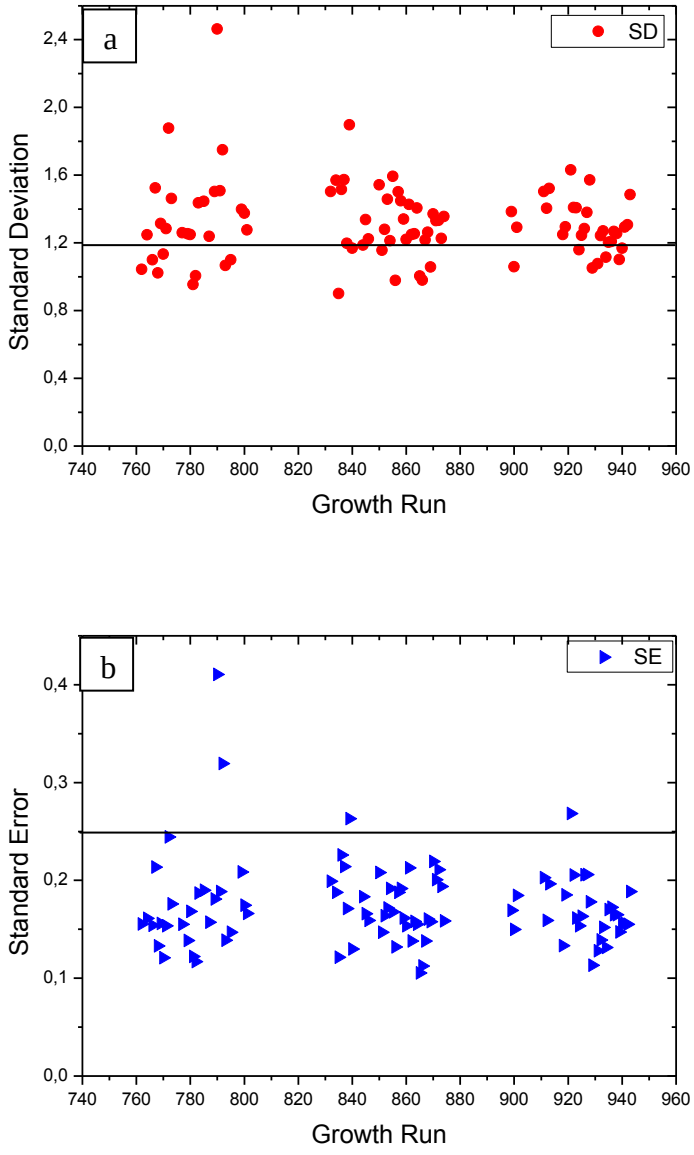

Figure 5.43. a) Standard deviation b) Standard error as CNT sequence of the samples grown by utilizing CO_2

When standard deviations (Figure 5.43a) and standard errors (Figure 5.43b) of the mean diameters are examined in detail; the growth sequence (CNT number) of all samples grown by utilizing CO_2 in this research is seen. It is shown that CNT diameters are span in a narrow interval. Standard deviations of all patterns are predominantly seen to be ranging from 1-1.6 nm. In addition to this narrow standard deviation interval, standard error of all the mean diameters is very small (~ 0.2 nm).

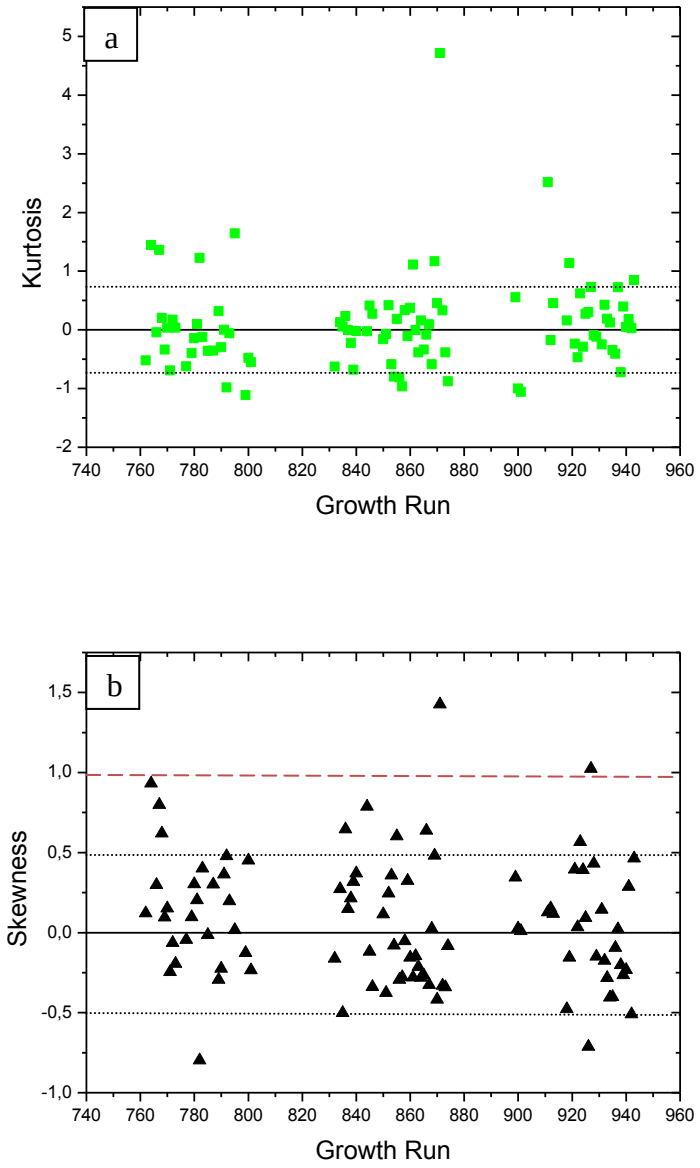

Figure 5.44. a) Kurtosis variations b) Skewness variations with CNT sequence of the samples grown by using CO_2

Kurtosis value is a descriptor of the shape of a probability distribution such as optimal positive value and optimal negative value. Kurtosis value variation of CNT sequence (Figure 5.44a) results that values are generally seen to be between +1 and -1. There are few smaller values than -1, whereas there are more values with kurtosis value larger than +1 and, thus, explaining narrow distributions. While diameter distributions are necessary for Gauss distribution is normally expected, these high positive kurtosis values are indication that CNT diameters are within narrow range of mean diameters.

In addition skewness values are generally seen to be between +0.5 and -0.5 (Figure 5.44b). There are four smaller values than -0.5, whereas there are two values with kurtosis value larger than +1.

As the correlation between these statistical data examined, no correlation between standard deviation and kurtosis (0.02) and a large positive correlation between standard deviation and standard error (0.87) are seen. In addition, a small positive correlation between skewness and kurtosis (0.32), standard deviation and skewness (0.14) are seen.

CHAPTER 6

CONCLUSIONS

In this work, the purpose was to investigate the effects of weak oxidizers (O_2, H_2O and CO_2) on CNTs grown on $Si/SiO_2/Al_2O_3$ substrates using different Fe thin film catalyst (FeAlO12, FeAlO14, FeAlO15, FeAlO16 and FeAlO17) by thermal CVD method during both pretreatment and growth duration. Due to the fact that CO_2 gave better results than the other two oxidizers in terms of CNT characteristics in the previous studies, CO_2 was used as oxidizer in the experiments. The reason for the use of CO_2 in the pretreatment process was to control the size of catalyst particle and in the growth process was to keep catalyst particle functioning throughout the growth time and to prevent amorphous carbon formation on the outer walls of CNTs. With these intentions, pretreatment time with oxidizer, the ratio of oxidizer in pretreatment to that of in growth and growth temperature were examined. Then, AFM, SEM and EDX were used to analyze catalyst thin films' structural properties. Moreover, the CNTs grown with CO_2 were evaluated with the help of SEM, STEM and Raman Spectroscopy to study their type, crystallinity and defect content.

There were two main goals for the study. The first one was to reduce the diameter by using oxidizer in pretreatment and growth processes and the other one was to control CNT diameters within very narrow diameter ranges. Nearly one hundred experiments were performed for these motivations. Ethylene was utilized as the carbon precursor, and its flow rate was kept constant at, 80 sccm for all growths. Ar gas at flow rate of 150 sccm was used as the carrier gas during the whole process of growth and also the sample was cooled to room temperature under Ar gas flow after the growth termination. CO_2 flow rates used during pretreatment and growth were 8:2, 10:2 10:8 and 10:10 (in unit of sccm). In addition, three different growth temperatures; 750 ^oC, 760 ^oC and 770 ^oC were studied. Different pretreatment times studied in the previous experiments showed that CNTs grown with 15 min. pretreatment time gave the best results. So pretreatment times were kept at 15 min. and CO_2 introduced in during pretreatment, 5 to 10 min. prior to the CNT growth in this work.

Very thin Fe films were grown on SiO_2/Si substrates with Al_2O_3 buffer layers. All Fe films intended to have similar thicknesses 1.5-2 nm. It is very well known that the film thickness have a major impact on the CNT diameters. Although there was a variation in CNT diameters for the growths carried on the different substrates, this change was not drastic and it could be said that the Fe film thickness was not an important factor in the observed diameter change. On the contrary, growth parameters are the main important parameters deciding diameters for the experiments.

From extensive statistical data we observe that most of the CNT diameters were within narrow range in the experiments performed with CO_2, which we believe due to positive oxidizer to keep metal catalyst sizes in a narrow range, therefore, resulted in an effective production of CNTs. However, CNTs with large diameters were obtained in some experiments indicating that, in some cases, positive effects of oxidizers were suppressed by growth parameters including the temperature. On the other hand, having larger diameters made the SEM analysis more trustworthy.

The results of experiments were evaluated with the statistical analysis including standard deviation, standard error, skewness and kurtosis. Several conclusions could be drawn from this analysis. Firstly, when the ratio of oxidizer in pretreatment to that of in growth was kept small, standard deviation was very narrow. Secondly, the CNTs grown with 15/5 min. pretreatment time (pretreatment time: 15 min., introduction of CO_2: 5 min., introduction of H_2: 10 min.) were seen to have wider standard deviation. Thirdly, the correlation between these statistical data yielded important results. There was no correlation between standard deviation and kurtosis (0.02). In addition, there was a small positive correlation between skewness and kurtosis (0.32), standard deviation and skewness (0.14). Furthermore, there was a large positive correlation between standard deviation and standard error (0.87), as expected, which showed that the statistical analysis were reliable. As the other result of evaluation, quite narrow standard deviations obtained for the diameters in this work are very important, since the diameter directly control most of the CNT properties. Even though CNTs grown in this work were mainly MWNTs, standard deviations were comparable with that of SWNT reported in the literature. STEM results of CNT diameters also supported this situation.

With the increasing temperature, skewnesses were seen to have larger positive values which mean that shifting to right. This shift indicated that the mobile catalyst particles formed larger clusters with the effect of high temperature when they were in the elemental form. Therefore, the optimum growth temperature was 760 °C.

It was shown that the importance of H_2 and CO_2 amounts and duration in the pretreatment and growth processes due to the fact that large nano particles are not very effective for CNT growth. Results indicated when CO_2 duration was kept shorter than that of H_2 at the pretreatment process of 15 min., CNTs grown had big diameters. This result further supported our initial hypothesis developed in this thesis work. According to the hypothesis, when CO_2 duration was kept longer than that of H_2 at the pretreatment process, CO_2 was shown to have a function in decreasing the negative effects of H_2.

REFERENCES

Amama, P.B., C.L. Pint, L. McJilton, S.M. Kim, E.A. Stach, P.T. Murray, R.H. Hauge, and B. Maruyama. 2009. Role of water in super growth of single-walled carbon nanotube carpets. *Nano Lett* 9:44-49.

Ando, Y., X. Zhao, T. Sugai, and M. Kumar. 2004. Growing carbon nanotubes. *Materials Today* 7:22-29.

Bachtold, A., P. Hadley, T. Nakanishi, and C. Dekker. 2001. Logic circuits with carbon nanotube transistors. *Science* 294:1317.

Baddour, C. and C. Briens. 2005. Carbon Nanotube Synthesis :a review R3. *Internation Journal of Chemical Reactor Engineering 3:20-22.*

Belin, T. and F. Epron. 2005. Characterization methods of carbon nanotubes: a review. *Materials Science and Engineering B* 119:105-118.

Bonard, J.M. 2006. Carbon nanostructures by hot filament chemical vapor deposition: growth, properties, applications. *Thin Solid Films* 501:8-14.

Bonard, J.M., P. Chauvin, and C. Clinke. 2002. *Nano Letters*. 2:665.

Cassell, A.M., J.A. Raymakers, J. Kong, and H. Dai. 1999. Large scale CVD synthesis of single-walled carbon nanotubes. *The Journal of Physical Chemistry B* 103:6484-6492.

Cheung, C.L., A. Kurtz, H. Park, and C.M. Lieber. 2002. Diameter-controlled synthesis of carbon nanotubes. *Journal of Physical Chemistry B* 106:2429-2433.

Chhowalla, M., K.B.K. Toe, C. Ducati, N.L. Rupesinghe, G.A.J. Amaratunga, A.C. Ferrari, D. Roy, J. Robertson, and W.I. Milne. 2001. *J. Appl.Phys* 90:5308.

Collins, P.G. and A. Zettl. 1997. Unique characteristics of cold cathode carbon-nanotube-matrix field emitters. *Physical Review B* 55:9391-9399.

Cui, H., G. Eres, J.Y. Howe, A. Puretkzy, M. Varela, D.B. Geohegan, and D.H. Lowndes. 2003. Growth behavior of carbon nanotubes on multilayered metal catalyst film in chemical vapor deposition. *Chemical Physics Letters* 374:222-228.

Dai, H. 2002. Carbon nanotubes: opportunities and challenges. *Surface Science* 500:218-241.

Dai, H., N. Franklin, and J. Han. 1998. Exploiting the properties of carbon nanotubes for nanolithography. *Applied Physics Letters* 73:1508-1510.

Darkrim, F.L., P. Malbrunot, and G. Tartaglia. 2002. Review of hydrogen storage by adsorption in carbon nanotubes. *International Journal of Hydrogen Energy* 27:193-202.

Deck, C.P., and K. Vecchio. 2006. Prediction of carbon nanotube growth success by the analysis of carbon-catalyst binary phase diagrams. *Carbon* 44:267-275.

Dresselhaus, M. and H. Dai. 2004. Carbon nanotubes: continued innovations and challenges. *MRS Bulletin* 29:237-243.

Dresselhaus, M., G. Dresselhaus, A. Jorio, A. Souza Filho, and R. Saito. 2002. Raman spectroscopy on isolated single wall carbon nanotubes. *Carbon* 40:2043-2061.

Dresselhaus, Mildred S., Gene Dresselhaus, and Phaedon Avouris, eds. 2001. *Carbon nanotubes: synthesis, structure, properties, and applications.* Berlin: Springer Publishers.

Dupuis, A.C. 2005. The catalyst in the CCVD of carbon nanotubes: a review. *Progress in Materials Science* 50(8):929-961.

Frackowiak, E., K. Metenier, V. Bertagna, and F. Beguin. 2000. Supercapacitor electrodes from multiwalled carbon nanotubes. *Applied Physics Letters* 77:2421-2423.

Futaba, D., K. Hata, T. Yamada, K. Mizuno, M. Yumura, and S. Iijima. 2005. Kinetics of Water-Assisted Single-Walled Carbon Nanotube Synthesis Revealed by a Time-Evolution Analysis. *Physical Review Letters* 95:056104-056107.

Futaba, D.N., J. Goto, S. Yasuda, T. Yamada, M. Yumura, and K. Hata. 2009. General rules governing the highly efficient growth of carbon nanotubes. *Advanced Materials* 21:4811-4815.

Futaba, D.N., K. Hata, T. Namai, T. Yamada, K. Mizuno, Y. Hayamizu, M. Yumura, and S. Iijima. 2006. 84% Catalyst activity of water-assisted growth of single walled carbon nanotube forest characterization by a statistical and macroscopic approach. *The Journal of Physical Chemistry B* 110:8035-8038.

Guo, T., P. Nikolaev, A. Thess, D. Colbert, and R. Smalley. 1995. Catalytic growth of single-walled manotubes by laser vaporization. *Chemical Physics Letters*. 243:49-54.

Harris, P.J.F. 2007. Solid state growth mechanisms for carbon nanotubes. *Carbon* 45:229-239.

Hart, A.J. and A.H. Slocum. 2006. Rapid growth and flow-mediated nucleation of millimeter-scale aligned carbon nanotube structures from a thin-film catalyst. *The Journal of Physical Chemistry B* 110:8250-8257.

Hasegawa, K. and S. Noda. 2011a. Millimeter-tall single-walled carbon nanotubes rapidly grown with and without water. *ACS Nano* 5:975-984.

Hasegawa, K. and S. Noda. 2011b. Moderating carbon supply and suppressing Ostwald ripening of catalyst particles to produce 4.5-mm-tall single-walled carbon nanotube forests. *Carbon* 49:4497-4504.

Hata, K., D.N. Futaba, K. Mizuno, T. Namai, M. Yumura, and S. Iijima. 2004. Water-assisted highly efficient synthesis of impurity-free single-walled carbon nanotubes. *Science* 306:1362-1365.

Hernadi, K., A. Fonseca, J. Nagy, D. Bernaerts, and A. Lucas. 1996. Fe-catalyzed carbon nanotube formation. *Carbon* 34:1249-1257.

Hofmann, S., G. Csanyi, A. Ferrari, M. Payne, and J. Robertson. 2005. Surface diffusion: the low activation energy path for nanotube growth. *Physical Review Letters* 95:36101.

Hornyak, G.L., J. Dutta, H. Tibbals, and A. Rao. 2008. *Introduction to nanoscience*. CRC Press Boca Raton, FL.

Hu, B., H. Ago, N. Yoshihara, and M. Tsuji. 2010. Effects of water vapor on diameter distribution of SWNTs grown over Fe/MgO-based catalysts. *The Journal of Physical Chemistry B 114*(9):3850–3856.

Huang, J., Q. Zhang, M. Zhao, and F. Wei. 2009. Process intensification by CO_2 for high quality carbon nanotube forest growth: Double-walled carbon nanotube convexity or single-walled carbon nanotube bowls? *Nano Research* 2:872-881.

Huang, S., M. Woodson, R. Smalley, and J. Liu. 2004. Growth mechanism of oriented long single walled carbon nanotubes using “fast-heating” chemical vapor deposition process. *Nano Letters* 4:1025-1028.

Iijima, S. 1991. Helical microtubules of graphitic carbon. *Nature* 354:56-58.

Iijima, S. and T. Ichihashi. 1993. Single-shell carbon nanotubes of 1 nm diameter. *Nature* 363:603-605.

In, J.B., C.P. Grigoropoulos, A. Chernov, and A. Noy. 2011. Hidden role of trace gas impurities in chemical vapor deposition growth of vertically-aligned carbon nanotube arrays *Applied Physics Letters*. 98:153102-153104.

Ivanov, V., J. B. Nagy, P. Lambin, A. Lucas, X.F. Zhang, and D. Bernaerts. 1994.The study of carbon nanotubules produced by catalytic method. *Chemical Physics Letters* 223:329-335.

Ivchenko, E.L. and B. Spivak. 2002. Chirality effects in carbon nanotubes. *Physical Review* B 66(15):155404-155413.

Jorio, A., G. Dresselhaus, and M.S. Dresselhaus. 2008. *Carbon nanotubes: advanced topics in the synthesis, structure, properties and applications.* Springer.

Joshi, M., Bhattacharyya, A., Wazed Ali, S. 2008. Characterization techniques for nanotechnology applications in textile. Indian Journal of Fibre & Textile Research 33:304-317.

Journet, C. and P. Bernier. 1998. Production of carbon nanotubes. *Applied Physics A* 67:1-9.

Jung, M., K. Yong Eun, J.K. Lee, Y.J. Baik, K.R. Lee, and J. Wan Park. 2001. Growth of carbon nanotubes by chemical vapor deposition. *Diamond and Related Materials* 10:1235-1240.

Kaufmann, D.R., and A. Star. 2008. Carbon nanotube gas and vapor sensors. *Angewandte Chemie International Edition* 47:6550-6570.

Kelly, P. and R. Arnell. 2000. Magnetron sputtering: a review of recent developments and applications. *Vacuum* 56:159-172.

Kim, S., C. Pint, and P.B. Amama. 2010. Evolution in catalyst morphology leads to carbon nanotube growth termination. *The Journal of Physical Chemistry B*. 1(6):918-922.

Kind, H., J.M. Bonard, C. Emmenegger, L.O. Nilsson, K. Hernadi, E.M. Schaller, L. Schlapbach, L. Forro, and K. Kern. 1999. *Adv.Mater* 11:1285-1289.

Kong, J., A.M. Cassell, and H. Dai. 1998. Chemical vapor deposition of methane for single-walled carbon nanotubes. *Chemical Physics Letters* 292:567-574.

Kong, J., N.R. Franklin, C. Zhou, M.G. Chapline, S. Peng, K. Cho, and H. Dai. 2000. Nanotube molecular wires as chemical sensors. *Science* 287:622-625.

Lee, C.J., J. Park, and J.A. Yu. 2002. Catalyst effect on carbon nanotubes synthesized by thermal chemical vapor deposition. *Chemical Physics Letters* 360:250-255.

Li, W., H. Zhang, C. Wang, Y. Zhang, L. Xu, and K. Zhu. 1997. Raman characterization of aligned carbon nanotubes produced by thermal decomposition of hydrocarbon vapor. *Applied Physics Letters* 70:2684-2686.

Liu, C., Y. Fan, M. Liu, H. Cong, H. Cheng, and M. Dresselhaus. 1999. Hydrogen storage in single-walled carbon nanotubes at room temperature. *Science* 286:1127-1129.

Liu, H., Y. Zhang, R. Li, X. Sun, F. Wang, Z. Ding, P. Mérel, and S. Desilets. 2010. Aligned synthesis of multi-walled carbon nanotubes with high purity by aerosol assisted chemical vapor deposition: effect of water vapor. *Applied Surface Science* 256:4692-4696.

Makita, Y., S. Suzuki, H. Kataura, and Y. Achiba. 2005. Synthesis of single wall carbon nanotubes by using arc discharge technique in nitrogen atmosphere. *The European Physical Journal D-Atomic, Molecular, Optical and Plasma Physics* 34:287-289.

Martel, R., T. Schmidt, H. Shea, T. Hertel, and P. Avouris. 1998. Single-and multi-wall carbon nanotube field-effect transistors. *Applied Physics Letters* 73:2447-2449.

Matthews, M., M. Pimenta, G. Dresselhaus, M. Dresselhaus, and M. Endo. 1999. Origin of dispersive effects of the Raman D band in carbon materials. *Physical Review B* 59:6585-6588.

Merkoçi, A. 2006. Carbon nanotubes in analytical sciences. *Microchimica Acta* 152:157-174.

Meyyappan, M. 2005. *Carbon nanotubes: science and application*. CRC Press.

Moisala, A., A.G. Nasibulin, and E.I. Kapauppinen. 2003. The role of metal nanoparticles in the catalytic production of single-walled carbon nanotubes.*Journal of Physics: Condensed Matter* 15:3011-3035.

Nessim, G.D. 2010. Properties, synthesis, and growth mechanisms of carbon nanotubes with special focus on thermal chemical vapor deposition. *Nanoscale* 2:1306-1323.

Nessim, G.D., A.J. Hart, J.S. Kim, D. Acquaviva, J. Oh, C.D. Morgan, M. Seita, J.S. Leib, and C.V. Thompson. 2008. Tuning of vertically-aligned carbon nanotube diameter and areal density through catalyst pre-treatment. *Nano Letters* 8:3587-3593.

Niu, Z., and Y. Fang. 2006. Effects of synthesis time for synthesizing single-walled carbon nanotubes over Mo-Fe-MgO catalyst and suggested growth mechanism. *Journal of Crystal Growth* 297:228-233.

Paradise, M., and T. Goswami. 2007. Carbon nanotubes-Production and industrial applications. *Materials & Design* 28:1477-1489.

Patole, S.P., P.S. Alegaonkar, J.H. Lee, and J.B. Yoo. 2008. Water-assisted synthesis of carbon nanotubes: Acetylene partial pressure and height control. *EPL (Europhysics Letters)* 81:38002-38007.

Petrucci, R.H., W.S. Harwood, F.G. Herring, and J.D. Madura. 1993. *General chemistry: principles and modern applications*. Macmillan New York.

Pint, C.L., S.M. Kim, E.A. Stach, and R.H. Hauge. 2009a. Rapid and scalable reduction of dense surface-supported metal-oxide catalyst with hydrazine vapor. *ACS Nano* 3:1897-1905.

Pint, C.L., S.T. Pheasant, A.N.G. Parra-Vasquez, C. Horton, Y. Xu, and R.H. Hauge. 2009b. Investigation of optimal parameters for oxide-assisted growth of vertically aligned single-walled carbon nanotubes. *The Journal of Physical Chemistry C* 113:4125-4133.

Popov, V.N. 2004. Carbon nanotubes: properties and application. *Materials Science and Engineering Reports* 43:61-102.

Puretzky, A.A., D.B. Geohegan, S. Jesse, I.N. Ivanov, and G. Eres. 2005. In situ measurements and modeling of carbon nanotube array growth kinetics during chemical vapor deposition. *Applied Physics A* 81:223-240.

Radushkevich LV, V.M. Lukyanovich. 1952. O strukture ugleroda, obrazujucegosja priTermiceskom razlozenii okisi ugleroda na zeleznom kontakte. *Zurn Fisic Chim* 26:88-95.

Saito, R., M. Fujita, G. Dresselhaus, and M. Dresselhaus. 1992. Electronic structure of chiral graphene tubules. *Applied Physics Letters* 60:2204-2206.

Saito Y, M. Okuda, N. Fujimoto, T. Yoshikawa, M. Tomita, T. Hyashi. 1994. Single wall carbon nanotubes growing rapidly from Ni fine particles formed by arc evaporation. *Japan Journal of Applied Physics Part 2- Letters* 33:526-529.

Schwartz, M. 2006. *New materails: process, and methods technology.* CRC Press.

Shanov V., Y.H. Yun, M.J. Schulz. 2006. Synthesis and characterization of carbon nanotube materials. *Journal of the University of Chemical Technology and Metallurgy* 41(4):377-390.

Smajda, R., J. Andresen, M. Duchamp, R. Meunier, S. Casimirius, K. Hernadi, L. Forró, and A. Magrez. 2009. Synthesis and mechanical properties of carbon nanotubes produced by the water assisted CVD process. *Physica Status Solidi* 246:2457-2460.

Stadermann, M., S.P. Sherlock, J.-B. In, F. Fornasiero, H.G. Park, A.B. Artyukhin, Y. Wang, J.J.D. Yoreo, C.P. Grigoropoulos, O. Bakajin, A.A. Chernov, and A. Noy. 2009. Mechanism and kinetics of growth termination in controlled chemical vapor deposition growth of multiwall carbon nanotube arrays. *Nano Lett* 9:738-744.

Stahl, H. 2000. *Electronic Transport in Ropes of Single Wall Carbon Nanotubes*. Achen University of Technology.

Thess, A., R. Lee, P. Nikolaev, H. Dai, P. Petit, J. Robert, C. Xu, Y.H. Lee, S.G. Kim, and A.G. Rinzler. 1996. Crystalline ropes of metallic carbon nanotubes. *Science* 273:483-487.

Thostenson, E.T., Z. Ren, and T.W. Chou. 2001. Advances in the science and technology of carbon nanotubes and their composites: a review. *Composites Science and Technology* 61:1899-1912.

Vesselényi, I., K. Niesz, A. Siska, Z. Kónya, K. Hernadi, J.B. Nagy, and I. Kiricsi. 2001. Production of carbon nanotubes on different metal supported catalysts. *Reaction Kinetics and Catalysis Letters* 74:329-336.

Walker, P.L., F. Rusinko, L.G. Austin. 1959. Gas reactions of carbon. *Advances in Catalysis* 11:133-221.

Wen, Q., W. Qian, F. Wei, Y. Liu, G. Ning, and Q. Zhang. 2007. CO_2 assisted SWNT growth on porous catalysts. *Chemistry of Materials* 19:1226-1230.

Wolf, E.L. 2006. *Nanophysics and nanotechnology:an introduction to modern concepts in nanoscience*. Wiley-VCH.

Wong, S.S., E. Joselevich, A.T. Woolley, C.L. Cheung, and C.M. Lieber. 1998. Covalently functionalized nanotubes as nanometer-sized probes in chemistry and biology. *Nature* 394:52-55.

Wynblatt, P. 1975. Supported metal crystallites. *Progres in Solid State Chemistry 9:*21-58.

Xiea, S.S., W.Z. Li, Z.W. Pan, B.H. Chang, and L.F. Sun. 1999. Carbon Nanotube Arrays. *The European Physical Journal* 9:1-4.

Xiong, G., Y. Suda, D. Wang, J. Huang, and Z. Ren. 2005. Effect of temperature, pressure, and gas ratio of methane to hydrogen on the synthesis of double-walled carbon nanotubes by chemical vapour deposition. *Nanotechnology* 16:532-535.

Xiong, G.Y., D. Wang, and Z. Ren. 2006. Aligned millimeter-long carbon nanotube arrays grown on single crystal magnesia. *Carbon* 44:969-973.

Yacaman, M.J., M.M. Yoshida, L. Rendon, and J.G. Santiesteban. 1993. Catalytic growth of carbon microtubules with fullerene structure. *Applied Physics Letters* 62:202-207.

Yamada, T., A. Maigne, M. Yudasaka, K. Mizuno, D.N. Futaba, M. Yumura, S. Iijima, and K. Hata. 2008. Revealing the secret of water-assisted carbon nanotube synthesis by microscopic observation of the interaction of water on the catalysts. *Nano Lett* 8:4288-4292.

Yamada, T., T. Namai, K. Hata, D.N. Futaba, K. Mizuno, J. Fan, M. Yudasaka, M. Yumura, and S. Iijima. 2006. Size-selective growth of double-walled carbon nanotube forests from engineered iron catalysts. *Nature Nanotechnology* 1:131-136.

Yang, Q., S. Bai, T. Fournier, F. Li, G. Wang, H. Cheng, and J. Bai. 2003. Direct growth of macroscopic fibers composed of large diameter SWNTs by CVD. *Chemical Physics Letters* 370:274-279.

Yudasaka, M., R. Kikuchi, T. Matsui, O. Yoshimasa, and S. Yoshimura. 1994. Specific conditions for Ni catalyzed carbon nanotube growth by chemical vapor deposition. *Applied Physics Letters* 67:2477-2482.

Zhang, G., D. Mann, L. Zhang, A. Javey, Y. Li, E. Yenilmez, Q. Wang, J.P. McVittie, Y. Nishi, and J. Gibbons. 2005. Ultra-high-yield growth of vertical single-walled carbon nanotubes: hidden roles of hydrogen and oxygen. *Proceedings of the National Academy of Sciences of the United States of America* 102:16141-5.

Zhao, Q., and H.D. Wagner. 2004. Raman spectroscopy of carbon-nanotube-based composites. *Philosophical Transactions of the Royal Society of London. Series A: Mathematical, Physical and Engineering Sciences* 362:2407-2424.

Zhong, G., S. Hofmann, F. Yan, H. Telg, J. Warner, D. Eder, C. Thomsen, W. Milne, and J. Robertson. 2009. Acetylene: a key growth precursor for single-walled carbon nanotube forests. *The Journal of Physical Chemistry C* 113:17321-17325.

Zhu, S., C.H. Su, J. Cochrane, S. Lehoczky, Y. Cui, and A. Burger. 2002. Growth orientation of carbon nanotubes by thermal chemical vapor deposition. *Journal of Crystal Growth* 234:584-588.

Zhu, W., C. Bower, O. Zhou, G. Kochanski, and S. Jin. 1999. Large current density from carbon nanotube field emitters. *Applied Physics Letters* 75:873-875.